Bejarano Durán, Fernando (2014) Miniature ultrasonic bone cutting device based on a cymbal transducer. PhD thesis.

http://theses.gla.ac.uk/5568

MINIATURE ULTRASONIC BONE CUTTING DEVICE BASED ON A CYMBAL TRANSDUCER

Fernando Bejarano Durán

A thesis for the degree of Doctor of Philosophy (PhD)

Submitted to the College of Science and Engineering,
University of Glasgow

September 2014

Declaration of Originality Form

This form **must** be completed and signed and submitted with all assignments.

Please complete the information below (using BLOCK CAPITALS).

Name: FERNANDO BEJARANO DURAN
Student Number: 0912675
Course Name: PHD
Assignment Number/Name:

An extract from the University's Statement on Plagiarism is provided overleaf. Please read carefully THEN read and sign the declaration below.

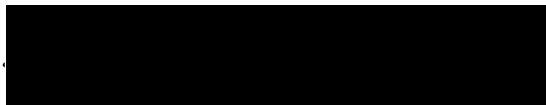| I confirm that this assignment is my own work and that I have:	
Read and understood the guidance on plagiarism in the Student Handbook, including the University of Glasgow Statement on Plagiarism	✕
Clearly referenced, in both the text and the bibliography or references, **all sources** used in the work	✕
Fully referenced (including page numbers) and used inverted commas for **all text quoted** from books, journals, web etc. (Please check with the Department which referencing style is to be used)	✕
Provided the sources for all tables, figures, data etc. that are not my own work	✕
Not made use of the work of any other student(s) past or present without acknowledgement. This includes any of my own work, that has been previously, or concurrently, submitted for assessment, either at this or any other educational institution, including school (see overleaf at 31.2)	✕
Not sought or used the services of any professional agencies to produce this work	✕
In addition, I understand that any false claim in respect of this work will result in disciplinary action in accordance with University regulations	✕

DECLARATION:
I am aware of and understand the University's policy on plagiarism and I certify that this assignment is my own work**,** except where indicated by referencing, and that I have followed the good academic practices noted above
Signed: Fernando Bejarano Duran

DECLARATION

I declare, Fernando Bejarano Durán, being the author of the thesis "MINIATURE ULTRASONIC BONE CUTTING DEVICE BASED ON A CYMBAL TRANSDUCER". This thesis is a record of the original work carried out by myself under the supervision of Prof. Margaret Lucas in the School of Engineering at the University of Glasgow, United Kingdom, during the period of January 2010 to August 2014. The copyright of this thesis therefore belongs to the author under the terms of the United Kingdom Copyright acts. Due acknowledgement must always be made of the use of any material contained in, or derived from, this thesis. The thesis has not been presented elsewhere in consideration for a higher degree.

Signature ___

Printed name: Mr. Fernando Bejarano Durán

Abstract

Ultrasonic cutting devices have been successfully used in several industries, especially the food industry. This knowledge, developed for industrial procedures, has been exported to other areas where it is having great impact. In medicine, during the last 30 years, different ultrasonic devices have been designed for a wide variety of surgical procedures involving soft tissue, and even more recently for cutting of bone. The increasing numbers of surgeons adopting ultrasonic devices as the device of choice has in turn increased the demand for devices which are able to be used increasingly in new procedures with more difficult to access surgical sites.

Currently, ultrasonic cutting devices consist of a Langevin piezoelectric transducer attached to a cutting blade both tuned to resonate in a longitudinal mode at a low ultrasonic frequency, usually in the 20-50 kHz range.

The first commercial ultrasonic devices for bone cutting applications, designed by the Italian company Mectron and called Piezosurgery®, were based on a Langevin piezoelectric transducer. Langevin transducers incorporate a piezoceramic stack capable of delivering a few microns of vibration amplitude, and therefore the transducer and the device as a whole must be resonant to achieve the required ultrasonic displacement amplitude at the cutting tip.

Because the ultrasonic blade is a tuned component its length must be a half-wavelength or a multiple of the half-wavelength at the driving frequency. Also, because Langevin transducers can only deliver a few microns of vibration amplitude, the blade profile must be carefully designed to provide sufficient vibration amplitude gain to meet the requirements of the material to be cut. Therefore the cutting blade itself incorporates high amplitude gain, which can lead to very high stresses, and the design of the blade geometry is somewhat restricted by the requirement for resonance.

These two geometry requirements can be very restrictive in the design of devices; a half-wavelength at a low ultrasonic frequency leads to quite a large cutting device and profiling for

high gain leads to very high stresses. This thesis investigates adapting the class V flextensional 'cymbal' transducer for power ultrasonic applications. The cymbal transducer consists of piezoelectric rings bonded to two end-caps with truncated conical shape. When the ring contracts radially under an AC voltage, the end-caps flex providing an amplified motion normal to the cap surfaces.

This thesis introduces a new prototype of an ultrasonic cutting device for bone surgery based on a cymbal transducer, optimised for use in power ultrasonics applications, which removes many of the geometrical restrictions on the cutting tip. For the proposed application, a cutting blade is attached to one of the vibrating end-caps with little effect on the operational frequency. Thus, the blade behaves nearly as a rigid body, without the need to be a tuned component of the device. The enormous benefit of this technology is that the cutting blade design can focus more closely on delivering the best interaction between the blade and bone to provide a highly accurate cut, and also the ultrasonic device can be miniaturised to allow the design of devices for delicate orthopaedic procedures involving minimal access surgery. The results show how the cymbal transducer can excite sufficiently high vibration displacement amplitude at lower driving voltages, by adapting the configuration of the cymbal to remove the problem of epoxy layer debonding and by optimising the cymbal end-caps and geometry through finite element modelling supported with experimental vibration characterisation. Preliminary trials of the resulting prototype ultrasonic bone cutting device, which operates near to 25 kHz, are presented to illustrate the success of this novel device design.

iii

Acknowledgments

First and foremost, I would like to express my sincerest gratitude to Professor Margaret Lucas for the effort, patience, guidance and the availability to always have time to discuss any aspects of this thesis despite busy agendas. With her helps I had the opportunity to present my work in various continents and meet researchers around the world that have made me love research and ultrasonics. Also I would like thank Professor Margaret Lucas for her patience and guidance to improve my English and to be able to write with success papers and this thesis. I must also specially thank Dr Andrea Cardoni, who was my first supervisor, for a short period of time, but was responsible for giving me the opportunity to develop my PhD in the University of Glasgow and to work on such an exciting topic.

I would like to thank the Engineering and Physical Sciences Research Council (EPSRC, grant EP/G046948/1) for funding the project, as well as the project's industrial partner, Mectron S.p.A. At Mectron S.p.A, I would specifically like to thank Mr Niccolò Cerisola for his time, help and knowledge during all the phases of this thesis and the opportunity of visiting Mectron S.p.A. in Italy to test the ultrasonic cutting device. From him I always had a yes for me, and this is something I indeed appreciate.

I also would like to thanks Professor Hamish Simpson, Dr Robert Wallace and Mr Antonio M. Spadaccino from the Department of Orthopaedic Surgery of the University of Edinburgh, for the collaboration in the performance of surgical procedures cutting rat bones.

Thank-you to the technical staff, Mr. Brain Robb and his colleagues, for their expertise, extensive help and assistance in the workshop and their kindness and patience during the long days trying to machine the different pieces of the ultrasonic cutting device. It was a challenge but without their help this device would have not been possible.

A special acknowledgement to the Power Ultrasonics group at Glasgow, because more than colleagues I consider them part of my life, we have shared knowledge, long talks, coffees and meals and friendship that made it feel like home from the first day I arrived in Glasgow. Although I consider all of them my friends, I have to specially thanks Andrew Feeney for all

Symbols and Abbreviations

List of symbols

f	effort
v	flow
L	Length
P_r	Spontaneous polarisation
T_c	Curie temperature
P	Polarisation
E	Electric field
P_s	Saturation polarisation
E_c	Coercitive field
S	Strain
D	Electric displacement
T	Stress
d,e,g,h,d_h	Piezoelectric constants
ϵ	Permittivity
s	Compliance
ε^T	Relative permittivity at constant stress
β_{mk}	Impermittivity
k	Coupling factor
Q_m	Mechanical quality factor
Z	Acoustic impedance
ρ	Density
υ	Wave speed
A	Cross-sectional area
ω	Angular frequency

λ	Wave length
C	Compliance
H	Degree of hysteresis
F	Force
R_c	Receptance
M_b	Mobility
v	velocity
a	Acceleration
D_s	Dynamic stiffness
Z_m	Mechanical impedance
D_m	Dynamic mass
D_c	Cymbal diameter
W_t	PZT thickness
w_t	End-cap thickness
C_d	Cavity diameter
C_h	Cavity depth
E_t	Epoxy thickness
A_d	Apex diameter
M	Mass matrix
K_{uu}	Displacement matrix
$K_{\Phi\ \Phi}$	Dielectric matrix
$K_{\Phi\ u}$	Piezoelectric coupling matrix
Q^M	Electrical charge vector
P^M	Mechanical force vector
ζ	Damping ratio
α, β	Damping parameters
Y	Young's modulus
σ	Poisson's ratio
f_r	Resonance frequency
f_a	Antiresonance frequency
R	End-cap radius
k_{eff}	Effective coupling factor
m	mass

List of abbreviations

HIFU	High Intensity Focused Ultrasound
GMM	Giant Magnetostrictive Materials
MSM	Magnetic Shape Memory
FSMA	Ferromagnetic Shape Alloy
PZT	Lead Zirconate Titanate
PDVF	Polyvinylidene Diflouride
PZN-PT	Lead Zirconate Niobate doped with Lead Titanate
PMN-PT	Lead Magnesium Niobate doped with Lead Titanate
MRI	Magnetic Resonance Imaging
FEA	Finite Element Analysis
BC	Boundary Conditions
OMA	Operational Modal Analysis
EMA	Experimental Modal Analysis
FRF	Frequency Response Function
LDV	Laser Doppler Vibrometer
FFT	Fast Fourier Transform
DOF	Degree of Freedom
SDOF	Single Degree of Freedom
OC	Original Cymbal Transducer
NC	New Cymbal Transducer
PNC	Prototype of New Cymbal Transducer

Contents

List of Tables

List of Figures

Chapter 1

Introduction

1.1 Introduction

Ultrasound is widely used in medicine, with a variety of applications that range from diagnosis to therapeutic procedures. The beginnings of ultrasound instrumentation started with the discovery of the piezoelectric effect by Pierre and Jacques Curie in 1880, who observed that applying an electric field to certain materials can cause high frequency mechanical vibrations and vice versa. One particular piezoelectric material, quartz, was then incorporated into the first ultrasound device, a hydrophone developed by Paul Langevin for sonar applications.

There exists a wide range of applications of high power ultrasonic techniques in therapy procedures. In many cases, the ultrasonic devices have substituted the traditional manual or mechanical tools due to the high precision, safety and effectiveness achieved by the actual devices. The incorporation of ultrasonic transducers into bone surgery has its origins in industry when researchers employed an ultrasonic cutting device developed for industrial applications in dentistry procedures.

In contrast to ultrasonic cutting in industry applications, the cutting procedure for biological tissues involves many factors apart from the effectiveness of cutting the material, such as correct accessibility to the zone to be cut, precision of the cut or preservation from damage of delicate tissues.

The incorporation of computer modelling software to the design of new ultrasonic transducers along with the development of more efficient materials, has allowed the designers to focus the transducer design to obtain a better performance of the device optimised for a better interaction with the medium in which it is employed. In this matter it is essential to develop devices that consider the point of view of the surgeon, to adapt the technologies to

the different procedures.

1.2   Actuator technologies

The word transducer comes from Latin *transducere* 'lead across' (from *trans-* (across) + *ducere* (lead)) [1]. Middelhoek and Hoogerwerf [2] define the process of transduction in a sensor as the conversion of a nonelectric energy into an electronic signal. This definition is restrictive as the transducer necessarily works to or from the electrical domain. Rossenberg and Karnopp go a step further, defining the transducer *as a device which couples subsystems in two different energy domains* [3]. In this case the description does not include conversions between types of energy belonging to the same domain. For Busch-Vishniac, however, a transducer is *a device which transforms energy from one type to another, even if both energy types are in the same domain* [4]. This broad definition doesn't make any restriction about types of energy nor domains and hence includes devices that were not thought of as transducers before.

According to the method of operation, transducers are divided into two classes: sensors and actuators. Sensors are devices that recover information from a system, for monitoring purposes, with minimum influence upon it. A example could be a temperature sensor in an engine. On the other hand, the function of actuators is to impose a particular state in the system they are coupled with, without being influenced by it. A loudspeaker is a clear example of an actuator, which imposes a condition (the sound pressure) in the system which it is coupled with (the air).

A general definition about what an actuator is was introduced by Pons referencing as a device that modifies the mechanical state of a system to which it is coupled [5]. This transducer can be represented as a two port device where some input energy is transformed and delivered, Figure 1.1. The signal at the input and the output is defined by an effort (force, torque, voltage, etc) and its correlated variable, a flow (velocity, angular rate, current, etc)

The ratio between those variables leads to one of the principal parameters, the impedance. Depending of the type of signal in each port it is possible to work with electrical impedance, mechanical impedance, acoustic impedance, etc.
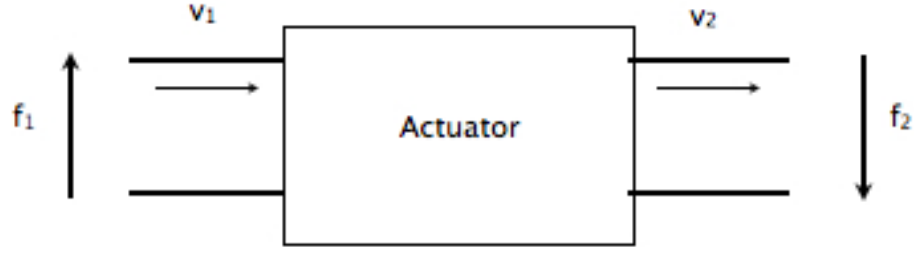
Figure 1.1: Two port schematic of an actuator

The actuator is hence a specific class of transducer, so that inside the device exists a conversion of energy to make it useful to impose a determinate state on a system.

Although there exist many different opinions about the delineation of energy domains, and this issue has generated controversial debates, it is possible to classify the transducers or types of transduction in seven main energy domains [5], chemical, electrical, magnetic, mechanical, optical, fluid and thermal. In general, the most common technologies require transducers that intervene in two of these mentioned domains, such as:

- Thermo-mechanical transducers. These devices convert thermal energy into a mechanical motion using different thermal properties of the material, direct effect, and vice versa, the inverse effect. An example is the compressional waves generator developed by A.H. Rich using the thermal expansion of a crystal compound of chromium modified manganese antimonide [6].

- Thermo-electric transducers. In this energy conversion process, a flow between the thermal and electric domains is created. Electrothermal transducers are common in MEMS devices and have been used in applications such as micro-actuator devices for read/write head positioning for data storage and solid state circuit sensor protector [7–10].

- Magneto-mechanical transducers. The process of transduction is based in material shape changes due to a change in its magnetic state and vice versa. These material changes produce mechanical energy. The magnetostrictive effect has been broadly used in the development of ultrasonic underwater sound projectors and receivers (sonars).

- Electro-mechanical transducers. The success of the conversion of electronics to microelectronics circuits has led to the development of transducers with a faster response and control. The exchange of energy occurs between the electrical domain and the

mechanical domain, although depending of the technology it is possible to find devices
with transduction between 3 different domains.

- Electro-magnetic-mechanical transducers. In these devices, previously mentioned
  as magneto-mechanical transducers, the magnetic energy is generated by an
  electric field. Based in the Lorentz law, some transducers are constituted by a
  magnet and an electric coil. Additionally it is possible to impose the necessary
  magnetic field in a magnetostrictive material by means of a electric circuit. In
  1977 Meeks studied the performance of rare earth iron rods made of terbium and
  dysprosium for their used as driver of ultrasonic underwater projectors [11].

- Electro-thermo-mechanical transducers. The thermal energy is generated by
  means of resistive heating using the Joule effect. The recent use of shape memory
  alloy materials like Nitinol, with 2 different elastic phases depending on the applied
  temperature, has led researchers to develop a wide range of new sensors and
  actuators.

- Electrorheological fluid (ERF) transducers. Related to ionic electroactive poly-
  mers, electrorheological fluids are colloidal suspensions, which reversibly transform
  into a semi-solid when subjected to an electric field. When the electric field
  is applied, electrorheological fluids change phase by forming fibrous structures
  parallel to the applied field.

- Piezoelectric transducers. Piezoelectric materials present an induced charge under
  the application of a force (deformation), this phenomena is called the direct effect.
  In the inverse effect, a strain is induced with the application of an electric field.
  These transducers are one of the most common transducer types on the market.

1.3   Ultrasonic transduction

It is possible to define ultrasound as energy generated by mechanical waves vibrating at
frequencies above 20 kHz (1 Hz is a cycle per second). Vibrations in solids and fluids can
be produced and detected by many different methods, so that there is not just one type of
transduction associated to the generation of ultrasonic waves.

Electro-mechanical transduction process groups the majority of transducers used in
medical and industrial applications, in which an electric signal, modulated at a frequency
above the mentioned threshold, is transformed to mechanical motion vibrating at the same

frequency, and vice versa. This work focuses on the development of devices based in this principle of energy conversion. The frequency range of ultrasounds present a broad spectrum from 20 kHz, which is the standard limit of frequency audible to humans to several Gigahertz. The upper limit is imposed only by the ability to generate the signals.

The most important parameters for the classification of ultrasonics applications are sound power (W), sound intensity (W/m^2) or sound energy density (Ws/m^3). Under these criteria ultrasonic applications can be assorted in two distinct groups: low energy (low power ultrasonics) ultrasound generates mechanical oscillations causing no physical or chemical alterations on the properties of the medium through which the ultrasonic wave passes. The particles oscillate due to the energy applied and return to their equilibrium position when the ultrasonic source is removed. These procedures are applied in non-destructive testing of materials, such as detection of failures and quality control of food, and medical diagnosis as ultrasonography.

It is not clear what is the upper power limit for these ultrasonic applications. While some researchers established this value in 1 W/cm^2 [12,13], up to which the ultrasonic wave causes no physical or chemical alterations in the properties of the material, recent studies in bone healing, as the work of Pilla et al, observed that the fibula osteotomy healing, in New Zealand white rabbits, increased when the bones were radiated with ultrasounds using intensities of 30 mW/cm^2 [14]. This demonstrates that the interaction with the media, causing alterations, in some cases occurs at very low intensities. This limit depends on the properties of the material in which the mechanical wave is propagated.

The other group is denominated high energy (high power ultrasonics or macrosonics) ultrasound, which exposes the medium to enough vibratory energy to alter permanently some part of the material or to generate a chemical reaction. The level of mechanical power depends on the application and the material under study. For industrial applications such as ultrasonic cutting and welding and ultrasonic cleaning, the power requirements usually encompass from tens of watts to several kiloWatts [15]. From a biomedical point of view, studies have concluded that an intensity of 2-3 W/cm^2 [16], is the limit between low level and high level ultrasound for HIFU (high intensity focused ultrasound) in applications such as cancer therapy, however, the characteristics of the medium and the application determine the energy required.

The most common applications of low power ultrasonics utilise frequencies in the range from hundreds of kilohertz to megahertz while high power processes usually use frequencies

from the lower ultrasonic range (20 kHz), up to a few hundred kilohertz, classifying the devices in high-power low frequency ultrasonic transducers and low-power high frequency ultrasonic transducers.

1.4 Power ultrasonic systems

Ultrasonic systems for high power applications can be classified as actuators, since their purpose is to modify the mechanical state of the material to which they are applied. In general, these devices consist of a power supply (signal generator and high power amplifier) and the electro-mechanical transducer, Figure 1.2. The transducers are typically composite devices in which the active part, that performs the transduction phenomena, is constituted by an electroactive material, commonly piezoelectric or magnetostrictive element, which changes dimensions in response to an electric (or magnetic) field. The power supply converts the available electric line low frequency signal into high frequency electric signal which is used to drive the electromechanical transducer.

The mechanical motion generated by the complete device might be improved by connecting mechanical amplifiers such as horns or end-caps, tuned at the operational frequency of the transducer, generating a higher output amplitude.

Although, as discussed above, the frequency range of power ultrasonic systems embraces several kilohertz, the different devices operate in a narrow frequency bandwidth. This limited operational frequency spectrum allows to concentrate the maximum energy in a specific vibrational mode, achieving high levels of efficiency.
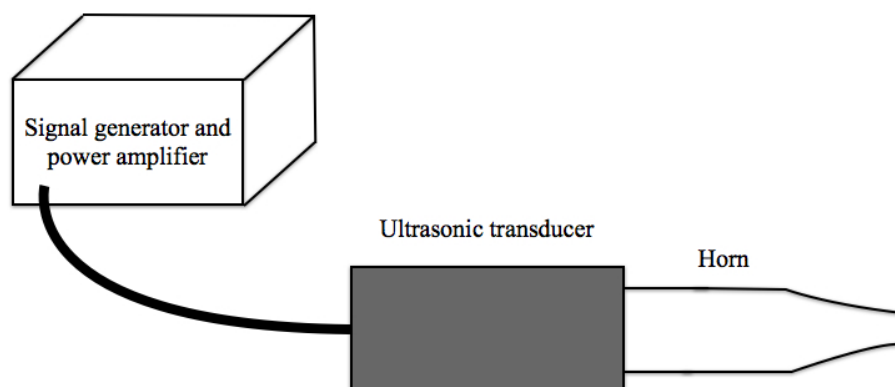
Figure 1.2: Schematic of a high power ultrasonic device

1.4.1 Magnetostriction

Ferromagnetic materials are those which present a spontaneous magnetisation, a net magnetic moment in the absence of an external magnetic field. This spontaneous magnetisation is due to the alignment of groups of magnetic dipoles in the crystalline structure creating regions with a certain magnetic moment. When an external magnetic field is applied the domains will re-orientate, aligning themselves with the direction of the applied field, and as a result the material is magnetised. When the applied field is removed some part of the induced domain alignment remains so that the body remains magnetised, Figure 1.3.
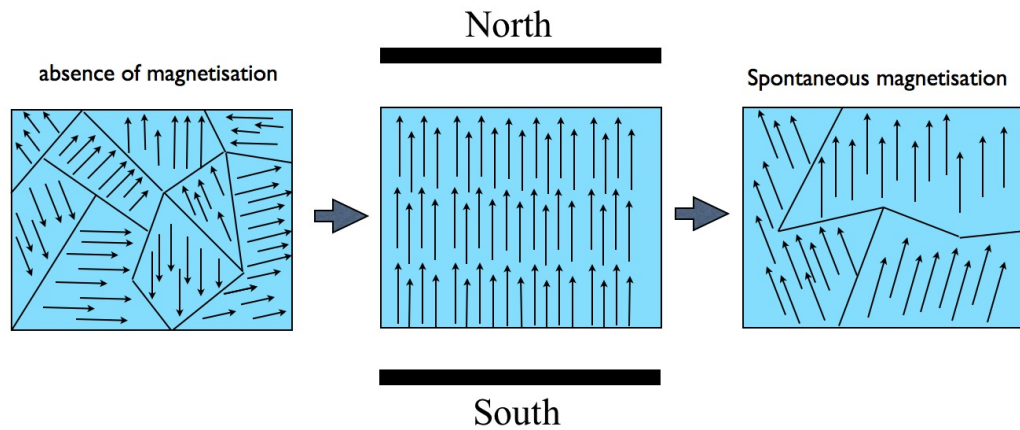
Figure 1.3: Orientation of domains in ferromagnetic material throughout magnetisation process

When a ferromagnetic material is exposed to an increment of temperature, the thermal motion or entropy competes with the tendency for dipoles to align. Above a certain temperature, the Curie point, the material becomes paramagnetic, the system reacts under the influence of a magnetic field but can no longer maintain a spontaneous magnetisation.

In 1842 Joule observed changes in the length of ferromagnetic materials (in particular nickel) when an external magnetic field was applied (Joule effect). During his experiments Joule obtained a contraction of the sample, known as negative magnetostriction. Subsequently studies with different materials exhibited an expansion or positive magnetostriction. In 1865 Villari discover the inverse effect, when a deformation of the material is exerted, a proportional magnetic field is generated by the material (Villari effect). There exist other additional effects in magnetostrictive materials such as the ΔE-Effect and Barret Effect,

although the most applied in actuator technologies are the Joule effect and the Widemann effect. This effect is similar to the Joule effect but in this case there is a conversion from a helicoidal magnetic field to torsional displacement, in the ferromagnetic material [5].

The first devices that used magnetostrictive transduction were built using transition metals such as iron, cobalt, nickel and its alloys. Although they present small elongation, the ratio of $\Delta L/L$ is typically of the order of 60 ppm (ppm = parts per million), a strain of around 0.006%. In later years researchers characterised new elements and alloys based in rare earth metals such as Terbium (Tb) and Dysprosium (Dy) which possess large magnetostrictive properties, and hence are known as Giant Magnetostrictive Materials (GMM). The most studied material was develop at the US Naval Ordnance Laboratory, with a composition of Tb-Dy-Fe, Terfenol-D, showing strains up to 4000 ppm [5,17–19].

The future of magnetostrictive materials is now largely associated with the shape memory alloy materials. Ullakko et al discovered in 1996 new magnetostrictive materials called Magnetic Shape Memory (MSM) alloys or Ferromagnetic Shape Memory Alloy (FSMA) materials. These materials exhibit giant magnetic field-induced strain based on the rearrangement of the crystallographic domains. FSMA materials can reach strains up to 10% [20,21].

1.4.2   Piezoelectricity

A dielectric is known as a material in which it is possible to induce an electric dipole when an electric field is applied. This phenomenon is known as electric polarisation of the dielectric [22].

Dielectric materials posses crystalline structure with geometric symmetries (point groups) that can be classified into 32 different point groups. According to their intrinsic crystallographic symmetry, among these classes of single-crystals 11 possess a centre of symmetry, due to the coinciding positive and negative charge sites, and are non-polar and 21 show a lack of centre of symmetry. In 20 classes of the non-centrosymmetric group, it is possible to induce a electric dipole when a mechanical stress is applied, this is known as the direct effect. These materials are known as piezoelectrics, meaning 'electricity by pressure' a definition that has its origin in the Greek word piezein meaning to 'press' or 'pressure' . Piezoelectric materials exhibit complementarily the inverse effect characterised by a strain being induced with the application of a potential difference [23].

Half of these piezoelectric materials, 10 point groups, present a unique polar axis,

providing a permanent polarisation in absence of an external electric field or stress, known as spontaneous polarisation. These crystals, known as pyroelectrics from the Greek '*pyr*' meaning fire, can generate, in addition to the piezoelectric behaviour, electric charges in their surfaces when a change in temperature is applied, due to the change in the ionic and electric forces of the dipole with temperature. In some pyroelectric materials the direction of the spontaneous polarisation can be modified by means of the applications of an electric field. This characteristic defines a new subgroup, ferroelectric materials. Not all piezoelectric and pyroelectric materials are ferroelectric, as shown in Figure 1.4.
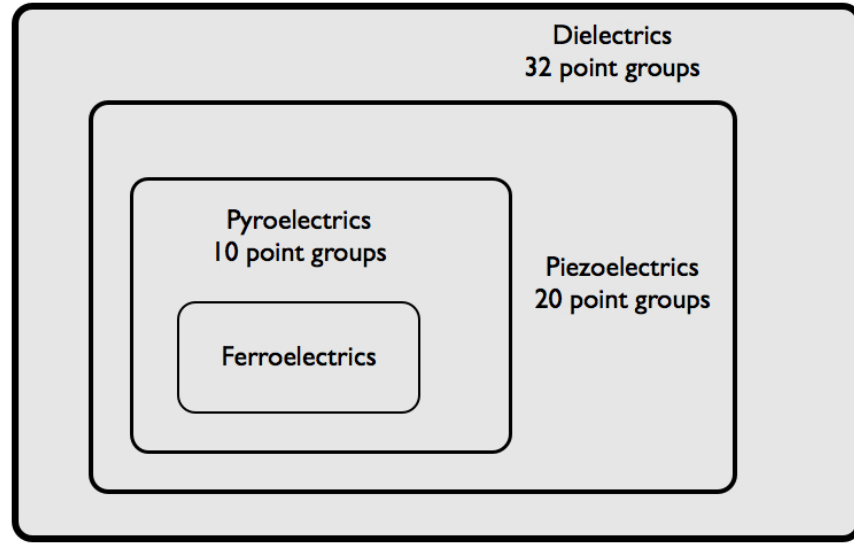
Figure 1.4: Point group division of the different dielectric materials

Ferroelectricity, analogous to ferromagnetism mentioned in the previous section, is a collaborative phenomenon. The spontaneous polarisation of one cell of the crystal interacts with its neighbour creating regions within the global structure of dipoles aligned in the same direction. These regions with a net polarisation are known as Weiss domains.

Within the material Weiss domains have different orientation depending on their polarisation vector, so that in the crystalline structure the angle between domains can vary. A difference of $180°$ between domains shows regions with an anti-parallel orientation, meanwhile a difference of $90°$ leads in a perpendicular orientation. It is possible to observe other orientations depending on the symmetry of the crystal.

The vast majority of ferroelectric ceramics have a perovskite crystal structure with the chemical formula ABO_3, with a quasi-cubic shape [24]. The element A represents a metal

with a monovalent, divalent or trivalent structure, and the second element B denotes a trivalent, tetravalent or pentavalent metal. Despite this crystal structure, which is commonly related with a geometric symmetry, it is necessary to have a lack of centre of symmetry in order to behave as a piezoelectric material, therefore ferroelectric ceramics with piezoelectric properties are internally anisotropic. Some typical examples of a ferroelectric ceramic, with a perovskite structure, are barium titanate BT (BaTiO3), discovered during World War II, $PbTiO_3$ (PTO), $(Ba,Sr)TiO_3$ (BST), and lead-based solid solutions such as $Pb(Zr,Ti)O_3$ (PZT).

Ferroelectric polycrystalline ceramics are not generally piezoelectric. They are isotropic materials with a regular perovskite structure and randomly ordered domains. In this state the material shows the paraelectric phase with an absence of piezoelectricity. In order to become piezoelectric, it is necessary to subject the material to a poling process. Through this process, a strong electric field whilst at an elevated temperature just below the materials Curie temperature T_c is applied to the material to give the material a polar state. During this process saturation polarisation is reached. Internally the domains polarity is aligned to that of the applied field, which becomes the polarity direction [25]. When the electric field is removed, some of the domains remain aligned, and the resulting polarisation is known as remanent polarisation P_r, or the spontaneous polarisation.

The Curie temperature, T_c, is the upper limit of the piezoelectric operational range. At higher temperature the spontaneous polarisation is lost and the material becomes paraelectric. Below T_c the material is in the ferroelectric phase, where the piezoelectric effect can be observed. There exists a dependence between the internal perovskite structure of the material and the temperature. The ferroelectric phase is therefore characterised by different distortions of the original cubic cell, providing a lack of symmetry between charges.

The non-linear relationship between the polarisation P and the applied field E in a ferroelectric materials is a hysteresis loop, as can be observed in Figure 1.5.
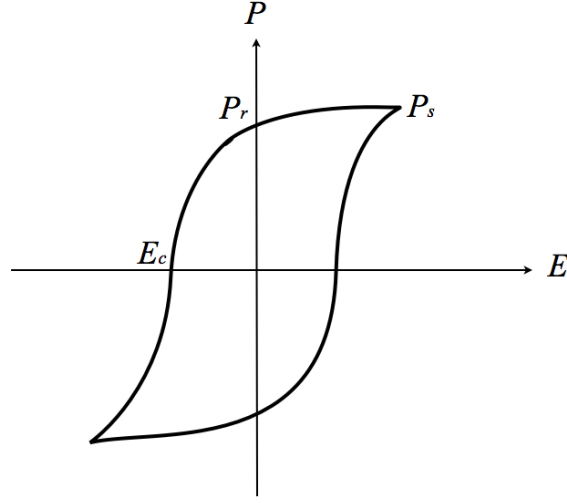
Figure 1.5: Relationship between the polarisation P and the applied electric field E in a ferroelectric material

In the analysis of these curves, it is possible to define the remanent polarisation P_r, which is the spontaneous polarisation in absence of an external electric field, the saturation polarisation P_s, above which the material acts as a 'monocrystal' and the coercive field E_c, that represents the electric field with opposite sign necessary to reduce the P_r to zero [22, 26, 27].

Similar analysis can be developed from the relationship between the applied electric field and the generated strain in the material. This corresponds to the inverse piezoelectric effect. In Figure 1.6 it is possible to observe the characteristic 'butterfly-shape' graph representing this relationship.
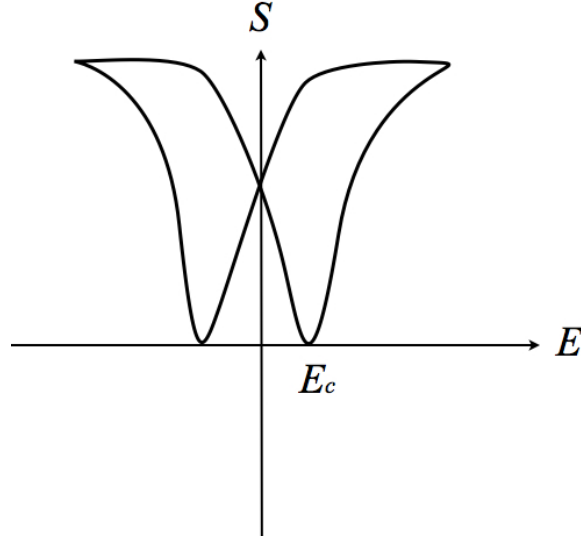
Figure 1.6: Relationship between the applied electric field E and the generated strain S in a ferroelectric material

The relationship remains quasi-linear for low levels of the applied electric field, and shows the maximum hysteresis when the coercive electric field E_c is reached. This is due the internal polarisation orientation in the material [5, 22].

Constitutive equations of piezoelectric materials

Piezoelectric materials are electromechanical and they are governed by both electrical and mechanical conditions. Therefore the mechanical and electrical parameters are coupled and must be involved in the constitutive equations.

As discussed previously, piezoelectricity is characterised by two complementary effects. The direct effect is the electrical response to a mechanical stimulation, the property to develop electric charge when a mechanical stress is exerted. Mathematically this can be expressed in a simple linear equation, (1.4.1):

$$D_m = d_{mi}T_i \tag{1.4.1}$$

where D_m is the electric displacement, T_i the stress component and d_{mi} is the component of the piezoelectric charge or strain coefficient, usually called the piezoelectric coefficient. On the other hand the inverse effect relates the mechanical strain produced in the material to the applied electric field. This relationship can be observed in equation (1.4.2) :

$$S_i = d'_{mi}E_m \tag{1.4.2}$$

where S_i is the strain component and E_m represents the electric field component. Electromechanical considerations show that $d_{mi} = d'_{mi}$, the coefficients that connect the electric field and the strain are the same as those that connect the stress and the polarisation. By convention, the first subscript of the piezoelectric constants indicates the direction of the electric field and the second the direction of the stress.

To complete the constitutive equation, it is also necessary to consider the mechanical and electrical relationship of any arbitrary non-piezoelectric material in the absence of interaction between stress and electric field. A material subject to zero stress, but a finite electric field E, can be described by the equation (1.4.3) :

$$D = \epsilon E \tag{1.4.3}$$

where ϵ is the permittivity of the material. On the other hand, when the same material is subject to zero electric field but has a stress T applied, a strain S is obtained. This can be observed in equation (1.4.4):

$$S = sT \tag{1.4.4}$$

where S is the resultant strain and s is the compliance of the material, that is defined as the inverse of the stiffness [28]. Combining (1.4.1) and (1.4.2) , and (1.4.3) and (1.4.4), gives the interactions between the electrical and mechanical cases, known as the piezoelectric constitutive equations [5, 29–32]:

$$D = dT + \epsilon^T E \tag{1.4.5}$$

$$S = s^E T + dE \tag{1.4.6}$$

Equation (1.4.5) defines the direct piezoelectric effect, while equation (1.4.6) defines the inverse effect. The superscripts in (1.4.5) and (1.4.6) denote the parameter being kept constant, in this case stress T and electric field E respectively.

In linear piezoelectricity the equations of linear elasticity, that usually define T and S, are coupled to the charge equation of electrostatics involving E and D by means of the piezoelectric constants. Depending on the selection of the independent variables (one mechanical and one electrical), it is possible to formulate four forms of the linear piezoelectric equations.

$$D_m = d_{mi}T_i + \epsilon^T_{mk}E_k$$
$$S_i = s^E_{ij}T_j + d_{mi}E_m \tag{1.4.7}$$

$$D_m = e_{mi}S_i + \epsilon^S_{mk}E_k$$
$$T_i = c^E_{ij}S_j - e_{mi}E_m \tag{1.4.8}$$

$$E_m = -g_{mi}T_i + \beta^T_{mk}D_k$$
$$S_i = s^D_{ij}T_j + g_{mi}D_m \tag{1.4.9}$$

$$E_m = -h_{mi}S_i + \beta^S_{mk}D_k$$
$$T_i = c^D_{ij}S_j - h_{mi}D_m \tag{1.4.10}$$

where, d, e, g and h are the piezoelectric constants, ϵ the permittivity and β_{mk} the impermittivity, found from the inverse of the permittivity matrix. Each pair of equations defines the direct and inverse effect of the piezoelectric material. Since the piezoelectric coupling is described by a linear relationship between a first order tensor or vector (D or E) and a second order tensor (T or S), the corresponding coupling coefficients d_{kij} (also called charge piezoelectric coefficients) form a third order tensor. The compliance, c, and the stiffness, s, are fourth order tensors. In the equations a matrix notation has been used following the Voigt convention, in order to simplify the notation [22, 31]. The directions assumed in the matrix notation are represented in Figure 1.7 :
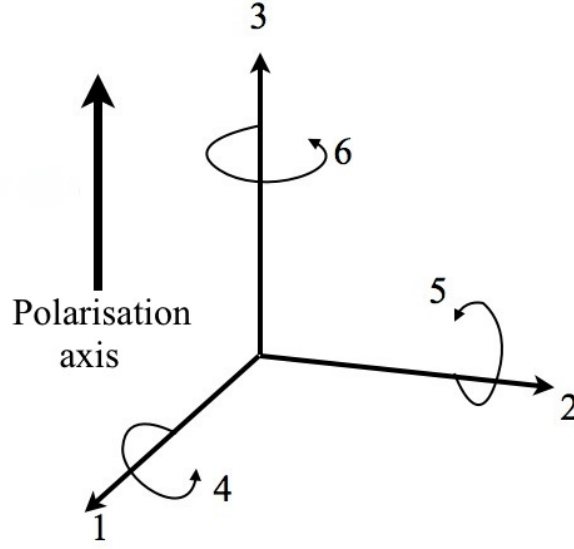
Figure 1.7: Matrix notation of the tensors in a piezoelectric material

Considering the order of all tensors in the constitutive equations and the reductions due to the crystallography symmetry of the material (i.e. a third order tensor has 27 independent components, reduced to 18 due to the crystallography equivalences), the electromechanical relationship in a piezoelectric material would be completely defined by 21 independent elastic coefficients, 18 independent piezoelectric constants and 6 independent dielectric constants. However, since poled ferroelectric ceramics have cylindrical symmetry, so the directions 1 and 2 are equivalents and their properties are different from direction 3. Therefore the number of independent coefficients can be reduced, following Neumann's principle: the symmetry elements of any physical property of a crystal must include the symmetry elements of the point group of this crystal. Hence, some poled ferroelectric only has five elastic constants, three piezoelectric and two dielectric [5, 22].

In matrix notation the constitutive equation can be represented by:

$$\begin{bmatrix} S \\ D \end{bmatrix} = \begin{bmatrix} s & d \\ d & \epsilon \end{bmatrix} \begin{bmatrix} T \\ E \end{bmatrix} \tag{1.4.11}$$

where the representations of the different variables are:

$$S = \begin{bmatrix} s_{11} & s_{12} & s_{13} & 0 & 0 & 0 \\ s_{12} & s_{11} & s_{13} & 0 & 0 & 0 \\ s_{13} & s_{13} & s_{33} & 0 & 0 & 0 \\ 0 & 0 & 0 & s_{44} & 0 & 0 \\ 0 & 0 & 0 & 0 & s_{44} & 0 \\ 0 & 0 & 0 & 0 & 0 & s_{66} \end{bmatrix} \tag{1.4.12}$$

$$\epsilon = \begin{bmatrix} \epsilon_1 & 0 & 0 \\ 0 & \epsilon_1 & 0 \\ 0 & 0 & \epsilon_3 \end{bmatrix} \tag{1.4.13}$$

$$d = \begin{bmatrix} 0 & 0 & 0 & 0 & d_{15} & 0 \\ 0 & 0 & 0 & d_{15} & 0 & 0 \\ d_{31} & d_{31} & d_{33} & 0 & 0 & 0 \end{bmatrix} \tag{1.4.14}$$

where

$$s_{66} = 2(s_{11} - s_{12}) \tag{1.4.15}$$

1.4.3 Piezoelectric materials

It is possible to classify the piezoelectric materials which are used for ultrasonic transduction into seven groups: quartz crystal, water-soluble crystals such as Rochelle salt and KH_2PO_4 (KDP), single crystals such as LN, LT, PZN-PT, PMN-PT, piezoelectric semiconductors such as cadmium sulphide (CdS) or zinc oxide (ZnO), piezoelectric ceramics such as barium titanate (BT) or lead zirconium titanate (PZT), piezoelectric polymer materials such as polyvinylidene difluoride (PDVF) and piezoelectric ceramic composites [22, 30, 33].

Piezoelectric ceramics are currently the leading materials for ultrasonic actuators in high power applications. Between the different ceramics, the PZT family possesses high piezoelectric coefficients d, T_c and k, easiness to develop a large variety of shapes with different directions of the polar axis and a reasonably high mechanical quality factor, Q_m. The piezoelectric coefficient d can be defined as the polarisation generated per unit of mechanical stress applied or as the mechanical strain experienced per unit of electric field applied. The k parameter, known as the coupling factor, represents the fraction of electrical energy that is converted into mechanical energy. The mechanical quality factor, Q_m, indicates the level of damping and, along with the k, indicates the efficiency. All these qualities have made this

type of piezoceramic the most favourable material for high-power ultrasonic transducers.

PZT was discovered by the Japanese researchers [5], but it was the US company Clevite Corporation who studied the piezoelectric properties and patented it in 1950s. Lead zirconate titanate in its general forms is composed of 52-43 % molar lead zirconate $PbZrO_3$ and 46-48 % molar lead titanate $PbTiO_3$.

The addition of dopants to the original formula can produce a significative impact on its properties. Doping the PZT material with donor ions such as La^{3+}, Nb^{5+} or Ta^{5+}, leads to the creation of cation vacancies, usually Pb-vacancies. The result increases the wall mobility, between domains, which means that less energy is required to reorientate the dipoles with the direction of the applied electric field. As result the material exhibits high permittivity, elastic compliance and k values. On the other hand this produces high dielectric losses with a reduction of the Q_m value. These ceramics, known as 'soft' PZTs exhibit low coercive electric fields (14-16 kV/cm) and high piezoelectric coefficients. On the other hand, doping the ceramic with acceptors such as Fe^{3+}, Sc^{3+} or K^{1+} generates the creation of oxygen vacancies. These vacancies generate a field that stabilises the domain structure when the dipoles are oriented in the same direction, reducing the wall mobility. The result is PZT with lower piezoelectric coefficients, low permittivity and dielectric losses, with high Q_m and high coercive electric fields (20 kV/cm). These ceramics are known as 'hard' PZTs, since it is more difficult to pole (and depole) the ceramics [5, 22, 26, 29, 31].

Due to their characteristics 'soft' PZTs are preferred for low power applications, such as sensors, and 'hard' PZTs, with higher Q_m, are the basis of high power actuators.

In the 1990s researchers discovered the piezoelectric properties of lead zirconate niobate doped with lead titanate (PZN-PT) and lead magnesium niobate doped with lead titanate (PMN-PT), known as 'single crystals'İmprovements in the growing techniques for the generation of the single crystals, such as flux methods or Bridgman method, allows the fabrication of elements such as disc, rings or bars with a reasonable big size. For this reason, in recent years, single crystal materials have been incorporated into high frequency devices. Due to the large k, piezoelectric coefficients and low Q_m and T_c, they are generally found in low power application.

Recently, a new generation of single crystal ceramics, such as PIN-PMN-PT and PMN-PZT, have shown a much higher Q_m and much higher energy densities than the previous compositions. Using the same experience acquired with the PZTs, doped counterparts of the pure piezocrystals, now offer Q_m of nearly 1000 [34–36]. This new line of single crystal

shows tremendous promise for incorporating in ultrasonic transducers and electromechanical actuators for high power ultrasonic applications.

1.5   Piezoelectric ultrasonic transducers

A single element of a piezoelectric material, such as piezoceramic disc, constitutes by itself alone the most basic configuration of an ultrasonic transducer. The electromechanical transduction phenomenon takes place when an electric signal is applied along the polarisation axis of the material driving it in one of its possible modes of vibrations, and vice versa. If during this process the aim is to impose a new state in a medium, the transducer is acting as an actuator. If instead, the medium is the subject to be analysed the transduction phenomenon defines the transducer as a sensor.

Both types of configuration of transducer, actuator and sensor, can be classified in terms of energy and frequency. In general, high frequency ultrasonic transducers are designed for low power applications, meanwhile the most common high power applications are developed at a low ultrasonic frequency. Only high power ultrasonic transducers for application at a low ultrasonic frequency will be discussed in detail. High frequency ultrasonic transducers are out of the scope of this thesis and are not included.

1.5.1   Langevin transducer

In the early stages of the application of ultrasonic technologies, researchers focused their knowledge on the development of underwater signalling. One of the main problems the researchers had to face was the design of low frequency resonators, due to the physical dimensions of the single quartz crystal. Langevin solved the problem by sandwiching a thin quartz crystal between two metal blocks [37, 38], to resonate at a low resonance frequency, hence reducing considerably the dimension of the quartz.

With the development of piezoelectric ceramics such as barium titanate, transducers consisted of simple blocks or cylinders due to the easiness of growing this material in those shapes. However, due to the weakness of the ceramics, those transducers did not prove to be very useful for high power applications. In order to solve this limitation, the sandwich transducer designed by Langevin was modified introducing a pre-stress in the ceramic between the metal blocks. Since a ceramic material has much greater mechanical strength at compression, than at extension, pre-stressing increases the reliability of the transducer. A piezoceramic element under pre-stress, can achieve higher maximum tensile stress before

exceeding its dynamic fatigue limit, therefore allowing the transducer to be driven at high power.

The simplest version of the sandwich transducer consists of a piezoceramic ring sandwiched between two identical metal blocks by means of a compression bolt [39]. The transducer is therefore a resonator of half wavelength restricted to the longitudinal mode of vibration. In Figure 1.8 a schematic of the sandwich transducer is shown.
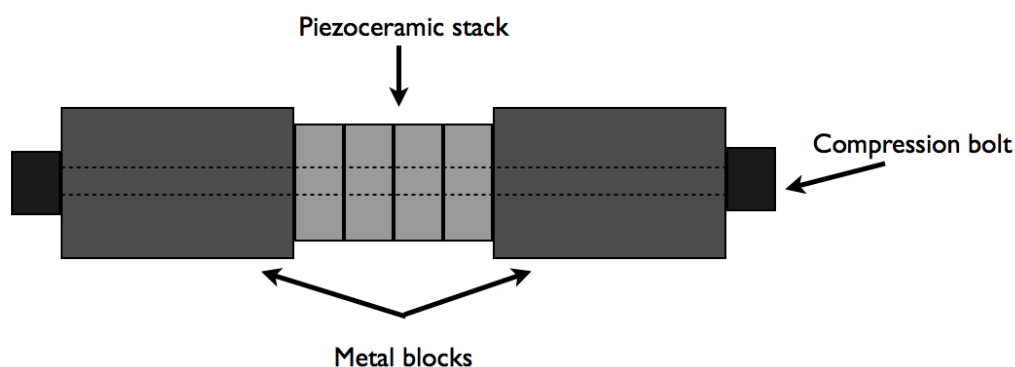
Figure 1.8: Schematic of the sandwich transducer

Generally a stack of ceramics is used instead of a single element, allowing a higher pre-stress, simplified electrical connections and increased output displacement of the transducer. An even number of ceramics is preferred for connection purposes. The ceramics are connected in pairs polarised in opposite directions and separated by an electrode connected to the positive lead, Figure 1.9. In the case of a couple of ceramics, the end-metal blocks are the ground lead and the electrode in between the ceramics the positive lead.
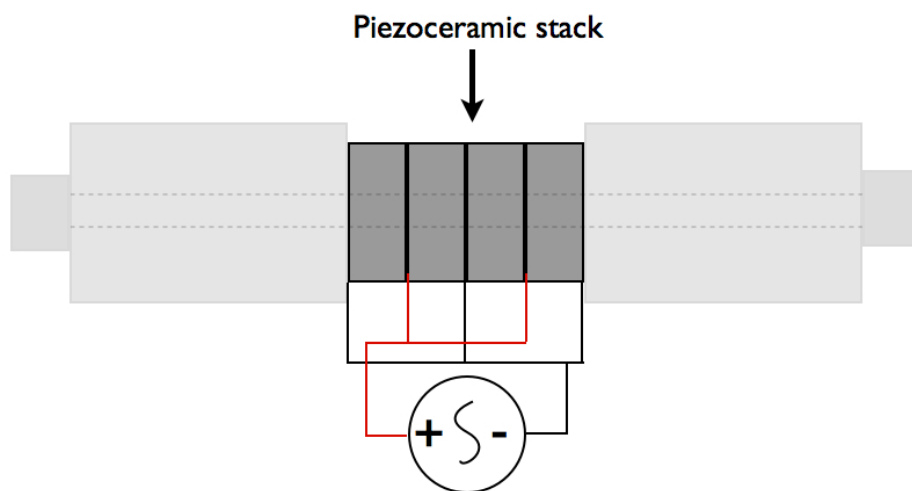
Figure 1.9: Electrical connection of a stack of four piezoceramics in a sandwich transducer

If the basic architecture of a symmetrical pre-stressed sandwich transducer is considered to resonate in the free-free half wavelength longitudinal mode, the nodal plane is situated in the middle of the ceramics, in the positive electrode. Considering the propagation of a plane stress wave through the different materials, and by applying resonant boundary conditions at either end, and velocity and force-continuity at the interface between the ceramic and the metal block, the relationship between the resonant frequency, acoustic impedance between materials and their lengths can be obtained using Equation 1.5.1 [39]:

$$\frac{Z_m}{Z_c} \tan \theta_m \tan \theta_c = 1 \qquad (1.5.1)$$

Z_c and Z_m represent the acoustic impedances of the piezoceramic element and metal blocks respectively, and can be defined as:

$$Z_c = \rho_c \nu_c A_c; Z_m = \rho_m \nu_m A_m; \theta_c = \frac{\omega_c}{\nu_c}; \theta_m = \frac{\omega_m}{\nu_m} \qquad (1.5.2)$$

where ρ, ν and A are the density, longitudinal wave speed and cross-sectional area of the respective material, and ω is the resonance frequency measured in radians. Although this equation is known as the frequency equation it can't be used to obtain the resonance frequency of the transducer, but can be used to obtain an unknown dimension such as cross-sectional area or length of the different elements of the transducer.

The symmetric sandwich transducer has both faces radiating in opposite directions. In practice, most applications require a transducer with a single radiating face. In order to obtain this, the metal blocks are made of metals of different density, and therefore different dimension, increasing the vibration amplitude of the radiating face and minimising energy loss through the back section [40]. In other applications it is necessary to support the transducer with the minimum of damping, which corresponds with the nodal plane. In this case the displacement node is moved away from the ceramic or the electrode between the ceramics to a different position, generally situated in one of the metal blocks [39, 40]. One of the most common designs of the asymmetric sandwich transducer, used as a sound projector, is the Tonpilz transducer [41], Figure 1.10.
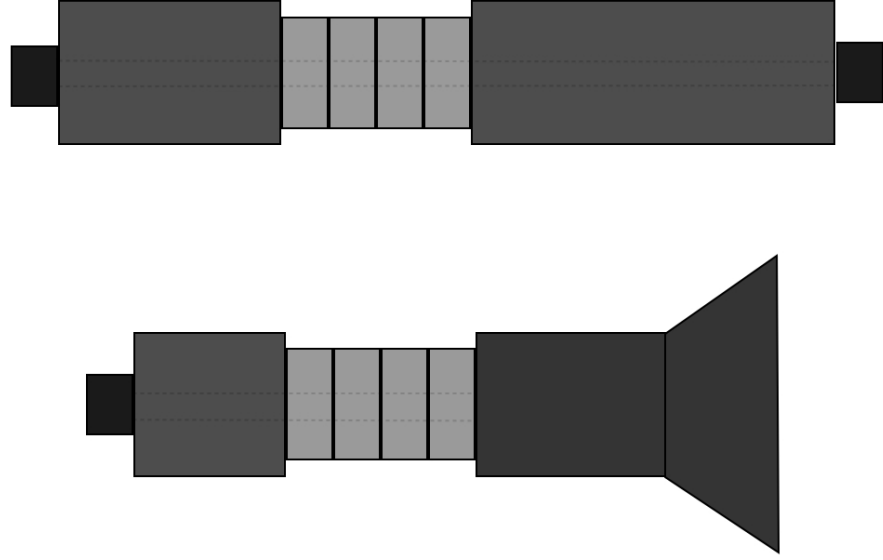
Figure 1.10: Schematic of the asymmetric sandwich (up) and Tonpilz-type transducer (down)

The effect of the mechanical pre-stress on the resonance frequency and the performance of the transducer has been studied for different material combinations by Arnold and Mhlen [42, 43]. They concluded that the minimum value of mechanical pre-stress that must be applied to the ceramic in order to obtain an effective acoustical matching between elements and hence to define a correct resonance frequency must be 30 MPa, for the configurations considered.

Some high power applications require considerably higher displacements at the output end. In this case, sandwich transducers may include mechanical amplifier or horn. In order to resonate at the same resonance frequency as the transducer, the length of these horns must be tailored at $\lambda/2$ or multiples. Depending on the geometry of the horn, generally conical, exponential, catenoidal or stepped, different levels of amplification can be achieved [40, 43, 44] as shown in Figure 1.11.
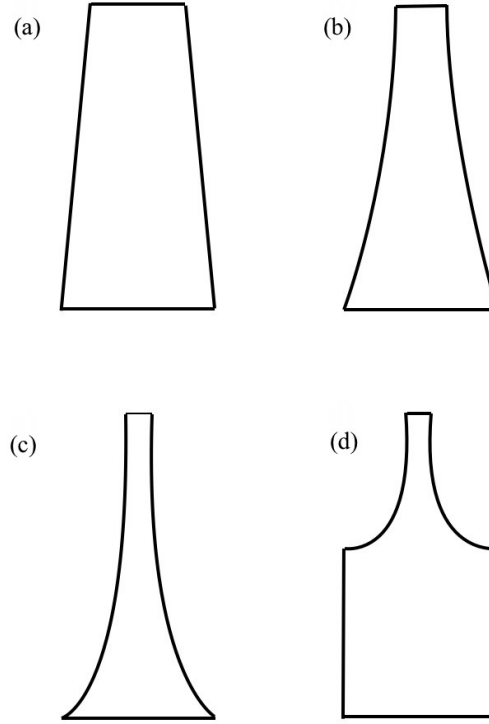
Figure 1.11: Common horn shapes. (a) conical, (b) exponential, (c) catenoidal and (d) stepped

One principal advantages of the sandwich transducer design is the low cost of fabrication. Due to the high capacitance and low impedance, the transducer is suitable from an aspect of low frequency applications. The pre-stress introduced into the ceramics allows the transducer to be driven at higher power levels. Moreover, the tensile bolt used for pre-stressing the ceramics facilitates the coupling of any additional mechanical amplifier or horn to the transducer. [39].

On the other hand, the main problems with this transducer are the limitations in power due to the physical properties of the materials. The exactitude of the dimensions of the different parts of the transducer, tailored to resonate at the desirable resonance frequency, imposes a significant limit on the allowed tolerances. Problems with mechanical loss are due to lack of flatness and smoothness in the contact surfaces of the different parts and loss of displacement when the nodal point is located away from the piezoelectric ceramic elements [45].

1.5.2   Flextensional transducer

The design of low-frequency transducers entails several difficulties related to the size and power requirements of the device. Researchers started to develop very low-frequency transducers initially for underwater sound projectors and receivers (sonar). These transducers work at resonance in order to maximise the power and efficiency, thus their size is inversely proportional to the operating frequency [46]. Applying this scaling to conventional longitudinal transducers, the results lead to intolerable sizes and weights. In Table 1.1, from the scaling study reported by Woollett [47], the relationship between size and resonance frequency is summarised.

f_r(Hz)	Diameter (m)	Length (m)	Weight (kg)	Power (W)	Peak displacement (μm)
500	0.12	0.30	12	113	5.1
100	6	15	1.5×10^6	2.8×10^5	260
10	60	150	1.5×10^9	2.8×10^7	2600

Table 1.1: Scaling study of low-frequency ultrasonic transducers

Other problems related with low-frequency transducers, in this case focused on sound projectors, are the displacement and power requirements, which are intrinsically connected. At a very low frequency the diameter of the radiating face of the transducer is in most cases smaller than the acoustic wavelength. This represents a small value of the radiation impedance [46], therefore in order to compensate it, high electrical and mechanical driving levels are required.

The large size of these devices, which is a direct consequence of the high stiffness of the piezoelectric ceramic stack, can be significantly reduced by utilising materials with higher compliance such as Terfenol-D, which has a lower Young's modulus than piezoelectric ceramics and possesses large magnetostrictive properties. However, a more effective solution is to employ a different transduction mechanism. Instead of using the longitudinal mode of vibration of the transducer, a higher compliance can be obtained by using flexural modes of vibration with a considerable reduction in the size of the whole device.

The flexural transduction mechanism is the basis of flextensional transducers. This transducer is a coupled system, in general consisting of a piezoelectric ceramic or stack and a mechanical shell coupled at the boundaries of the ceramic or stack. The device operates generally at the first mechanical resonance frequency, which corresponds to the first flexural

mode of the shell. The piezoelectric ceramic produces a high impedance small extensional motion that is transmitted to the mechanical shell, which is transformed into a low impedance large flexural motion and delivered to the medium. In general, the shell flexes and the ceramic or stack extends, the combination of both motions giving rise to the name of this type of transducer as flextensional.

The shape of the shells is designed to allow them to flex easily. This characteristic reduces the resonance frequency of the transducer and enhances the output displacement. Due to the small motion of the driver, it is necessary to employ a reasonably large volume of ceramic stack in relation to the mechanical shell. As explained previously, piezoceramic materials need to be under stress in order to prevent failure when high drive conditions are required. In the case of the flextensional transducer, the piezoceramic stack is embedded in the mechanical shell which provides the necessary pre-stress.

The first flextensional transducer was developed and constructed by Hayes in 1929 at the Anacostia Naval Research Laboratories (NRL). This transducer was designed to work as sound projector replacing the much larger pneumatical foghorns at that time placed on lightships [48]. Hayes describes the advantages and drawbacks of the 'bow' type transducer, that corresponds with the mechanism of a flextensional transducer, in the 1936 patent 'Sound generating and directing apparatus' [49]. In Figure 1.12 the different drawings that Hayes realised to describe his transducer are shown.
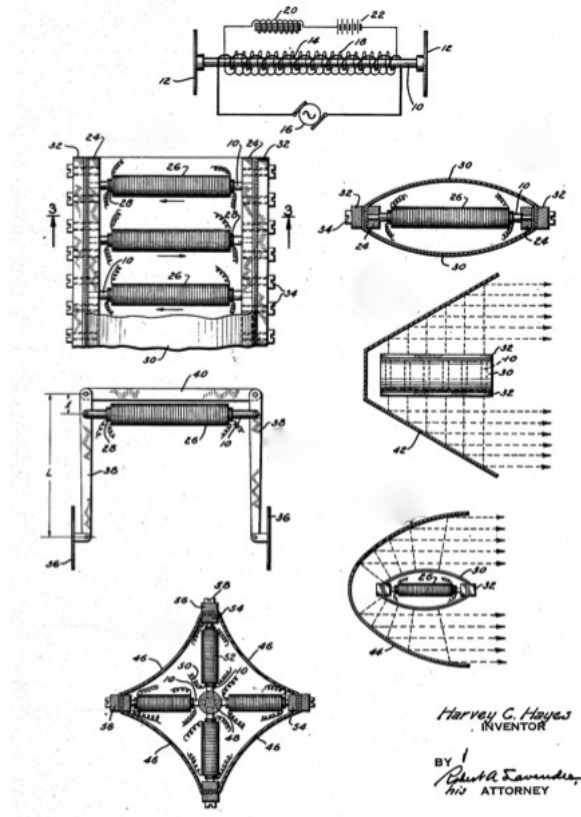
Figure 1.12: Hayes's bow type transducer. Reproduced from the patent [48]

Although Hayes's transducer showed promise for low frequency radiators, due the lack of funding the research was stopped. There were no more advances in this field until the mid 1950s with the work of Toulis.

Many authors attributed to Toulis the discovery of the flextensional transducer because there was no notice about Hayes work, for that reason, it is assumed that Toulis, who didn't mention Hayes's device, reinvented the flextensional transducer.

Toulis was investigating compliant tubes for sonar when he developed the flextensional transducer [48]. This work generated two patents in 1966 [50, 51], one where the author described the transducer and the mechanism and the other where a system to compensate for the external pressure, to which the transducers are subjected when they are submerged in water, is introduced. The Toulis's transducer is shown in Figure 1.13.
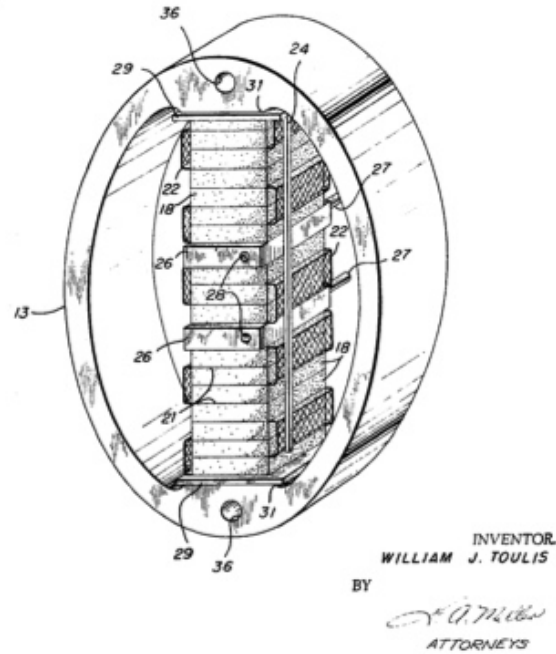
Figure 1.13: Toulis's flexural-extensional electromechanical transducer. Extracted from [48]

The design described by Toulis is very similar to that developed by Hayes. The main differences are that Toulis's transducer is designed for underwater applications whereas Haye's device operates as air resonator. Another important difference is that Toulis introduced a pre-stress into the ceramic stack. This pre-stress is applied to the piezoelectric material by the mechanical shell, with a specific shape to enhance it. This solves one of the main drawbacks pointed out by Hayes with respect to his flextensional transducer.

The potential shown by flextensional transducers, has led many other researchers to investigate this technology. Merchant [48] developed a transducer where the main difference with Toulis's design was the geometry of the shell, which was concave instead of the convex design developed by Toulis. Due to the proliferation of different types of flextensional transducer authors, for example Royster [52] classified the transducers into 5 different classes, class I to class V.

The class I flextensional transducer usually consists of a piezoelectric stack and a surrounding mechanical shell with a quasi-cylindrical shape. The shell is coupled to the piezoceramic stack through two end plates. Excitation of the stack results in extensional motion of the end plates in the axial direction, which is transformed into radial motion via

flexure of the surrounding shell. One successful transducer was developed at the University of Miami and is known as the University of Miami flextensional, in Figure 1.14.
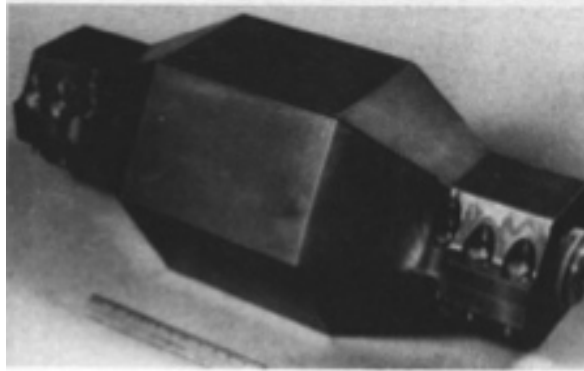
Figure 1.14: Class I flextensional transducer, the University of Miami transducer. Extracted from [48]

The class II and class III flextensional transducer, following the Royster's classification, are variations of the class I, Figure 1.15. The class II presents longer cylindrical end sections, which allow for increase of the volume of the piezoelectric stack placed in the shell. This represents a transducer able to generate higher power at higher frequencies.
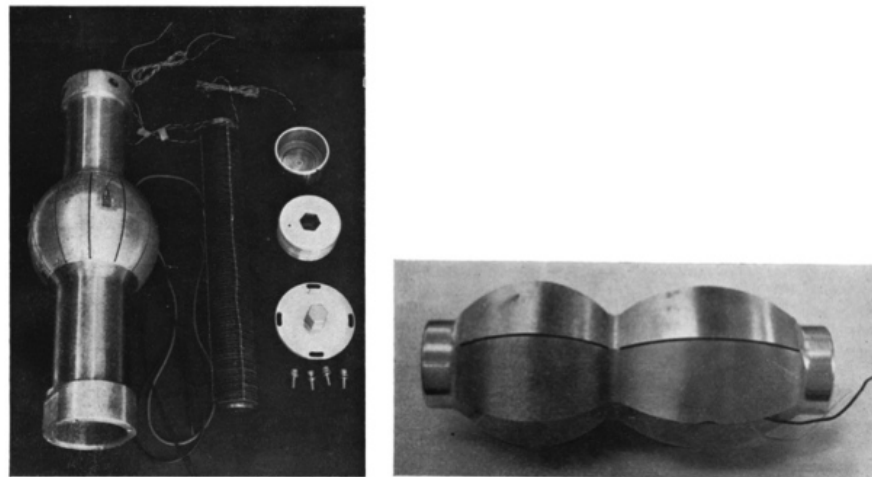
Figure 1.15: Class II flextensional transducer (left) and Class III flextensional transducer (right). Extracted from [48]

The second variation, called class III, defines a transducer with a double elliptical section of different sizes. The two curved sections forms a double resonant system, increasing the bandwidth of the transducer by having two close resonant modes. These three classes are also known as barrel-stave flextensional transducers and are generally designed for sonar

applications [53].

The class IV flextensional transducer consists of a shell in the form of an elliptical cylinder, inside which the driver is fitted along the major axis. The driver is, in most cases, a piezoelectric ceramic stack. This transducer has the same internal mechanism as those developed by Hayes and Toulis.

Although before World War II Pallas [48] had investigated a type of transducer that uses the flexural movement of a membrane between an electrostrictive ring, the first class V flextensional transducer, was attributed to Abbott and was patented in 1955 [54]. This device consisted of a thin magnetostrictive or piezoelectric ring polarised in the radial direction to each face of which is bonded a shallow convex, or concave, membrane. The ring is driven radially, transforming the motion to a much larger axial movement due to the action of the membranes. In the same work, Abbott also described a method for pressure compensation, to prevent the collapse of the transducer under water pressure, by injecting a compressed gas into the transducer. Figure 1.16 shows the class V flextensional transducer designed by Abbott. Since Abbott's work, many different versions of this class have been studied.
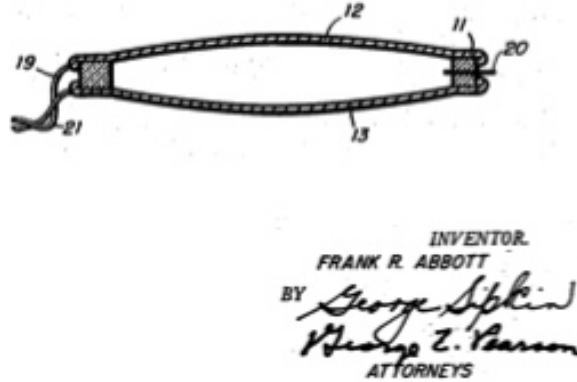
Figure 1.16: Abbott's class V flextensional transducer. Extracted from [54].

The miniaturised class V moonie and cymbal transducers

In the late 1980s, in the Materials Research Laboratory at the Pennsylvania State University, a miniaturised class V flextensional transducer was developed for underwater applications, generally as a hydrophone. The transducer is composed of a piezoelectric ceramic disc poled in the thickness direction sandwiched between two metal plates with a shallow cavity (end-caps), with the shape of a half moon, thus giving rise to the name 'moonie' [55, 56].

The aim of this study was to try to solve the problem of competing between the d_{31} and d_{33} coefficients in the active material, that represent the radial and axial coefficients

respectively. For a single piezoceramic disc these parameters possess opposite sign, therefore the hydrostatic piezoelectric coefficient d_h, 1.5.3, that can be defined as the hydrostatic strain per unit electric field, is obtained by the subtraction of both, so the resulting d_h values are low. The presence of the cavities in the moonie allows the metal end-caps to serve as a mechanical transformer for transforming and amplifying a portion of the incident axial stress into radial stresses of opposite sign. Thus, the d_{31} and d_{33} contributions of the PZT now add together (rather than subtracting) in the effective d_h value of the device [56]. The moonie transducer is shown in Figure 1.17.

$$d_h = d_{33} + 2d_{31} \tag{1.5.3}$$
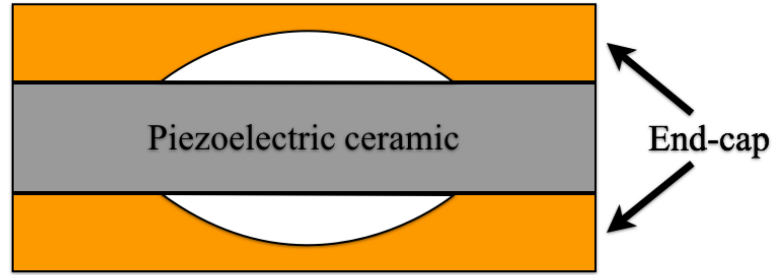
Figure 1.17: Moonie transducer

Generally the average size of the moonie transducer is around 11-12 mm diameter and 3 - 5 mm thickness. If compared with the sizes of other types of flextensional transducer that can possess several meters in length with weights that can reach several kilograms, this miniaturised transducer shows an omnidirectional sound radiating pattern in the low ultrasonic frequency, due to the wavelength being much larger than the size of the transducer. This miniaturised transducer represents a new generation of devices with large generative forces and amplitudes, inexpensive for mass production due to its simple design and has a good profile for assembly in arrays.

One of the main drawbacks of this transducer was the high concentration of stress in the metal plates, just above the edge of the ceramic to metal bonding layer near the edge of the cavity, due to the flexural movement [56–58]. This stress concentration reduces the displacement that can be generated by the transducer, and hence the sensitivity of the transducer when working as a receiver or sensor.

The first attempt to solve this problem involved introducing a ring-shaped groove on the exterior surface of the end-caps in the area of maximal stress. The aim was not to eliminate the stress completely but to concentrate it in a small area [58, 59]. The small groove on the surface of the end-cap enhances the displacement of the transducer, since the metal cap in the area of the slot has a higher compliance. The use of finite element analysis to study the stress distribution in the moonie, led to the design of a new shape of end-cap with a cymbal shape [58]. The new transducer is known as the 'cymbal' transducer [60]. The three configurations of the moonie end-cap, the grooved moonie end-cap, and the cymbal end-cap are shown in Figure 1.18.
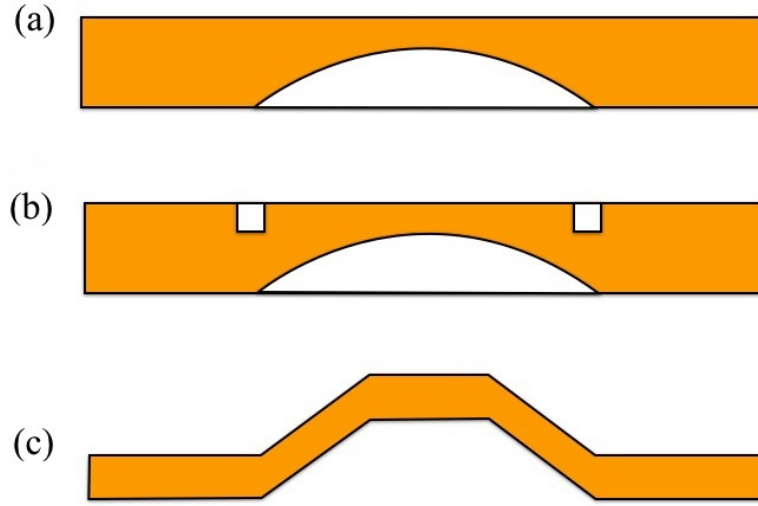
Figure 1.18: (a) Moonie end-cap, (b) grooved moonie end-cap and (c) cymbal end-cap

The cymbal end-cap is the result of removing part of the metal of the moonie end-cap in the area of the maximal stress concentration, and is defined by a truncated cone cavity. The result is an end-cap with uniform thickness. This new end-cap with a higher compliance exhibits a considerably higher displacement [58, 60], approximately double that of its predecessor. Despite the mechanical transduction of the moonie's end-cap, that exhibits a flexural movement, the cymbal's end-cap transforms the radial motion of the ceramic into a flexural and rotational motion. The cymbal transducer displacement motion is shown in Figure 1.19.
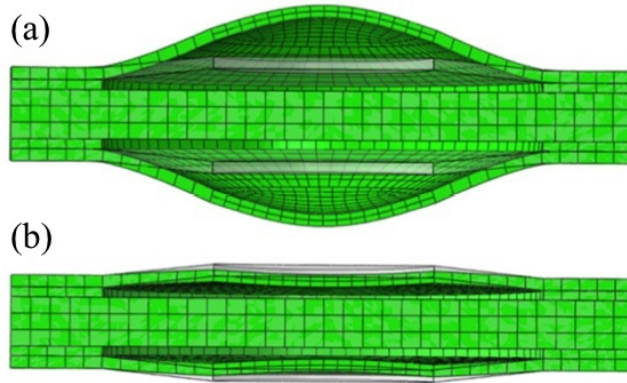
Figure 1.19: Schematic of the cymbal transducer showing (a) expansion and (b) contraction motion half-cycles of the end-caps

In the moonie transducer, the displacement is highly dependent on the position from the centre of the end-cap, being maximum at the centre of the device. Due to the regular geometry of the cymbal end-cap, the displacement remains uniform along the top surface, Figure 1.20. This characteristic increases the amount of generative force of the transducer since the active surface areas are enlarged.
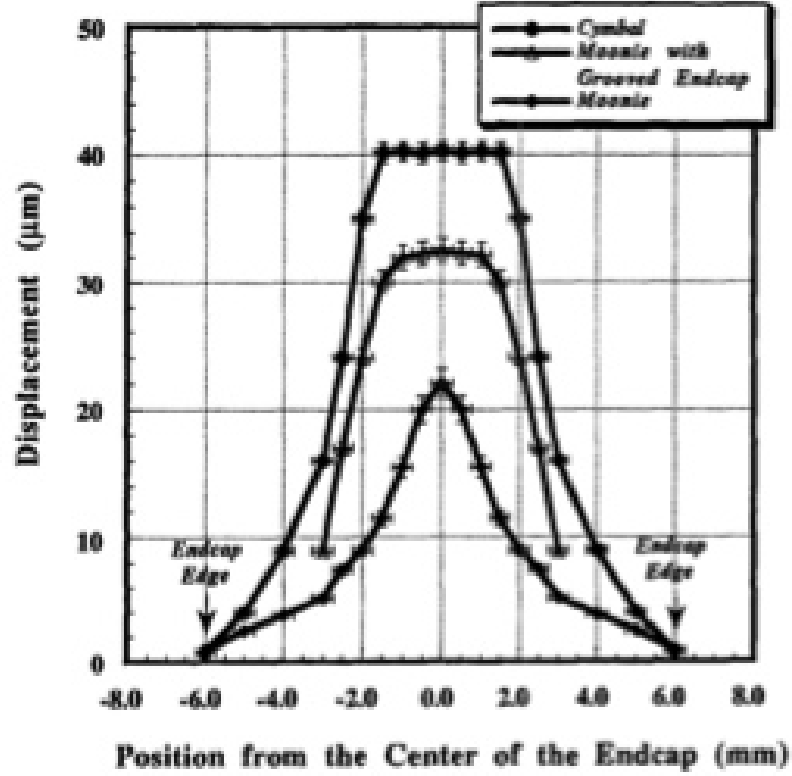
Figure 1.20: Comparison of the displacement dependence on the position on the end-cap of the moonie, grooved moonie and cymbal transducers. Extracted from [58]

The development of the cymbal transducer also introduced an improvement in the end-cap fabrication. A die tool was designed that performs a precision cut and punch of a metal sheet, defining the truncated conical shape of the cavity [58, 60]. The end-caps are then bonded to the piezoelectric ceramic using an epoxy layer. The electrodes are connected directly to the flange of the metal end-cap.

The cymbal transducer design exhibits high piezoelectric coefficients, high vibrational displacement and acceleration sensitivity at low ultrasonic frequencies, ease of tailoring the desired properties by the choice of the cap and driver materials and geometries [61], and cost effective manufacturing. This transducer is therefore a potential device for using as a sensor or actuator such as hydrophone, accelerometer, motor and sound projector.

1.6   Power ultrasonics in medical applications

Ultrasonic techniques are currently well-established in medicine, in surgery, therapy and diagnosis. It is possible to divide the ultrasonics in medical applications in two main

groups, low power diagnostic ultrasound and high power therapeutic ultrasound. Diagnostic ultrasound encompasses all the procedures where the aim is to obtain the required diagnostic information without causing biologically significant cellular effects. Commonly known as sonography or ultrasonography, diagnostic ultrasound consists of acoustic visualisation systems focused on the extraction of images of the interior of the human body. In contrast, therapeutic applications require that the exposed target tissue undergoes reversible or irreversible change, depending on the goal of the treatment. This group also includes all surgical applications.

In diagnostic applications the signal emitted by the transducer is enhanced to obtain images with good spatial and temporal resolution in order to delineate all the interfaces between media. Due to the low intensities of ultrasound employed, a good compromise between the type of signal, match of impedances, and power is necessary to give an acceptable signal to noise ratio.

Therapeutic ultrasound which corresponds with higher power applications, can be further divided into low power therapy applications such as sonophoresis, thrombolysis, sonoporation, gene therapy and bone healing, and high power therapy applications encompassing treatment procedures for cancer and kidney stones, dental hygiene and surgical procedures such as cataract removal, hard and soft tissue dissection. In the following sections, the ultrasound techniques related to these therapeutic medical procedures, are briefly described.

1.6.1   Low power therapeutic procedures

These procedures utilise the ultrasonic waves generally for two main purposes, enhancing or accelerating biological processes and to modify the mechanical structure of the tissue in which it is applied. The effects of exposure to low power therapy ultrasound are in general reversible and disappear when the ultrasound beam is removed.

Bone healing

Bone healing after a fracture or trauma involves the spatial and temporal action of many different cell types, proteins and genes, working towards the total restoration of the mechanical strength and correct function of the affected area. The treatment, with an ultrasonic beam, of the damaged area reduces considerably the time of the healing process. The exact biological effect of the ultrasound in the healing process remains unclear, however it is possible to classify the interaction with the bone at two different levels, molecular level

and mechanical level.

It has been found that low intensity ultrasound enhances the processes involved in endochodral osteogenesis, that is the generation of bone from cartilage, that represents the main process in bone healing. Ultrasonic mechanical waves alter the physiology of the osteoblasts stimulating the assimilation of calcium ions and potassium into the cells as well as numerous genes that accelerate and ultimately augment the processes of callus formation [62, 63]. At a mechanical level, the acoustic pressure waves promote fluid micro-streaming in the radiation area, therefore enhancing the transport of nutrients to the cells. Moreover the ultrasonic energy dissipates in the cells, transformed into small temperature fluctuations, facilitating some enzymatic processes such as the production of collagenase, which assists in destroying extracellular structures.

During the treatment the ultrasound beam can be applied using two different techniques, trans-cutaneous application or trans-osseous application. In trans-cutaneous application, the ultrasound transducer is coupled directly to the skin under which the bone fracture is located, whereas in trans-osseous application, small transducers are implanted surgically on the surface of the bone. In general, treatments consist of periodic sessions of a duration of ten minutes with an ultrasound beam of around 30mW/cm^2 of intensity at typical operating frequencies in the range from 0.2 MHz to 2.5 MHz.

Different studies during the last decade have shown a reduction of between 30 and 50% of the healing time in patients treated with ultrasound, compared with processes where no ultrasound treatment is employed. Between the two different techniques, the trans-osseous application presents the best results due to the better acoustic coupling between the transducer and the bone [63, 64].

Ultrasound therapy for bone healing is also being applied in dentistry as a method to repair and re-grow teeth. The mechanical waves increase the formation and growth of the tooth by reparation of the root and stimulation of the generation of reparative cementum [65, 66].

Drug delivery

The application of ultrasound in the penetration of pharmacologically active drugs, proteins and genes through different biological tissues, has been an important area of study in the last two decades. Although there are many applications of ultrasonics in drug delivery, it is possible to group the different procedures into two main groups: sonophoresis, that consists of the use of a low frequency ultrasonic wave that temporary permeabilises the skin in order to

deliver drugs into soft tissues; and sonoporation which refers to the utilisation of ultrasound to deliver the drug directly into the cells [67].

The physical mechanism of the relationship between the permeability of tissue and ultrasound is not well understood. Although it is assumed that the main phenomenon responsible is cavitation, other mechanisms such as thermal and mechanical effects also contribute to the transportation and delivery of the drug [67–69].

Due to the pressure oscillations generated by ultrasonic waves in the medium, micro-bubbles can be produced during the rarefactions that expand and contract at the same frequency as the applied ultrasound. When the tension on the wall of a bubble reaches its tensile strength it collapses violently, generating high temperatures and high-energy microjets. It has been observed that when the bubble is near a surface the microjet is directed towards the surface, in the case of biological tissue. This increases significantly the tissue permeability [70].

In order to enhance the local absorption, drugs can be incorporated into bubbles, for example encapsulated within the bubble, to target a specific site of disease when they enter an insonated field [67, 68, 70].

For different types of drugs the operational frequencies and intensities are different depending of the procedure. Generally the range of frequencies is between 20 kHz and 3 MHz and intensities from 0.5 to 3.0 W/cm^2 [68, 70].

There are several procedures where ultrasonic drug delivery is employed, such as treatment of cancer, gene therapy, and sonothrombolysis that consists of the dissolution of blood clots either utilising the cavitation effect or in combination with microbubble contrast agents and fibrinolytic drugs, and drug delivery in delicate areas such as the brain and the eyes.

1.6.2   High power therapy procedures

The effect of high power ultrasonic waves in therapy applications causes irreversible changes in the physical and biological nature of the tissue. The majority of the techniques are related to surgical procedures.

High intensity focused ultrasound (HIFU)

High intensity focused ultrasound (HIFU) encompasses a series of surgical procedures where a high intensity ultrasound beam is focused in a specific area in order to destroy the tissue. The principal physical mechanism involved in the process is the ablation of tissue by coagulative

necrosis due to thermal absorption. Coagulative necrosis can be explained as a lack of oxygen and nutrients due to a dramatic rise in temperature, above approximately 60°, leading to cell death. Another effect that must be considered is cavitation, although its effect can be negligible when the frequency is above 1 MHz.

In order to generate a focused beam, transducers can be designed with a concave single element or an array of piezoelectric elements configured in a concave shape. The high intensity ultrasound is hence concentrated in a region of approximately a few cubic millimetres. The intensity at the focus varies depending on the procedure but is in the range of 10^3 - 10^4 W/cm^2. The range of operating frequencies is approximately between 0.5 and 10 MHz, although the vast majority of procedures are performed at 1.5 MHz. In order to ensure correct energy absorption in the area to be treated, the irradiating time can be up to 30s, leading to instantaneous cell death and coagulative necrosis, with a margin of a few cells between live and dead cells at the edge of the focal zone [67, 71–73].

Due to the irregularities of different tissues and the precision required to maintain the correct position of the focal point, HIFU procedures are usually combined with medical non-invasive imaging techniques to guide the ultrasound, such as magnetic resonance imaging (MRI), known as 'Magnetic resonance-guided focused ultrasound' (MRgFUS) or ultrasound imaging [71, 72].

Since the first applications in neurosurgery procedures, HIFU has been applied in numerous medical processes, such us the treatment of different types of cancer, located in the prostate, liver and breast, as well as for treatment of haemostatasis and vascular occlusion, where the ultrasonic beam seals blood vessels and interrupts flow in vessels [67, 71–73].

Cataract removal

Early evidence of cataract surgery can be found in Ancient Rome in the 1st century AD. These procedures tried to eliminate, by means of a needle, the substance inside the eye that disrupts vision. Although it has been studied throughout the centuries, it was in the 18th century when intracapsular cataract extraction, and afterwards extracapsular cataract extraction were developed. These manual techniques consist of creating a large incision in the eye to remove the damaged lens, and the capsule in the case of intracapsular extraction or the prolapsing of the lens, leaving the capsule intact in the case of extracapsular extraction and replacement [74].

The use of ultrasound in cataract surgery received the name of phacoemulsification,

generally consisting of an ultrasonic transducer with a needle that can vibrate in a longitudinal or torsional mode at a frequency around 40 kHz. Through a small incision in the cornea of 1.5 to 3mm, the vibrating needle fragments and emulsifies the lens nucleus and cortex. The emulsified lens is then aspirated from the capsule where a prosthetic inatraocular lens is placed once the cavity is empty [74–76].

The small size of the incision in the case of phacoemulsification reduces the risk of such postoperative complications as astigmatism and traumatic wound rupture [74]. Despite the advantages, it is necessary to control cavitation and high temperature in order to prevent damage. To minimise these problems, recent studies in the development of transducers for cataract surgery have demonstrated that devices that exhibit a torsional mode generate a lower operational temperature than those with a longitudinal mode of vibration [77]. Also, modifying the irrigation solution by saturation with CO_2 may reduce or even eliminate acoustic cavitation [78].

Oral prophylaxis

Plaque and calculus removal was one of the first and most studied applications of ultrasound in dentistry. Bacterial deposits on teeth, that constitute plaque, produce acids that desmineralise the tooth leading, in the worst case, to periodontal disease such as gingivitis or tooth loss. Consequently, an exhaustive dental hygiene and periodic plaque control is highly recommended to maintain good oral health.

Mechanical methods have been demonstrated to be the most effective procedures in dental plaque removal, commonly known as scaling. Traditionally dentists have utilised manual scalers to remove plaque from teeth, but the incorporation of ultrasound transducers in dentistry in 1950s, saw a new line of scaling devices that exhibit better performance. Studies demonstrated that the utilisation of ultrasonic scalers, where the tip of the tool in contact with the tooth vibrates at high velocity, reduces the average time necessary for the dentist to remove the plaque and reduces discomfort of the patient during the process [79–81].

In parallel to the development of ultrasonic scalers, researchers investigated a variation of the vibrating tool known as the sonic scaler. The main difference between these devices was the transducer and the operational frequency. In sonic scalers a turbine unit moves the vibrating tip at a lower frequency, between 3 and 8 kHz, whereas in ultrasonic scalers a piezoelectric stack transducer delivers the mechanical movement to the tip motion at a frequency between 25 and 45 kHz [82]. In Figure 1.21 an ultrasonic tip performing a scaling

procedure is shown.

Figure 1.21: Scaling procedure. Courtesy of Mectron S.p.A

In ultrasonic scalers three mechanical processes intervene in the removal of the plaque. The main process is due to the mechanical amplitude of the tip at high frequency, in a range from 10 to 100 μm, that breaks and removes the dental plaque. The amplitude of the tip depends on the input power but also on the shape and material of the tip [82, 83]. Due to the utilisation of a cooling system to reduce the internal rise of temperature in the transducer and the consequent irrigation on the vibrating tip, the effects of cavitation and micro-streaming enhance considerably the effectiveness of the device, improving the cleaning process [80–82, 84].

Soft and hard tissue dissection

Ultrasonic surgical devices for biological tissue cutting, ablation or fragmentation represent a division of surgical tools operating at high-power and low operational ultrasonic frequency, from 20 to 60 kHz. Generally, these devices are designed to generate a high longitudinal vibration in which the action of the ultrasonic tip cuts or shatters hard tissue and cuts, emulsifies and cauterises soft tissue [85]. The transduction mechanism is common for all the applications, however the design of the tip and the operational frequency and power tailors the device for a specific application.

The application of ultrasonic cutting in soft tissue procedures has resulted in a significant improvement in laparoscopic surgery over other technologies, such us laser surgery or electrosurgery. In electrosurgery, dissection or ablation is achieved by the action of a high frequency electric current applied to tissue, meanwhile in laser surgery the process is realised by application of a high intensity electromagnetic beam focused on the area to be treated.

Both methods present important drawbacks that are necessary to be considered. Due to the utilisation of an electric current and a high intensity laser there exists the possibility of putting the safety of either the patient or the surgeon in danger, and there is a risk of damaging surrounding tissues. Also, smoke generated during the process limits the surgeon's vision of the operation site [86, 87].

The physics of the ultrasonic cutting process for soft tissue involves two different mechanisms. The main mechanism is the cutting action of the sharp blade, which exhibits high vibration displacement, generally up to 100 μm, at frequencies in the region of 50 kHz. The second is fragmentation by cavitation. Fragmentation is strictly related to the fluid (water or fat) content of the tissue: the higher the water content, the easier the fragmentation. Cavitation induces vaporisation of the fluid in tissue leading to its fragmentation. The principal advantages of ultrasonic laparoscopic procedures are that during the cutting process the dissected tissue is immediately cauterised thus preventing blood leaks, and the high precision achieved in the cut plus the absence of smoke during the process [86–88]. In Figure 1.22 it is possible to observe a typical ultrasonic laparoscopic procedure.

Figure 1.22: Ultrasonic laparoscopic soft tissue dissection. Courtesy of Ethicon

Ultrasonic laparoscopic devices have different tips depending on the specific task to be performed. Sharp blades, hooks and shears attached to the ultrasonic transducer facilitate correct access and manipulation of the area to be treated by the surgeon. Control of temperature in the zone of the cut is achieved by minimising the time of the cutting process and the utilisation of a coolant, in order to prevent damage to nearby tissue by necrosis [86, 88–91].

Dissection of bone, known as osteotomy, constitutes one of the most delicate surgical techniques in maxillofacial surgery because the bones are surrounded by delicate tissue, such as vestibular and lingual/palatal soft tissues that provide bone vascularisation. However,

bone is a hard tissue that requires aggressive methods to perform a cut, and traditional devices are saws and drills. The principal problem of these types of tool is the excessively high temperature due to friction that results in osteonecrosis and tissue necrosis that impairs bone regeneration [92, 93].

The first commercial ultrasonic cutting device designed for osteotomy, the Piezosurgery® device, was developed in 2001 by the Italian company Mectron S.p.A under the supervision of the maxillofacial surgeon, Vercellotti [94]. The device consists of a piezoelectric stack transducer, which operates in a longitudinal mode of vibration, connected to one of a variety of different cutting inserts. The final shape of the cutting tip allows for either a longitudinal or a combination of longitudinal-flexural vibration motion. These inserts are designed to perform different procedures ensuring a correct access to the surgical site. In Figure1.23 it is possible to observe a vibrating tip which operates in a longitudinal-flexural vibration mode. The surgical procedures adopting this device range from oral surgeries to maxillofacial operations such as orthognathic surgeries [94].

Figure 1.23: Cutting blade with a longitudinal-flexural vibration. Courtesy of Mectron S.p.A

The Piezosurgery® device operates in a frequency range of 24 to 36 kHz with micrometric vibration displacement of the cutting tip between 60 to 210 μm [92, 94, 95]. The operating frequency can in some cases also incorporate a low frequency modulation (30 Hz or less) to prevent overheating and bone compaction [96]. The device incorporates a cooling system that is delivered directly to the tip of the cutting insert. The cavitation produced maintains the operating site clean of blood and debris [93, 95–97].

The low operational ultrasonic frequency allows Piezosurgery® to perform a selective cut only in mineralised tissue. Neurovascular tissue and other soft tissue would only be cut by

a frequency above 50 kHz, therefore the risk of damage to delicate tissue is considerably
reduced [98]. In comparison with traditional cutting methods, the micrometric vibrations of
the Piezosurgery® provide an extremely high precision during the cutting process, reducing
the total amount of blood loss. In Figure 1.24 an ultrasonic dental osteotomy performed
using the Piezosurgery® is shown. The low heat generation, improved by the utilisation of
the coolant, minimises tissue damage by necrosis near the cutting area, therefore reducing
the time of total recovery [96, 97].
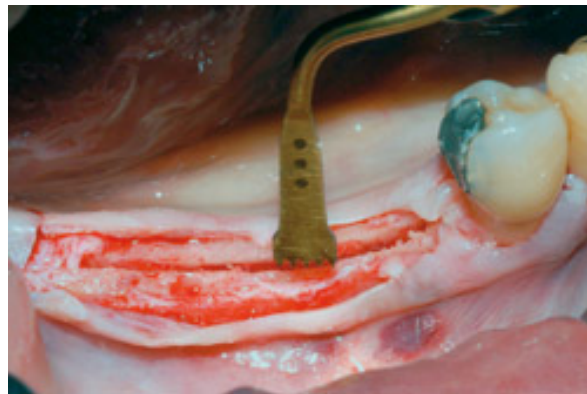
Figure 1.24: Ultrasonic dental osteotomy. Courtesy of Mectron S.p.A

1.6.3 Cymbal transducers in medical applications

Flextensional transducers, such as the cymbal transducer, have been used mostly in ultrasonic
underwater applications either as hydrophones or sound projectors. The low volume of the
cymbal transducer and its inexpensive cost of manufacture facilitate the design of arrays,
increasing the efficiency and the spatial ultrasound field generated. These features have
attracted great interest in ultrasound mediated transdermal drug delivery applications.

As was mentioned previously, in sonophoresis a low intensity beam of low frequency
ultrasound is generated to perform transdermal delivery of drugs. Although there are several
possible low frequency transducer designs that can be used in a drug delivery application,
such as Tonpilz low frequency longitudinal resonant transducers, many researchers have
investigated developing portable small-size transducers so that the patient can wear them
during the process [99]. Cymbal arrays are therefore excellent candidates for this type
of treatment, as they can be efficient, light (less than 50g), and low-profile in the desired
frequency band with similar spatial intensities as stack transducers [100].

Different studies realised in rabbits, pigs and rats, have demonstrated the feasibility of
this type of transducer array for delivering insulin [101–103]. Despite the small dimensions of

each cymbal, with diameters around 12.7 mm, the size of the array does not have significant effect on the reduction of blood glucose after the procedure [102], therefore small arrays of 2 x 2 elements can perform a correct insulin delivery.

1.7 Scope of the work

The aim of this work is to design a novel ultrasonic cutting device for orthopaedic surgical procedures based on the flextensional class V cymbal transducer. The reference device is the commercial Piezosurgery®, developed by the Italian company Mectron S.p.A, based on a pre-stressed Langevin transducer. This allows the research to focus on novel devices with comparable or improved performance from an existing, commercially successful, ultrasonic bone cutting device.

A combination of numerical analysis (finite element analysis) and experimental methods are used to characterise the vibration response of the cymbal transducer under different operational conditions. In a second stage, a modification is introduced in the design of the cymbal transducer to optimise its response for high power ultrasonic applications.

Finally a new design, developed and optimised using finite element analysis is investigated. This device is designed to support different types of vibrating inserts in order to perform a wide range of surgical procedures. The experimental characterisation of the device is complemented with a series of cutting trials, that include dissection of real bones in collaboration with the Department of Orthopaedic Surgery of the University of Edinburgh.

Chapter 2

Literature survey

2.1 Historical review of ultrasound

The history of ultrasound cannot be understood without the historical knowledge of acoustic. The origins of acoustics as a branch of physics, as nowadays is known, are intrinsically related with the study of music. Since the ancient Greece, musical sounds and music theory have traditionally been associated with arithmetic, geometry and astronomy. The first documented studies can be traced back to the 6th century BC in the figure of Pythagoras of Samos. These documents describe how Pythagoras was investigating the generation of arithmetical ratios to characterise the musical intervals, mainly in strings of different length, thickness and tension. From these experiences it also was observed the relationship between the pitch (or frequency) of the sound and the geometry and physical properties of the string [104].

Few centuries later, around 350 BC, Aristotle postulated that a sound wave resonates in air through the motion of the air, the movement of a part of the air moves its neighbours, although this was a philosphy-based hypothesis more than one of experimental physics. This hypothesis introduced one of the basic concept of acoustic; the sound needs a medium to be transmitted [105]. The first scientific observation of this concept was realised in 1490 by Leonardo da Vinci who wrote: *If you cause your ship to stop, and place the head of a long tube in the water and place the outer extremity to your ear, you will hear ships at a great distance from you* [106]. This is considered for many researchers as the beginning of underwater acoustics, since the methodology utilised by Leonardo described the basic principle of the passive sonar.

The studies of Galileo Galilei in Italy and Marin Mersenne in France, during the 16th and 17th centuries, continued the work of Pythagoras and developed the laws of vibrating

string and bodies that generate the sound waves. These works were complete by Newton who established a mathematical and physical analysis of the sound waves in a compressible medium [104].

Until the end of the 18th century, the concept of acoustics was intrinsically related to mechanical waves with a frequency within the limits of the human hearing. The first studies that proposed the existence of sounds out of the human range started with the work of Lazzaro Spallanzani in 1794. He tried to understand the ability of bats to avoid all kind of obstacles when flying in the dark. The conclusions of these first experiences lead to Spallanzani to postulate that bats possessed a 'sixth sense' . However in 1798, after other experiences realised by the Swiss zoologist L. Jurine, both researchers assumed that was the ear the sense that bats utilised to navigate in the dark [107, 108]. Although their hypothesis, rejected by their contemporary, were based in the idea of the utilisation of sound to locate obstacles, they could not explain which range of frequencies were used by bats. It was not until 1938 when Pierce and Griffin found that bats emit a high frequency sound. In posterior works they discovered that bats use sound and echoes of ultrasonic pulses to locate objects, that was defined as echolocation.

During the 19th century, when the relation between pitch and frequency was clearly demonstrated, many researches tried to delimit the hearing threshold of human as well as of animals. Despretz in 1845 set at 30 kHz the limit of audibility for humans, while Helmholtz set the limit at 38 kHz [107, 108]. Although they used devices able to generate sound at high frequencies, the appearance during the trials of sub-harmonics within the audible range (up to 20 kHz in average), distorted the results due to the limitations of the devices employed.

The proliferation of this type of research, led to the development of devices and apparatus focused on the generation of ultrasonic sound waves. Although in 1830 Savart designed a toothed wheel to produce sounds with a range of frequencies up to 24kHz, the most common devices, used during 1800s, were high frequency whistles. Developed from bird call whistles, they were employed to study both, the reactions of birds and other animals and humans, to high frequency sounds. The most well known of these whistles was invented by Galton on 1883, and it is considerate the first true ultrasonic generator. All these devices can be considered the first generation of ultrasonic transducers, although two important discoveries, occurred during the 1800s, would change, in a later date, the transduction mechanism of ultrasound.

In 1842 J. P. Joule discovered the magnetostrictive effect with the identification of the

change in dimensions of a magnetic material under a magnetic field. This preliminary work, included in the first law of thermodynamic as a footnote, became the centre of numerous subsequent studies such as the Villari in 1865 who discovered the converse effect. Although the most important contribution arrived with the discovery of the piezoelectric effect by Pierre and Jacques Curie in 1880. The phenomenon was observed as a consequence of studies examining the relationship between pyroelectric phenomenon and crystal symmetry in materials such as the Rochelle salt. In this first study the Curies discovered the direct piezoelectric effect in several materials as the before mentioned Rochelle salt but also in crystals of tourmaline, quartz, topaz, and cane sugar; among which quartz and Rochelle salt exhibited the most piezoelectricity. The possibility of the converse effect was predicted theoretically by Lippmann a year later, and it was promptly validated experimentally by the Curies [107–109].

The first real application of ultrasound was related with submarine acoustic. During the outbreak of the WWI, the imminent menace of submarine attacks led the governments of France and Great Britain to invest in the development of programs of underwater detection. Previous the start of the war, the interest on the detection of submarine objects and the communication between ships and submarines rose after the sinking of the RMS Titanic on 1912 after crashed into an iceberg [107, 108, 110].

In US the Canadian inventor Fessenden, who realised great advances on radio broadcasting, designed a low-frequency system for underwater localisation of objects, known as the Fessenden oscillator. Subsequently, this system was commercialised and used in real naval operations. During the same period, in Great Britain the English meteorologist Richarsond patented a method of underwater echolocation of objects using ultrasound, however the system never was developed and implemented in real applications. Based on the work of Richarsond, in 1915 the Russian electrical engineer Chilowsky proposed to the French physicist Langevin the development of an echolocation system using a magnetic transducer. After the first tests, and due to the growth that piezoeelectric materials were experimented by improving the preparation and manufacture of quartz crystals, both scientists built a device using a single quartz crystal embbebed in wax as electromechanical transducer. First this device was used only as a hydrophone in detection acoustic waves tasks. The large size and dimensions of the quartz crystals used, along with the high voltages levels needed, limited the use of this type of transducer as sound projector. To solve this problem Langevin redesigned the initial proposal using an array or mosaic of smaller quartz crystals cemented

between two steel plates. This development, now referred to as the sandwich or Langevin transducer, enhanced the level of acoustic energy radiated by improving the coupling between the transducer and water, as well as dropping its resonant frequency to 50 kHz. With this device, for the first time, it was possible to send signals and hear clear echoes at long distances. It can be asserted that the era of modern ultrasonic started with Langevin's quartz sandwiched transducer [107, 108, 110].

Although the submarine industry attracted the greatest advances in ultrasonic applications, after the end of WWI, the successful results obtained with the use of piezoelectric materials in the device designed by Langevin, created an intense interest on the development of this technology on further areas. Arose from war stimulated research, Professor Walter Cady implemented the use of quartz crystal in frequency control systems, crystal resonators. Cady found that the stability of the frequency of the electrical signal generated by a quartz crystal, vibrating in resonance, could be used in applications such as radio broadcasting and in stabilization of transmitted and received signals. During the period between the end of the WWI and the beginning of WWII many other applications were initiated. Apart from the frequency stabilizers, other devices such as microphones, pick-ups, accelerometers or phonographs, were developed. [107–109].

An important issue in ultrasonics was the development of pulsed-echo ultrasonic metal flaw detectors. Although the concept of ultrasonic metal flaw detection was first suggested by the Soviet scientist Sokolov in 1928, the first practical industrial application of ultrasound was developed between 1939 and 1945, independently in America by Firestone and Britain by Desch et alt. This was the first application of ultrasound outside of underwater applications, for locating flaws in materials and for measuring the thickness of materials with reduced accessibility to both sides [107, 108, 110]. Now a days, this technique competes with x-ray and other inspection methods and it has an important role in medical process for non-invasive diagnosis of the inside of the body and biological tissues.

Parallel to the development of new applications, some researchers focused their work on investigating the effects on biological tissues when they were insonated with high intensity ultrasound. These effects were first assessed by Langevin when reported the death of fish in the sea and pain in the hand when exposed to a high intensity ultrasonic field. Despite of the report of Langevin, these effects were not the subject of great interest from the scientific community. However these studies were continued and expanded by Robert Wood and Alfred Loomis [111], who studied both physical and biological effects due to the application of

ultrasonic beams of high intensity in living tissues. In their work, they described effects such as drilling, fogging, agglomeration, crystallization, creation of bubbles (cavitation), destruction of tissue and even the death of animals. They introduced ultrasound to chemistry, that were the beginnings of what is now known as sonochemistry . The work of Wood and Loomis initiated a line of research that was quickly followed by numerous researchers, and represents the basis on which many current applications, both industrial and medical, are based on [107–110].

During WWII it proliferated the use of magnetostrictive materials in low frequency ultrasound applications. Although the magnetostrictive effect was discovered by Joule in 1842, it was not until 1928 when Pierce developed the first magnetostrictive oscillator. Ferroelectric alloys such as nickel-iron and cobalt-iron alloys showed better performances at low ultrasonic frequencies since they were found to be more robust, and less expensive than the quartz crystals manufactured [107, 108].

The growth magnetostrictive transducers coincided with a limitation to find natural piezoelectric materials, in this case quartz crystals with the required quality. With the discovery of ferroelectricity in 1921, independent research groups searched for piezoelectric artificial materials in the form of ceramics. The first generation of these new ferroelectric materials were developed mainly from the ammonium and potassium dihydrogen phosphate, denominated ADP and KDP respectively. These new materials presented reasonable better piezoelectric properties than quartz crystals and Rochelle salt, with minor production costs to produce different shapes and volumes. However the principal drawbacks were the low Curie temperature and that they are water soluble. The most important ferroelectric material of this first generation was the barium titanate compound, BaTiO3, reported in 1945 by researchers at the MIT, although groups in Russia and Japan discovered this material almost at the same time. After WWII barium titanate, which was initially commercialised as a transducer material, became the most used ferroelectric material in ultrasonic applications [22, 107, 109, 110].

The second generation of ferroelectric materials appeared with the use of lead zirconate titanate, in its most common form known as PZT. The PZT solution was originally developed in 1954 by the Japanese researchers Gen Shirane, Sawaguchi Etsuro et al. although the enormous potential of the compound piezoelectric was discovered by Jaffe, Roth and Marzullo a year later. Clevite Corporation took the most important PZT patents for transducer applications. Due to the advantageous properties of PZT in comparison with the rest of

ferroelectric and ferromagnetic materials, this type of piezoelectric ceramics quickly became the most widely used material in almost all ultrasonic applications and the basis for the development of transducers for high power ultrasonics applications [5, 22, 109].

During 1940s and 1950s ultrasonic transducers technology attracted the interest of many researchers in order to develop more efficient devices. Current technology, inheriting of the work developed by Langevin, suffered from a clear power limitation due to the low tensile strength of piezoelectric materials. In 1945 Manson proposed the use of an exponentially tapered half wave length rod, working in resonant with the transducer, in order to amplify the vibration energy generated by the piezoelectric element. However the most important advance in the development of ultrasound technology for high power applications came from the hand of Miller in 1954. Miller designed the pre-stressed sandwich transducer, where the stack of ceramics is subjected to a compression stress, by means of a compression bolt, increasing the mechanical strength of the transducer, solving on this way the problem of fracture due to high stress concentrations in the piezoelectric material. Further development and implementation of such technology had a great impact in industrial processes such as, metal forming and welding, drilling, cutting and ultrasonic cleaning, and in applications in medicine [107, 108].

Classically the design of transducers relied on the use of a lumped-element approach. The method consist on the assumption that the transducer can be represented by a number of mass elements interconnected by springs and dampers. Derivation and computation of the various parts is fairly easy to do for a transducer of simple geometry; however, for many ultrasonic transducers which employ flexing motions or cavity resonances the task becomes significantly more difficult and analysis is best carried out using numerical methods.

Finite Element Analysis (FEA) was first developed in 1943 by Courant [112]. It consisted of a method of numerical analysis and minimisation of variational calculus to obtain approximate solutions to vibration systems. The method was first developed by American and European aircraft industries for the analysis of aircraft structure, and shortly after a broader definition of numerical analysis was established [113]. Within a decade it was soon recognised that the finite element technique could be applied to the solution of many other classes of problems. By the early 1970s, the first software packages which implemented finite element methods appeared, but their use was limited to expensive mainframe computers generally owned by the aeronautics, automotive, defence, and nuclear industries.

The utilisation of a numerical treatment for piezoelectric elements [114], allowed the

finite element method to be applied to the field of ultrasonic transducer design. Transducer designers were gradually exploiting the technique to model the highly complex geometry of different devices. Although it was during the 1980s, when the application of finite element (FE) techniques to the design of ultrasonic transducers progressively increased. This is essentially due to the increasing availability of powerful personal computers. Since FEA provided the designer with a wealth of accurate data regarding the behaviour of a transducer, it became not only a complementary technique of analysis, but the principal tool previous to the fabrication of the prototypes. On example is the development of the cymbal transducer in 1997 that was an outgrowth of results obtained via finite element analysis using SAP90, MARK, and ANSYS, on transducers with the moonie-style cap [115]. The introduction of an end-cap with a different geometry in the FE model solved the problem of stress concentration in the regions above the bonding area.

Today computer modelling makes extensive the use of the finite element method, and it is an important part of the development of new transducers. Commercially available packages have made it easy for the transducer designer to study not only the structural mechanics variables, such us resonance modes, velocity profiles, static and dynamic stresses, and the acoustic output of transducers, but the possibility of realising electro-mechanic and thermo-mechanic analysis of the devices, in order to have a complete characterisation of the device previous the experimental analysis. Thus both the development time and the final cost are considerably reduced.

2.2 Ultrasound in surgical applications

It can be asserted that the use of ultrasound technology in medical applications started with the work of Wood and Loomis [111]. In 1917 Wood, who witnessed part of the experimentation process realised by Langevin and his transducer, was very impressed with the effect that the powerful ultrasonic beam produced in living organisms, able to kill small fish when swimming within the sound field generated. When returned to America, Wood and his collaborator Loomis developed a series of experiments that led to the publication of an article in 1927. In this comprehensive work, the authors studied different physical and biological effects observed from the use of high power ultrasonic beams. For the realisation of these experiments an ultrasonic transducer, based on the one designed by Langevin, was built using quartz discs with a frequency of operation between 100 and 700 kHz.

Wood and Loomis analysed the biological effects on cells, unicellular organisms, fish and

small mammals and amphibians such as mice and frogs. They observed that the activity at the cellular level was interfered when organisms were exposed to short ultrasonic pulses, leading to destruction if exposure was continued. For small fish frogs and mice, death appeared after an exposure of approximately 2 minutes. The first hypothesis proposed by the authors about the death at cellular level, was the temperature rise inside the subject, although they could not provide empirical data of such fact. The results taken from the work of Wood and Loomis on the biological effects of ultrasound did not generate great interest in the scientific community of 1928, apart of a German patent describing a method for transferring ultrasonic vibrations into the human body [107, 109, 111, 116].

The first practical applications of ultrasound in therapeutic applications, called ultrasonotherapy appeared in the early 1930s in Germany and central Europe. In 1938 Polhman compiled a series of experimental and clinical studies describing the therapeutic effects of ultrasound in human tissues. Despite the proliferation of different therapeutic applications, from treatment of sciatica, to the cure of abscesses or warts, the lack of an understanding of physical phenomena involved in the processes and the disparity between results obtained, hampered further investigations for the application of ultrasonic techniques in therapeutic processes [107, 109, 111, 116].

In the 1950s, in the aftermath of the WWII, the rise of the speciality of physical medicine, and the incorporation of techniques developed originally for industrial processes, rekindled the interest in the use of ultrasound in medical applications. It is possible, during these years, to make a clear difference between processes for therapeutic purposes, diagnostic procedures, surgical procedures and dental applications.

The first applications of ultrasound in surgery were specialized in two different procedures, neurosurgery and ear surgery. The first studies began in the early 1950s with the work of Fry et al. about the interaction of the application of focused ultrasonic beams in biological processes. These studies led to the development of techniques applied to neurosurgery. The first device, designed by Fry and his team, was comprised of an array of transducers where various quartz discs vibrate in thickness mode at a frequency of 1 MHz fitted with a polystyrene lens. With a fixed focal length, the transducer was immersed in a saline solution that acted as mechanical coupling for the ultrasonic wave between the transducer and the brain of the patient. In a further modification, a device with a single piezoelectric element mounted on a parabolic reflector, to obtain a more focused pattern of radiation, was developed. In Figure 2.1, an image of the device used by Fry is shown [107, 117–119].
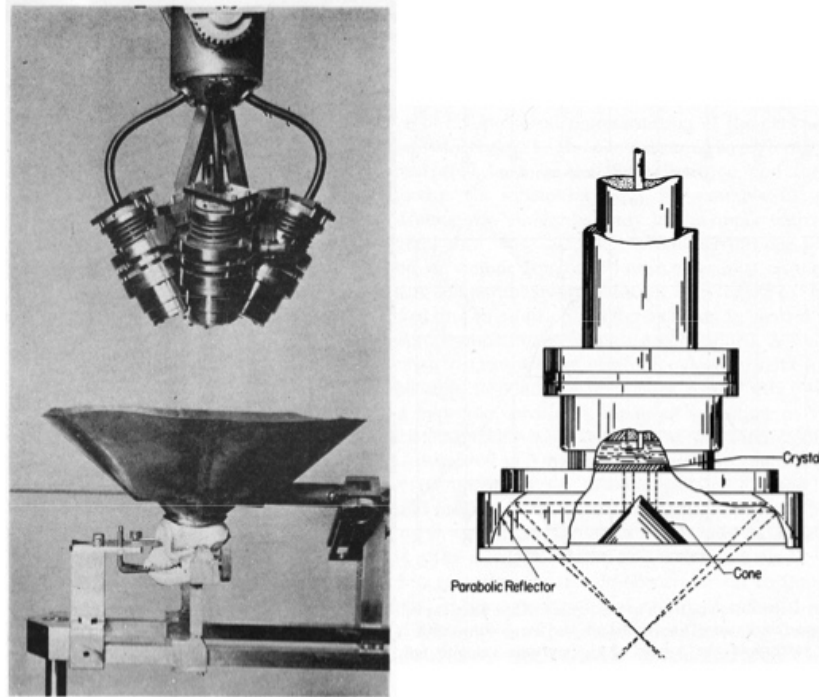
Figure 2.1: Ultrasonic device for neurosurgery designed by Fry et alt. Extracted from [117]

In 1965 Fry conducted a series of studies in patients using the ultrasonic neurosurgery technique primarily in the treatment of Parkinson disease and the destruction of the pituitary gland for the treatment of some cancers. Parallel to the work of Fry, Krejci in 1952 conducted a study on the use of focused ultrasonic beams for the treatment of Ménière's disease. The size of the transducer in this case was reduced in order to facilitate a better access to the work area. For that purpose a metallic probe was designed and coupled to the transducer. As in the previous case, a saline solution was used to obtain an efficient acoustic coupling [119].

The difficulty to obtain a correct focus of the ultrasound beam in the area to be treated generated a poor performance, since the risk of damage in adjacent sensitive areas was very high. Today these ultrasonic techniques are used in conjunction with other imaging techniques such as the magnetic resonance imaging (MRI). In this way, the surgeon has during the whole process a direct visual access to the zone in real time, so that the position of the ultrasonic focus can be corrected if necessary. Normally, in a first step, the area to be treated is irradiated with a pulse of low intensity which raises the temperature of biological tissue enough to be recorded by the MRI, so that it can be verified with precision the area which is radiated. Once the correct position of the focus of the ultrasonic beam is verified, a second pulse of higher intensity is delivered in order to proceed with the surgical procedure.

The first application of ultrasound in dentistry was reported by Catuna in 1952 [120],

when used an industrial drilling machine for cavity preparation in human teeth. The device was originally designed by Balamuth in 1945 [121] for cutting hard and brittle materials such as glass and ceramics. The device consisted of a magnetostrictive Langevin transducer that delivered a longitudinal vibration energy to a vibrating cutting tip. The mode of the cutting action was divided into longitudinal, using straight tips and a combination of a longitudinal and flexural motion using tips with curve shapes. The ultrasonic drill required of an abrasive slurry of aluminium oxide applied on the surface of the teeth to assist the process of cutting or grinding enamel and dentine. After the first results obtained with patients, Balamuth et al. [122,123] designed an ultrasonic cutting device optimised for dental applications based on the same principle as the original industrial design and an ultrasonic knife for cutting bone and flesh. Balamuth pointed as main advantages of these devices a high cutting precision with a low pressure on the cutting area, that reduced the risk of tearing and damaging of the areas surrounding the cut. The second vantage was the control of the heat generation during the cutting process through a cooling system embebed in the device, allowing a self-cleaning action when cutting soft and viscous materials, and reducing the heat when penetrated delicates tissues.
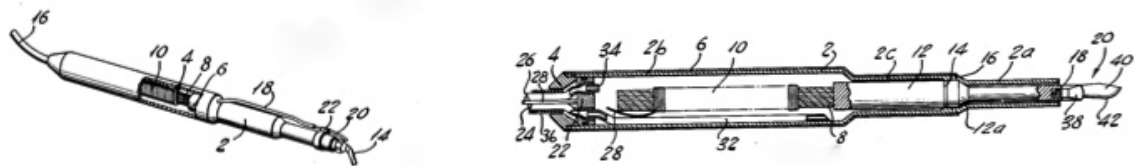
Figure 2.2: Ultrasonic cutting devices for bone surgery designed by Balamuth. Extracted from [122-123]

Although the first results drawn from works such as those by Oman et al. and Postle [80, 124] reported a wide acceptance by both patients and dentists, ultrasonic cavity preparation never became popular. The poor visual access, the large amount of alumina slurry needed and the more effective high speed air powered rotary drills which were developed around the same time, hampered the development of this technology.

During the decade of the 50s, the main use of ultrasonic techniques in dentistry was focused on oral prophylaxis treatments. In 1955 Zinner [125] proposed the use of an ultrasonic transducer connected to a modified scaling tip based on the tip used in hand scaling instruments. The action of the ultrasonic vibration of the tip in conjunction with the

application of water coolant improved the effectiveness in the removal of plaque and calculus from teeth. Two years later Johnson and Wilson [126, 127] conducted a comprehensive study on the application of ultrasound in dental scaling procedures. As result of this study, the authors improved the efficiency of both the device and the technique used during the scaling process. Initial trials of early ultrasonic scalers produced favourable results over hand instruments, reducing procedure time, patient discomfort and damage of soft tissue surrounding the tooth [128]. Soon after ultrasonic scaler became completely established in the removal of dental plaque and calculus procedures.

Parallel other studies, such as the conducted by Richman [129], suggested ultrasonic vibrations might be used for endodontic treatments to prepare and clean the root canal of teeth. However this technique was not developed further and used clinically until the work realised by Martin in 1976 [127, 130], where combined the use of the ultrasonic vibration of the tip with a biocial agent to lead a more efficient bactericidal synergism during the root cleaning.

Richman also investigated the use of his ultrasonic device in dental surgical procedures such as removal of the apical portions of roots of teeth. The main difference between this device and the cutting device designed by Balamuth was the absence of the abrasive slurry. In his study Richman reported the results of several clinical trials where the grade of acceptance in patients was significant. Subsequent studies such as the conducted by Poliakov in 1972 [85] and Horton et alt. in 1975 and 1981 [131, 132] also reported successful clinical evaluations of the use of ultrasonic instruments in cutting, sawing and uniting bone fractures. The generation of micro displacements at the cutting edge of the ultrasonic inserts, allow to remove mineralized tissue without damaging soft and delicate tissues. The principal vantages included ease of instrument application and use at surgical sites, preciseness of bony removal, haemorrhage control, uneventful healing with lack of postoperative damage, and patient acceptance with minimal discomfort. The use of a coolant during the process also improved the procedure eliminating the debris due to the appearance of cavitation and acoustic microstreaming and reducing the heating in the cutting zone due to the frictional movement of the vibrating tip.

The use of ultrasound in osteotomy and bone cutting during 70s, 80s and 90s was limited to the performance of sporadic clinical studies and laboratory tests without finding a definitive continuity to become an alternative to conventional methods. It was not until 2001 when the first ultrasonic device designed specifically for maxillofacial bone surgery appeared

in the market. The maxillofacial surgeon, Vercellotti, and the Italian company Mectron s.p.a. created the Piezosurgery Device® [93, 96, 133]. The special collaboration between an engineering company and surgeon allowed to combine both technological expertise with medical experience to design a device to support the needs of the surgeon and optimised for a wide range of surgical procedures. The device has been designed to perform procedures from oral prophylaxis to oral surgeries and maxillofacial operations such as orthognathic surgeries (correction of problems relating to the jaw and face, such as jaw realignment or the treatment of a cleft palate). Several clinical studies have shown wide acceptance by both surgeons and by patients who report less inconvenience and a speedy recovery [92, 95, 134, 135].

Chapter 3

Cymbal transducer

3.1 Introduction

In this chapter the materials used for fabrication of the cymbal transducers and the assembly process are discussed The transducer design used is the original proposed by Newnham and Dogan [60] in 1998. Furthermore, both the numerical and experimental analyses used for the characterisation of the cymbal transducers are defined.

Piezoelectric transducers, such as the cymbal transducer, show different operating conditions depending if working as sensors or actuators. So far, the design and characterization of cymbal transducers has been mainly oriented towards the study of the frequency response and the study of their characterization as underwater transducers and sound projectors. Cymbal transducers, along with all other types of flextensional transducers, are generally small compared to the wavelength of sound in the usable frequency range, usually out from their first resonance frequency. In addition, most of the radiating surface area of the end-caps moves in phase, thus the resulting acoustic radiation pattern is quasi-omnidirectional, resembling an acoustic monopole. The omnidirectional characteristics of flextensional transducers create significant problems in projection transducers. Therefore, in order to produce the desired beam pattern, so as to increase the acoustic power and radiating surface, it is usual to configure the cymbal transducers in arrays.

In high power applications, such as ultrasonic cutting or drilling, the mechanical energy generated by a single transducer is transmitted to a vibrating tip. As mentioned in chapter 1, the basic architecture of a high power ultrasonic such as the Langevin transducer is considered to resonate in the free-free half wavelength extensional mode. The Langevin transducer also includes a metallic amplifier, or horn, which produces displacement amplification at

the working end. This horn must be tailored to $\lambda/2$ or multiples of the half wave length. Therefore, both transducer and horn are designed to resonate at the same frequency. In order to study the capability of cymbal transducers to drive horns or vibrating tips, in the last section of this chapter the response of a single cymbal transducer, as an actuator when different masses are connected to the end-caps, in a non-resonant mode, will be discussed. The aim is to observe the behaviour of the cymbal transducers when different masses are connected to the end-caps.

3.2 Design and assembly of the cymbal transducer

3.2.1 Piezoceramic driver

The active element of a cymbal transducer, which performs the electromechanical transduction, is produced from piezoelectric material. Such piezoelectric elements are conventionally formed into discs or rings polarised in the thickness direction. The top and bottom surfaces of the element are often prepared through processes such as screen printing or plating, by which a layer (3 μm to 10 μm thick) of an electrical conductive material, such as silver, chromium or nickel, is deposited on to the surface. In this way leads can be soldered straight to the prepared surface of the piezoceramic. In the cymbal transducer, as well as the others flextensional transducers, the mechanical movement (radial expansion/contraction) of the piezoceramic disc or ring is transmitted to the metal end-caps, which amplify the motion in the perpendicular direction. In the case of the cymbal transducer the output movement is generated in the axial direction, perpendicular to the radius of the ceramic.

Under an applied electric field, when a piezoceramic disc or ring expands radially in proportion to the material's piezoelectric d_{31} coefficient, it also contracts longitudinally as a function of the piezoelectric d_{33} coefficient, and vice versa. Therefore, in the cymbal transducer, due to the design of the metal end-caps, the axial displacement comes from two different sources. One is the longitudinal displacement of the ceramic itself through d_{33}, and the other is the flextensional motion of the metal end-caps arising from the radial motion of the ceramic through d_{31}. Although the two parameters contribute to generate the output displacement, it can be asserted that the axial displacement is determined almost exclusively by the action of the metal end-caps.

The type of piezoelectric materials selected for use within a cymbal transducer, is generally preferred to have large piezoelectric coefficients, in particular a large d_{31} coefficient, in order

to obtain the largest displacement possible. These materials can be represented in general by soft PZT, the most common is PZT 5H, and single crystals such us PMN-PT [61, 136–138]. Although single crystals show the best performance, due to the high cost of production of single crystal discs and rings, soft PZT has been the preferred option for mass production.

Both the cymbal transducer as its predecessor, the moonie, are miniaturised variations of the class V flextensional transducer with a practical operational frequency range from several kHz to hundreds of kHz. Since the design of the metal end-caps allows high control of the resonance frequency and displacement of the transducer, the dimensions of the piezoceramic disc or ring are selected to be as small as possible in order to decrease the cost of production. However, the geometry of the piezoceramic element can also have a significant influence on the performance of the transducer, therefore it is important to consider, before the design of the transducer, factors such as the diameter, thickness and number of elements [139]. The diameter of the piezoelectric disc or ring has a high influence on the resonance frequency and the displacement of the transducer. For example, a variation between 10 and 50 mm in diameter of the piezoceramic produces a reduction in the resonance frequency of around 30 kHz. On the other hand, piezoceramic discs and rings with large diameters generate larger radial displacements, increasing the axial displacement of the transducer. The thickness of the piezoceramic element does not have a significant influence on the resonance frequency of the transducer, tending to remain practically constant when the thickness is more than 3 mm. However the thinner the piezoceramic element is, the better the electric field uniformity, the higher the effective electromechanical coupling coefficient and lower its impedance (higher flow of current and hence amplitude for a given driving voltage). It is not common to use more than one piezoceramic element due to the additional complexity and cost of the transducer without significant improvement or control of the resonance frequency and displacement. Also, increasing the number of piezoceramic elements leads to inefficiency due to mechanical losses (caused through increasing the number of join interfaces without a strong mechanical coupling) and drive problems, as too many elements can induce phase shifts among the elements causing them to counteract one anothers oscillations. For these reasons the utilisation of a cymbal transducer with a double piezoceramic driver only occurs in applications where the control of the directivity radiation pattern of the transducer is important [140].

For the construction of the cymbal transducers two different hard PZTs disc, PKI-402 from Piezo Kinetics and PIC181 from PI Ceramics were employed for reasons of convenient.

The properties of the piezoceramic materials can be seen in Table 3.1. The reason of using hard PZTs instead of soft PZTs, is because, as mentioned in chapter 1, power ultrasonic devices, due to their driving conditions of high electrical field and high strain as well as low losses, exhibit better performances with hard PZTs, due to the low permittivity and dielectric losses and high Q_m values. The geometry of the piezoceramic disc utilised for the fabrication of the cymbals transducer is showed in Table 3.2.

Parameter	Units	PKI-402	PIC181
Density	kg/m^2	7900	7850
C_{11}^E	N/m^2	$1.47E^{11}$	$1.52E^{11}$
C_{12}^E	N/m^2	$8.11E^{10}$	$8.90E^{10}$
C_{13}^E	N/m^2	$8.11E^{10}$	$8.54E^{10}$
C_{33}^E	N/m^2	$1.32E^{11}$	$1.34E^{11}$
C_{44}^E	N/m^2	$3.13E^{10}$	$2.23E^{10}$
C_{66}^E	N/m^2	$3.06E^{10}$	$3.16E^{10}$
d_{31}	m/V	$-1.50E^{-10}$	$-1.08E^{-10}$
d_{33}	m/V	$3.25E^{-10}$	$2.53E^{-10}$
d_{15}	m/V	$4.80E^{-10}$	$3.89E^{-10}$
ϵ_{11}^T		1239	1224
ϵ_{33}^T		1084	1135

Table 3.1: Properties of the piezoceramic materials

Piezoceramic	Diameter (mm)	Thickness (mm)
PKI-402	12.7	1
PIC181	27	3

Table 3.2: Dimensions of the piezoceramic discs

3.2.2 Metal End-caps

In the cymbal transducer, the piezoceramic disc or ring is sandwiched between two symmetric truncated conical cymbal-shaped metal end-caps, with shallow cavities at their inner surface. The name 'cymbal' is used because of the similarity in the shape of the end-caps to that of the musical instrument. The end-caps are usually bonded with the piezoceramic element by means of an epoxy layer applied at the flat flange, creating an air-filled cavity [58, 60, 141].

The end-caps transform the high impedance, low radial displacement of the piezoceramic element into low impedance, high axial displacement of the end-caps. Working as actuators the radial motion of the piezoceramic is converted into flextensional and rotational motions in the metal end-caps, Figure 3.1. With a fixed piezoceramic geometry, the resonance frequency, force and displacement of this structure can be tailored through the choice of the cap materials and dimensions [58, 61, 136, 137, 139, 142, 143]. The relationship between the resonance frequency and displacement is in all cases inverse, when the resonance frequency increases the axial displacement decreases. The dimensions with higher influence over the resonance frequency and displacement are the base cavity diameter and the thickness of the end-cap. The influence of the end-cap material on the resonance frequency and displacement of the transducer is not as great as the geometry. The resonance frequency has a close relationship with the velocity of sound of the material. Materials with higher sound velocity tend to show higher resonance frequencies. On the other hand, the displacement has a strong dependance on the Young's modulus of the material. Materials with lower values of Young's modulus present higher displacements than stiffer materials [61, 137, 139, 141–143].
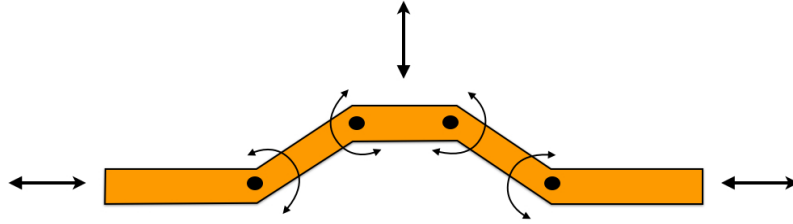
Figure 3.1: Flextensional and rotation motion of the end-cap

In most studies reported in the literature, end-caps are produced from sheet metal by punching and then pressing to shape the end-cap to its final cymbal geometry [58, 61, 136]. Whilst this is a highly repeatable process for precise, high volume production, there are some drawbacks. Accuracy of the cavity dimensions is paramount in ensuring an efficient transducer, however punching results in the edge between the inner cavity and the flange becoming rounded. Consequently, when the epoxy resin is deposited a portion can escape into the inner cavity area, affecting the vibration response of the transducer [61]. On the other hand, during the pressing process, pre-stress is introduced in the end-caps that can hamper the rotational movement of the wall of the cavity. An alternative is to cut the end-caps, so there is no rounded edge thus reducing, but not eliminating, the chance of epoxy resin entering the cavity. In this case there is not any pre-stress so the movement from the

piezoceramic element can be transmitted more efficiently.

For this thesis three different materials have been used, brass, steel and titanium, for the construction of the end-caps, in order to analyse the influence of the end-cap material when the cymbal transducer performs as an actuator. The three materials with different values of density and Young's modulus are listed in Table 3.3. The end-caps were cut from 0.25mm-thick sheets using a a thread mill, Datron VH-Gewindefrser, controlled by CAD software in order to automate the fabrication process, Figure 3.2.

Material	Density (kg/m^3)	Young's modulus (GPa)	Poisson's ratio
Brass	8325	106	0.35
Steel	7723	179,18	0.31
Titanium alloy Ti-6-4	4418	110.4	0.342

Table 3.3: Properties of the end-cap materials
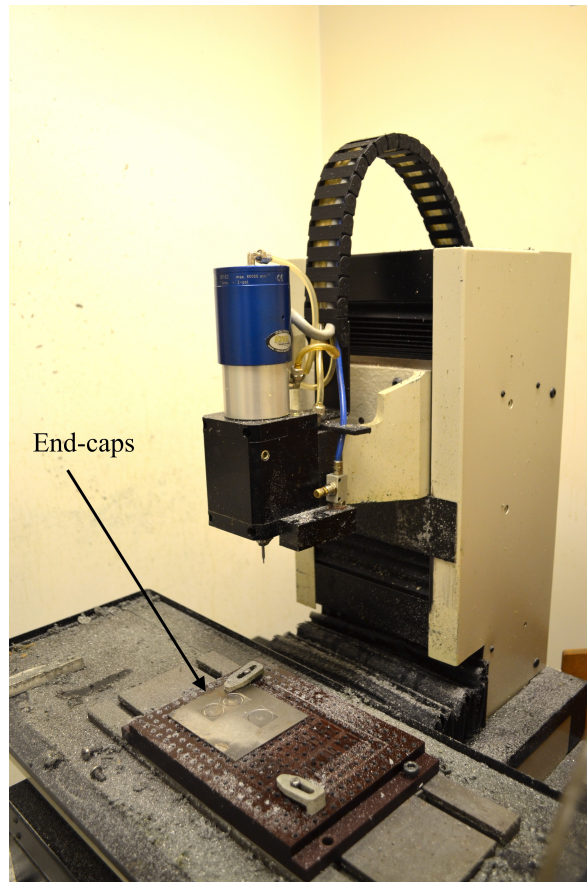
Figure 3.2: Machining process of the end-caps

3.2.3 Bonding agent

The end-caps are usually bonded to the piezoceramic through an epoxy layer. Thus the mechanical radial motion of the ceramic is transmitted to the end-cap through a single mechanical coupling. This epoxy layer is deposited in the flat flange of the metal end-caps avoiding leaking into the cavity.

In the cymbal transducer both faces of the piezoceramic element are enclosed by the end-caps, therefore the electrical leads are connected to the flange of the metal end-caps. For this reason the epoxy must have an adequate electrical conductivity, but more importantly, sufficient shear strength and low mechanical damping. Due to the flextensional motion of the end-caps, the largest stress concentration is observed at the inner edge of the bonding layer [144, 145]. In this area there is a tensile stressed region which induces a critical loading mode into the epoxy layer, in the form of cleavage.

Although the use of conductive epoxy guarantees an optimal current flow to the piezoceramic, the main drawback of this type of epoxy is its low tensile strength. In general, the end-caps are therefore bonded to the driver using a high-strength insulating epoxy [143]. To avoid the formation of microcracks leading to the degradation of the mechanical coupling between the piezoceramic and the end-cap, the epoxy should be able to withstand stresses caused by motion of the end-caps. On the other hand, in order to assist optimal current flow to the ceramic, several small spots of conductive epoxy are placed on the ceramic. Because the surface of the piezoceramic is a conductive material, this ensures adequate electrical potential distribution.

The geometry of the epoxy layer, specifically the thickness, has a small effect on the resonance frequency of the transducer. The relationship between the thickness of the epoxy layer and the resonance frequency is inversely proportional. It has been calculated that the difference between an ideal end-cap/piezoceramic coupling without epoxy and an epoxy layer of 1 mm, produces a reduction of 20% in the resonance frequency [146]. Usually the thickness of the epoxy layer varies from 0.1 to 0.5 mm, which entails an approximate range of 8% in the resonance frequency. The selection of the thickness of the epoxy layer must be concerned with efficiency parameters during the performance of the transducer. A thinner bonding layer causes adhesion and endurance problems; a thicker bonding layer leads to high compressibility of the bonding material resulting in mechanical losses across the layer. Depending on the final application, a correct compromise between damping and maximum stress supported by the epoxy must be considered when selecting the type of epoxy and its thickness.

For the construction of the cymbal transducer, a layer of Eccobond 45LV (black) insulating epoxy resin (Emerson & Cuming), at a ratio of three parts epoxy resin to one part resin catalyst, was deposited between each end-cap flange and the piezoceramic disc, to form an approximate 0.4 mm thick epoxy layer. This epoxy in comparison with other commercial insulating epoxies such as EPO-TEK or Masterbond, has shown higher flexibility [61, 144]. This provides more stress relief and higher strength. The curing process occurs at room temperature.

Since the elastic parameters of the epoxy depend on the mix of the two components, a tensile test of the ratio of three parts epoxy resin to one part resin hardener was performed, Figure 3.3. The results obtained from the analysis are shown in Table 3.4.

(a)   (b)
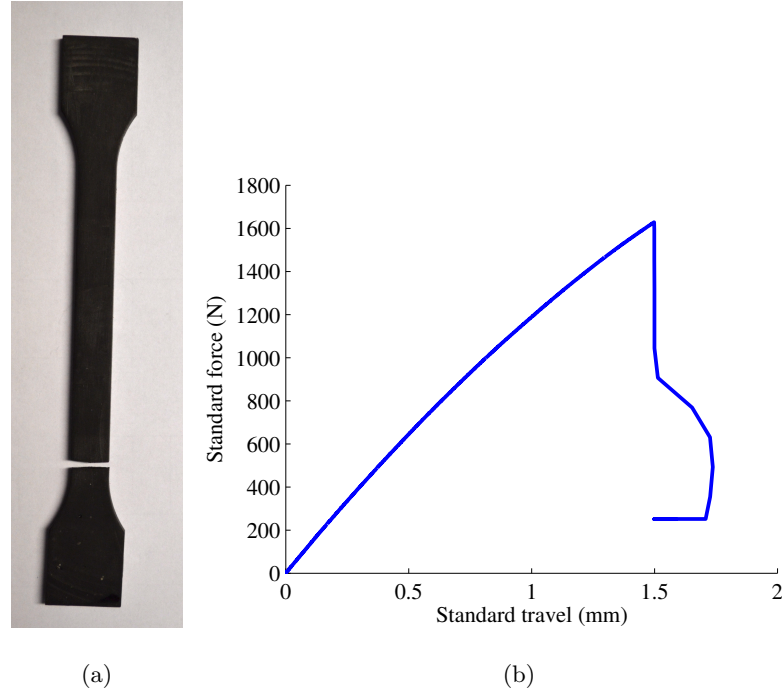
Figure 3.3: (a) Tensile test specimen and (b) tensile test result

Material	Density (kg/m^3)	Young's modulus (Pa)	Poisson's ratio
Epoxy	1496	2745283502	0.35

Table 3.4: Properties of the resin epoxy

3.2.4 Assembly process

The different parameters used to tailor the resonance frequency and displacement of the cymbal transducer are shown in Figure 3.4 and the dimensions utilized for the fabrication of

the cymbal transducers are listed in Table 3.5.
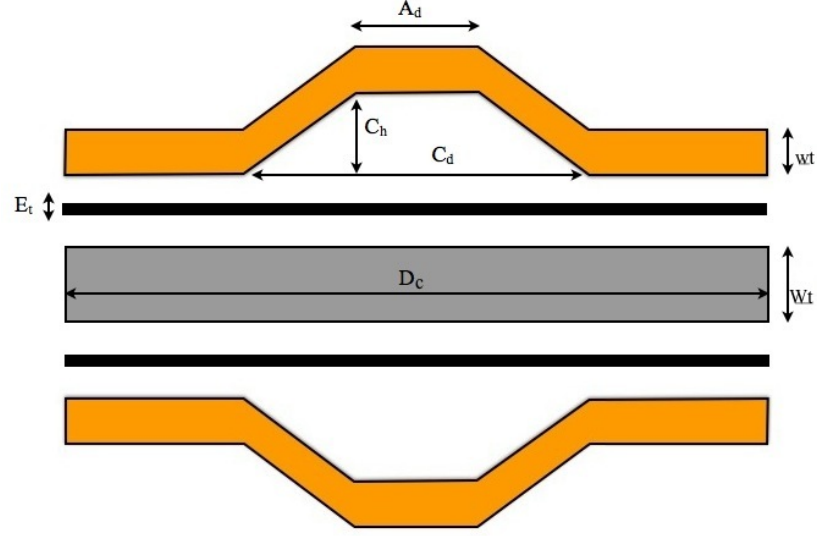
Figure 3.4: Description of the different parameters of the cymbal geometry

Parameter	Dimension (mm)
W_t	1.00
w_t	0.25
D_c	12.70
C_d	9.00
A_d	4.50
C_h	0.30
E_t	0.30

Table 3.5: Dimensions of the cymbal transducer

The assembly process starts with a preparation and cleaning of the different parts in order to ensure an optimal adhesion of the epoxy. Thus the flanges of the metal end-caps were ground using sandpaper to create a slight roughness on the surface of the metal. After this process, the end-caps were cleaned to remove dust and other residual contaminants.

As previously mentioned, in the cymbal transducer the electrical leads are connected to the flange of the metal end-caps. Since an insulating epoxy is used as the mechanical coupling, it is necessary to introduce some elements to improve the electrical conductivity between the end-caps and the piezoceramic. For this purpose, several solder spots were placed at the edge of the piezoceramic all around its circumference. These spots were approximately 0.4 mm in

thickness, and the number and position were selected to ensure the correct parallel alignment of the end-cap with the surface of the piezoceramic, with a direct electrical connection once the epoxy was deposited, Figure 3.5.
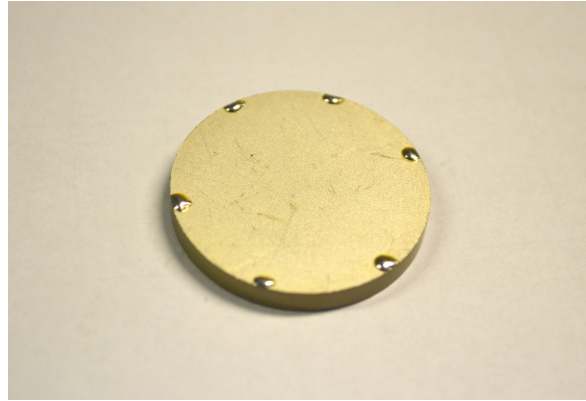
Figure 3.5: Distribution of the solder spots on the surface of the piezoceramic

For the assembly of the cymbal transducer, a metal rig was used in order to keep a correct alignment of the different parts during the curing process, as shown in Figure 3.6. The epoxy was deposited manually on the flange of the end-caps with special attention to the quantity utilised in order to reduce the possibility of any leaks of epoxy into the cavity. Afterwards the end-caps and ceramic were assembled into the rig. During the curing process the entire assembly was kept under uniaxial pressure at 170 kPa, for 24 hours at room temperature to allow the epoxy to cure. The pressure was applied uniformly on the area of union through metal rings with a wall width equal to the dimensions of the flanges of the end-caps.
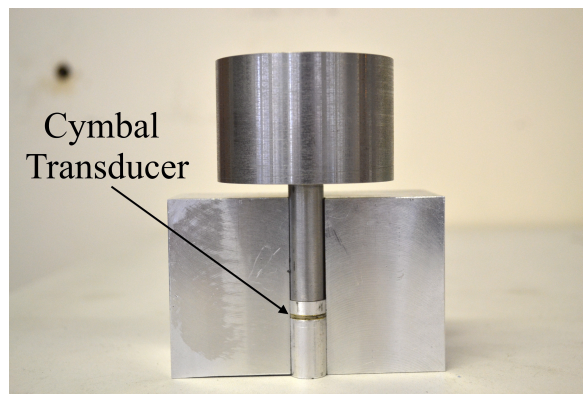
Figure 3.6: Curing process of the cymbal in a metal rig

After the curing process was completed, the electrical leads were soldered onto the flange of each end-cap, as shown in Figure 3.7. The wires used were enamelled copper wire with a

diameter of 0.213mm. The reason for using this particular wire was its small diameter and high flexibility, in order to introduce the minimal external effect on the vibration mode of the transducer. Two different methods were used to solder the wires, metal solder, for the brass end-caps and conductive epoxy, in the case of the titanium and steel end-caps.
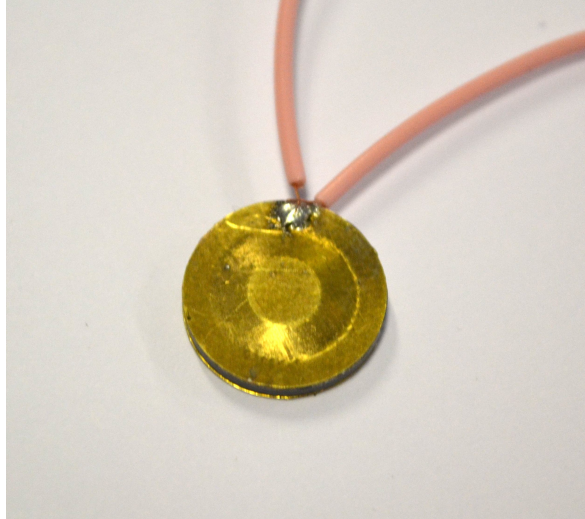
Figure 3.7: Cymbal transducer after the connection of the electrical leads

3.3   Finite element analysis

3.3.1   Introduction

The finite element method (FEM) is a numerical method to simulate the behaviour of a structure with infinite degrees of freedom (DOF), by modelling the structure with approximately the same material properties and geometry but with a finite number of DOF. In this model, the equilibrium equations are constituted by a limited number of unknown variables, therefore it is possible to find solutions not obtainable by analytical models. The true advantage of this numerical method is the opportunity of analysing complex structures by reducing the complexity of the mathematical development and computational time. However, since it is an approximate method, it is extremely important to determine what simplifications have to be introduced in the model in order to obtain a valid result.

In the FEM the structure or domain is divided into a finite number of non-intersecting smaller subregions or finite elements. In each element the physical variables of interest, that correspond with the DOFs, are interpolated based on their values at a discrete number of points or nodes, that are situated on the element boundaries and in the centre and are common to adjacent elements. These nodal points are given by co-ordinates relative to a set

of global axes (x, y, z). The geometry of each element is defined in terms of these co-ordinates by shape functions that map the points onto a local co-ordinate system. The mapped nodal points are given by co-ordinates relative to a set of local axes (ξ, η, ζ).

The set of elements, that depend of the structure's geometry, describe a mesh where the density of the mesh determines the accuracy of the solution, therefore an increased number of elements within the mesh produces an improved approximation. As the number of elements used to model the domain tends to infinity, the accuracy of the solution approaches that of the differential equation, but the computational cost is increased. The success of the numerical model relies on the combination of an efficient mesh selection, material model, a proper definition of the boundary conditions (BC) and the correct interpretation of the results obtained.

Since the 1980s, in conjunction with the development of more powerful computers, the finite-element method has been used extensively in modelling complex transducer structures. Many different finite element (FE) software packages are commercially available, such as ANSYS, ATILA, COMSOL, PZFLEX, Abaqus, etc. For this thesis, the commercial multidisciplinary FE software package utilised is Abaqus/CAE v6.10-2. This software is used to simulate the vibrational behaviour of the transducer. It is also used to study the linear dynamic behaviour of the transducer through harmonic excitation analysis. This software constitutes a powerful tool for the analysis of mechanical structures in two or three dimensions.

The type of elements available for the finite element analysis depends on the software used. Abaqus has an extensive element library to provide a wide range of solutions for different types of analysis and problems. The most common elements used in Abaqus are showed in Figure 3.8 [147].
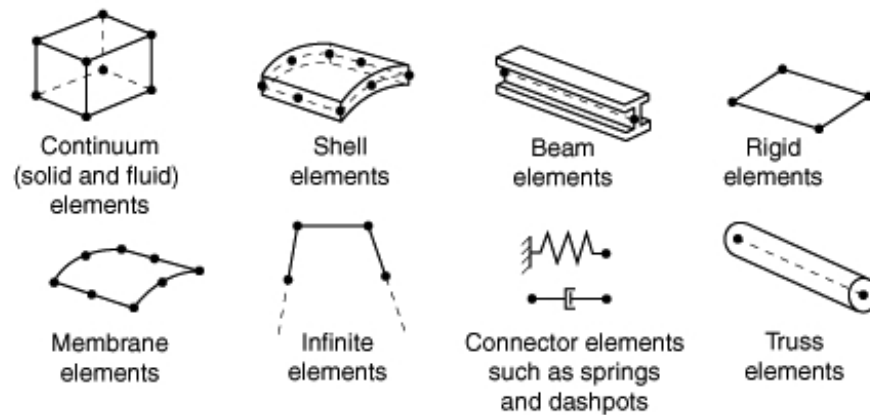
Figure 3.8: Type of elements available in Abaqus

The selection of the type of element must attend to two general criteria: the spatial dimensionality of the model and the type of the analysis required. There are one-dimensional (1D) elements for heat transfer, coupled thermal/electrical, and acoustic applications. 2D elements are represented by an area without thickness. The most common are the plane stress and plane strain elements. 3D elements are used when the geometry and/or the applied loading are too complex for any other element type. Cylindrical elements are a subgroup of 3D elements with a circular or axisymmetric geometry subjected to general, non-axisymmetric loading. Axisymmetric elements are used to discretise objects with an axial symmetry (revolution symmetry) and axisymmetric loading conditions. These elements are essentially 2D elements that simulate 3D behaviour [147].

Depending on the type of analysis, is important to define the nature of the object to be analysed. For the design of ultrasonic transducers, involving a piezoelectric and mechanical elements, it is necessary to consider parameters such as stress/strain, piezoelectricity, heat/electric transfer. In Abaqus, the solid (or continuum) elements can be used for linear analysis and for complex nonlinear analyses involving contact, plasticity, and large deformations. They are used for stress, heat transfer, acoustic, coupled thermal-stress, coupled pore fluid-stress, piezoelectric, and coupled thermal-electrical analyses [147].

The 3D solid elements available in Abaqus for stress/displacement and piezoelectric analysis are tetrahedron, prism and bricks with two different geometric orders, first or second order. First order elements, that use linear interpolation to approximate the solution, correspond with an element with a node placed in each corner. Second order elements, that use quadratic interpolation, correspond with elements with additional nodes placed in the

middle of the edges between corner nodes [147].

3.3.2 General formulation

Based on the constitutive equations of the piezoelectric effect, in conjunction with the equilibrium and conservation equations, the system of equations that Abaqus employs for modelling piezoelectric transducers, is derived in terms of nodal quantities [147]:

$$M^{MN}\ddot{u}^N + K^{MN}_{uu}u^N + K^{MN}_{\phi u}\phi^N = P^M \tag{3.3.1}$$

and

$$K^{MN}_{\phi u}u^N - K^{MN}_{\phi\phi}\phi^N = -Q^M \tag{3.3.2}$$

where

$$M^{MN} = \int_V \rho N^M N^N dV \tag{3.3.3}$$

is the mass matrix (no inertia terms exist for the electrical flux conservation equation)

$$K^{MN}_{uu} = \int_V B^M_u D_m B^N_u dV \tag{3.3.4}$$

is the displacement matrix

$$K^{MN}_{\phi\phi} = \int_V B^M_\phi D_\phi B^N_\phi dV \tag{3.3.5}$$

is the dielectric matrix,

$$K^{MN}_{\phi u} = \int_V B^M_\phi e B^N_u dV \tag{3.3.6}$$

is the piezoelectric coupling matrix,

$$P^M = \int_V N^M P_v dV + \int_S N^M P_s dS + P^M_c \tag{3.3.7}$$

is the mechanical force vector, and

$$Q^M = \int_V N^M Q_v dV + \int_S N^M Q_s dS + Q^M_c \tag{3.3.8}$$

is the electrical charge vector.

In the above expressions u^N and ϕ^N are the vector of displacement and electrical potentials respectively, ρ is the mass density and N^M and N^N are the array of interpolating functions. B^N_u, B^M_u, B^N_ϕ and B^M_ϕ are the spatial derivatives of N^M and N^N. D_m is the mechanical constant, D_ϕ is the electrical constant and e is the piezoelectric constant of the constitutive equations. The force and electrical charge vectors include the volume, surface, and concentrated quantities. The unknowns are the nodal displacements and potentials. Once these are determined, the strains and potential gradients are computed using the expressions given above. The stresses and electrical flux densities are computed by means of constitutive relationships.

3.3.3 Modal and dynamic analysis

Abaqus offers a wide range of different types of analysis depending on the requirements of the problem. The software divides the model analysis into steps. A step corresponds to an analysis with a specific output request. In Abaqus, analysis steps are classified into two categories: general steps, where the response is nonlinear, and linear perturbation steps, which provide the linear response of the model related to a base state. In a model it is possible to define different steps to create a sequence of analysis. The base state is the current state of the model at the end of a previous nonlinear step. If a linear perturbation is the first step then the base state is considered to be the default initial step that is provided by Abaqus code. The linear perturbation approach allows general application of linear analysis techniques in cases where the linear response depends on preloading or on the nonlinear response history of the model. For the analysis of the cymbal transducer two complementary linear perturbation steps were realised, modal and dynamic analysis [147].

Generically, for the modal analysis of a piezoelectric transducer, the system of equations, in matrix notation, is reduced to:

$$\begin{bmatrix} K^{MN}_{uu} - \omega^2 M^{MN} & K^{MN}_{\phi u} \\ [K^{MN}_{\phi u}]^T & K^{MN}_{\phi\phi} \end{bmatrix} \begin{bmatrix} U \\ \phi \end{bmatrix} = \begin{bmatrix} 0 \\ -Q^M \end{bmatrix} \tag{3.3.9}$$

where, ω is the angular frequency.

To predict modal parameters of the transducer, that is assumed to be under free conditions, the program performs an eigenvalue extraction procedure to calculate the natural frequencies and the corresponding mode shapes. Abaqus allows extraction of all the eigenvalues or a specific number within a frequency range selected. For this analysis the eigensolver used in Abaqus was the Lanczos algorithm.

The dynamic analysis is developed by studying the performance of the transducer under a harmonic excitation. The system of equations that govern this analysis is:

$$\begin{bmatrix} K_{uu}^{MN} - \omega^2 M^{MN} & K_{\phi u}^{MN} \\ [K_{\phi u}^{MN}]^T & K_{\phi\phi}^{MN} \end{bmatrix} \begin{bmatrix} U \\ \phi \end{bmatrix} = \begin{bmatrix} P^M \\ -Q^M \end{bmatrix} \tag{3.3.10}$$

Abaqus estimates operating amplitudes, stress and strain within the transducer under specific BCs defined by the user. Linear dynamic operating conditions of the transducers are obtained by simulating the inverse piezoelectric effect of the piezoceramic. The excitation is applied during this step through the BCs of the piezoceramic disc. These BCs correspond with a potential difference applied across the disc in the polarisation direction, in this case the thickness direction of the piezoceramic [147]. When simulating dynamic behaviour, the damping effect must be considered in order to obtain accurate results. In Abaqus two different forms of damping are supported: material damping, that is due to material properties, and 'global damping' that introduces uniform structural damping to the model. Both damping parameters are defined through Rayleigh damping.

Rayleigh damping is defined by the equation [148]:

$$C = \alpha M + \beta K \tag{3.3.11}$$

where C is the material damping matrix, M is the material mass matrix and K is the material stiffness matrix. α and β are the mass multiplication factor and the stiffness multiplication factor respectively. They are determined through the damping ratio (ζ):

$$\zeta = \frac{\alpha}{2\omega} + \frac{\beta\omega}{2} \tag{3.3.12}$$

Rayleigh damping can be divided, therefore, in two damping constants. From the damping ratio formula it can be observed that the influence of the α component decreases as the frequency increases, resulting in β being the dominant component. Due to the high frequency of the cymbal transducer, it can be assumed that the effect of the α component is negligible, therefore, the expression for Rayleigh damping is a viscous damping determined by the β component:

$$\beta = \frac{1}{\omega Q_m} \tag{3.3.13}$$

where ω is the angular frequency and Q_m is the mechanical quality factor.

3.3.4 FE model of a cymbal transducer

The FE model of the cymbal transducer created in Abaqus is shown in Figure 3.9. The model is constituted of four parts with three different material properties; the piezoceramic disc, epoxy layer and metal end-cap.
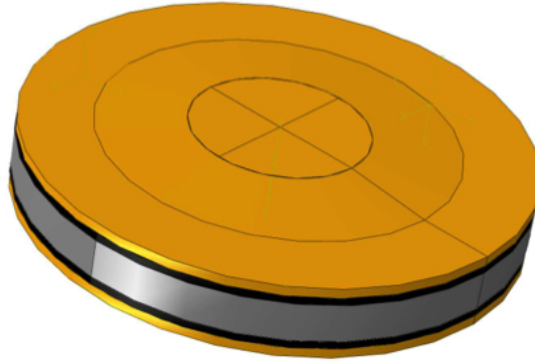
Figure 3.9: The cymbal transducer modelled in Abaqus

The cymbal transducer shows symmetry along the axial plane. This particularity would allow analysis by creating a 2D model using axisymmetric elements. The use of an axisymmetric model significantly reduces the computation time and memory required. In the following chapters, different models of ultrasonic cymbal transducers coupled with surgical vibrating blades will be studied. The introduction of theses blades will remove the symmetry of the model, therefore it is necessary to use a 3D model. In order to maintain consistency, a 3D model of the cymbal transducer was analysed.

Material properties

For FE models, it is necessary to specify the properties of the materials of the different parts. The specification of material properties in the FE software depends on the nature of the material, for example if it is an isotropic, orthotropic or anisotropic material, it is necessary a different material properties in order to defined completely its behaviour [147].

The cymbal transducer is constituted of three different materials; a piezoelectric ceramic that is an anisotropic material, which means that its mechanical, piezoelectric and dielectric parameters are directionally dependent, and an epoxy and metal that are isotropic materials, where their parameters are directionally independent. For the modal and dynamic analysis, the properties of the materials that Abaqus requires for the metal and epoxy parts are the mechanical elastic properties, represented by the Young's modulus and Poisson's ratio and

the general mass properties represented by the material density [147]. With these parameters it is possible to define completely the mechanical properties of the materials since, in the case of the cymbal transducer, the dielectric properties of the epoxy layer and the end-caps are assumed to be negligible. These properties were listed in Tables 3.3 and 3.4.

In the case of the piezoelectric ceramic, in order to define the coupling between the electrical and mechanical properties of piezoelectric materials, the mechanical (density and elastic), the dielectric and the piezoelectric parameters must be defined. As mentioned previously, piezoelectric ceramic is an anisotropic material, therefore the elastic, dielectric and piezoelectric parameters are directionally dependent. In Abaqus, to define completely a piezoelectric material as anisotropic, it is necessary to introduce 21 elastic parameters, 18 piezoelectric constant (since the model corresponds to an actuator, the piezoelectric constant required is the piezoelectric strain constant d) and 6 dielectric parameters [147]. However, since a piezoelectric disc poled in the thickness direction has cylindrical symmetry, the number of elastic, dielectric and piezoelectric constant can be significantly reduced, as was shown in equation 1.4.11. With this assumption the material is orthotropic, in which the material properties are dependent on three mutually perpendicular symmetry planes. The properties of the piezoelectric materials used for the modelling of the cymbal transducers were listed in Table 3.1.

BCs of the model of a cymbal transducer

In the numerical model of the cymbal transducer, the BCs correspond with electrical potential. These BCs are applied to the piezoceramic disc creating a differential of potential between each face. In Abaqus, either for the dynamic or modal analysis, the electric potential degree-of-freedom must always be constrained at least at one node to remove singularities from the dielectric part of the element operator [147].

Mesh selection and convergence of cymbal transducer

For analysis where dynamic or modal behaviour of vibrating systems are investigated, quadratic interpolation elements should always be used to ensure accurate results and real mode shapes. In Abaqus the element used for the design of the 3D model of the cymbal transducer was the 20 node brick named C3D20R [147].

This element is a continuum solid element in which for stress-displacement analysis, the DOF corresponds with displacements calculated in the x, y, and z directions at each node.

The results are then extrapolated to all the nodes of the element by quadratic interpolation. For the design of a piezoelectric transducer this kind of element is used for the discretisation of isotropic elements, so that in the case of the cymbal transducer the metal end-caps and the epoxy layer are discretised using C3D20R. In the case of the piezoelectric elements it is necessary to consider both displacement and electric potential DOFs. In the Abaqus element library, the relevant continuum solid element with quadratic interpolation is the C3D20RE.

The model of the cymbal transducer after the creation of the mesh is shown in Figure 3.10. In order to discretise each part with the same type of element, the geometry was simplified dividing parts with a complex shape such as the end-cap, that contains corners, in parts with a much simple geometry in order to allow Abaqus creates automatically an uniform mesh with the same type of element. After meshing each part individually, during the assembly process all joined surfaces were governed by appropriated constrain conditions using the constraining option 'Tied' .
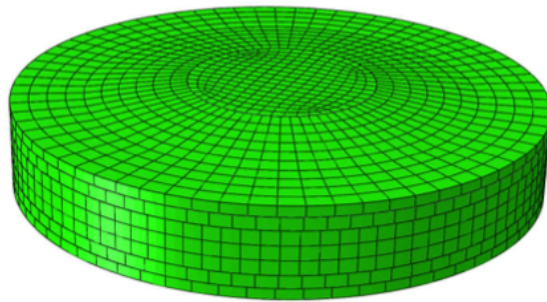
Figure 3.10: Mesh selection for the cymbal transducer model

Accuracy of results extracted from a FE analysis is affected by the element selection and the mesh density. A dense mesh produces a more accurate solution, however, as the number of nodes is increased the computational time and cost is increased. Therefore a balance must be achieved between accuracy and computing cost.

In order to determine the most efficient mesh density, a convergence test was conducted to determine the mesh size, from which a finer size does not result in a better approximation. For that purpose, to assess if the number of elements contained in the mesh used to model the cymbal transducer is high enough, mesh density with respect to the first resonant frequency convergence has been investigated. The results are shown in Figure 3.11.
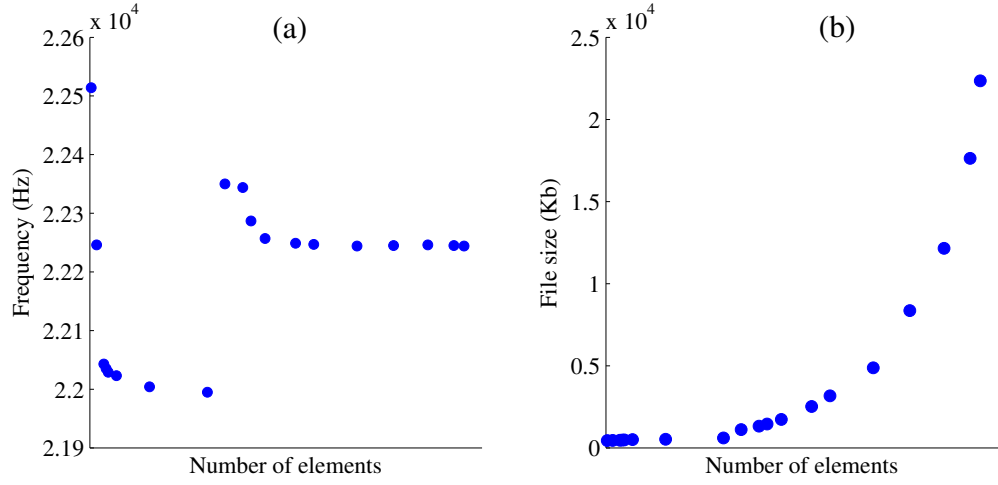
Figure 3.11: (a) Convergence of resonance frequency and (b) convergence of the size of the output file for different numbers of elements in the mesh

For a cymbal transducer it is not possible to calculate the resonance frequency accurately from an analytical model, due to the complexity of the flextensional motion of the end-caps. Researchers have previously utilised analytical methods, derived from shallow shell theory, to investigated the principal parameters that govern the fundamental resonance frequency of the transducer [142]. Equation 3.3.14 shows the proportional relationship of the resonance frequency in air with different end-cap parameters.

$$f_r \propto \sqrt{\frac{Y}{\rho_c}\left[\frac{1}{C_d(1-\sigma^2)}+\frac{1}{R^2}\right]} \tag{3.3.14}$$

where, ρ_c is the end-cap material density, C_d is the diameter of the cavity at its base, R is the end-cap radius, Y is Young's modulus of the end-cap, and σ is Poisson's ratio. This means that the validation of the results obtained from the FE modal analysis must be conducted by comparison with experimental analysis.

3.4 Experimental analysis of the cymbal transducer

The design of an ultrasonic transducer is divided in two complementary processes. The first process consists of an approximation of the transducer and calculation of its dynamic behaviour through analytical and/or numerical analysis. The low cost and time required to obtain accurate results provides essential information for the development of the first prototype. Despite the significant accuracy of the analytical and numerical models, it is

impossible to consider all the parameters that affect the behaviour of the real transducer. There are three different sources of uncertainty during the construction of an ultrasonic transducer: uncertainty of material properties and manufacturing tolerances, uncertainty during the fabrication process and uncertainty due to the boundary conditions in its operational mode. The second process is therefore the execution of a series of experimental analysis whose results, obtained under real operation conditions, are employed to validate and/or update the analytical and numerical models, as shown in the Figure 3.12. The correct feedback between processes determines the success of the development of the transducer.
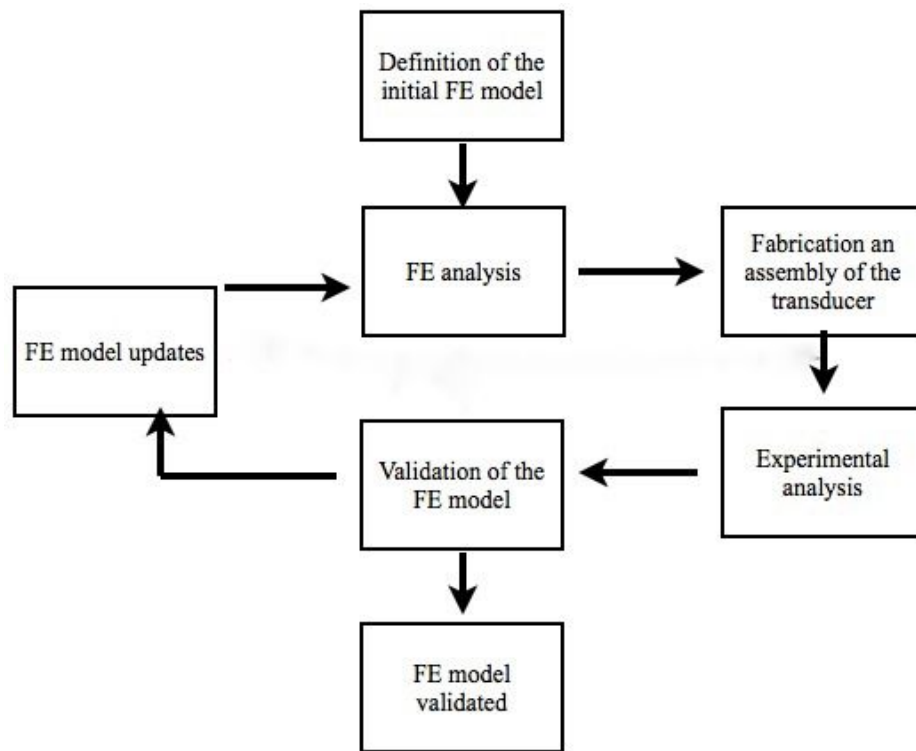
Figure 3.12: Design process for ultrasonic transducers

Due to the small dimensions of the cymbal transducer, the uncertainty of the manufacturing tolerances of the different parts, in particular small variations on the dimensions of the end-caps, affect significantly the response of the transducer. Therefore, before the assembly process and experimental analysis it is necessary to update the FE model with the real dimensions. However the most important source of uncertainty is due to the fabrication process. As explained previously, during the assembly process of the cymbal transducer it is difficult to control the deposition of the epoxy layer in order to avoid leaks into the cavity. Any asymmetry, due to differences on the epoxy layer on both end-caps, will be hidden by

the metal end-caps, this prevents to update the FE model with more accurate geometries. For these reason, for the validation of the FE model it is necessary to compare the results of several cymbal prototypes.

In this thesis three different types of experimental analysis were performed to characterise the electrical, modal and dynamic parameters of the cymbal transducers. Electrical impedance analysis is used to measure the electrical impedance frequency spectrum of the devices. This information is useful to calculate the resonance (f_r) and antiresonance (f_a) frequency for each mode of vibration, and hence, the effective coupling coefficient k_{eff}, that is the amount of electrical energy converted to mechanical energy, associated with each mode of vibration. The characterisation of the impedance spectrum, in the operating frequency range, is important to match the input impedance of the transducer with the output impedance of the power supply in order to avoid losses, and even critical damage, due to mismatching between transducer and power supply.

The modal parameters are extracted through of an experimental modal analysis (EMA). With this analysis it is possible to determine the resonance frequencies and the mode shapes over a selected frequency bandwidth. The extracted data is used to validate the FE model and the success of the fabrication process. The third experiment consists of an harmonic analysis, which is used to characterise the dynamic response of the transducer. In this analysis, the output response of the transducer (displacement of the end-cap) is measured with respect to a specific input signal at different excitation levels. The results extracted are used, in the first place, to update the damping coefficients of the FE model, and to validate the predictions when analysing transducers based on modifications of the original model.

3.4.1 Electrical impedance analysis of the cymbal transducer

The electrical impedance analysis was performed to investigate the frequency response of the cymbal transducer in a broad frequency band. The bandwidth was selected to include the principal modes of vibration of the transducer. For that purpose, an impedance analyser, Agilent 4294A, was used to excite the transducers and measure their electrical impedance and phase angle between voltage and current. By analysing the electrical impedance spectrum of an ultrasonic device, it is possible to observe the resonance and antiresonance frequencies of the different modes of vibration, with the assumption that a mechanical resonance frequency correspond with a minimum in the electrical impedance spectrum, and a mechanical antiresonance frequency with a maximum. To calculate the electrical impedance

a swept signal with a low excitation level, 0.5 V_{pp}, to guarantee that the minimum and maximum values on the impedance spectrum correspond with the mechanical resonance and antiresonance frequency, was applied to the transducers over a selected bandwidth. The experimental setup is shown in Figure 3.13.
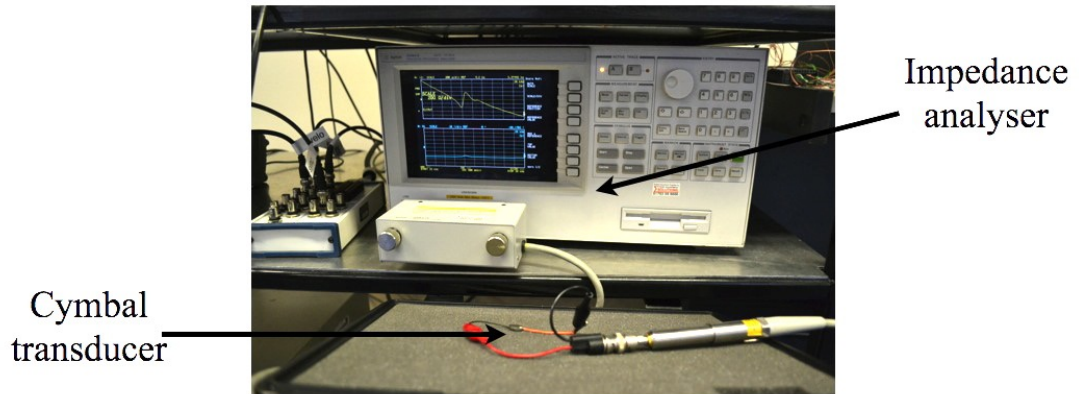
Figure 3.13: Experimental setup for the electrical impedance analysis

To ensure the validity of the results, before each measurement the test probe of the impedance analyser (PROPE 42941A) was calibrated using two loads: 0Ω load (short load, Agilent HRM 504) and a 50Ω load (Agilent HRM 601).

The electrical impedance analysis was also used to investigate the symmetry of the cymbal transducer after the assembly process. In the first resonance mode, the cavity resonant mode of the cymbal transducer, both end-caps vibrate symmetrically in a perfect flextensional motion of the cavities, as shown in Figure 3.14 a). However, approximately 80% of fabricated cymbal transducers exhibit in the impedance response a double peak instead of a single resonance frequency [143,149]. This is because of asymmetries in the cymbal transducer, due to differences in the geometry of the metal end-caps or differences in the epoxy layer. Each frequency corresponds with the cavity resonant frequency of each end-cap, but one frequency is associated with the cavity resonant mode, where both end-caps vibrate out-of-phase, and the second frequency is associated with the asymmetric mode where both end-caps vibrate in-phase, as shown in Figure 3.14.
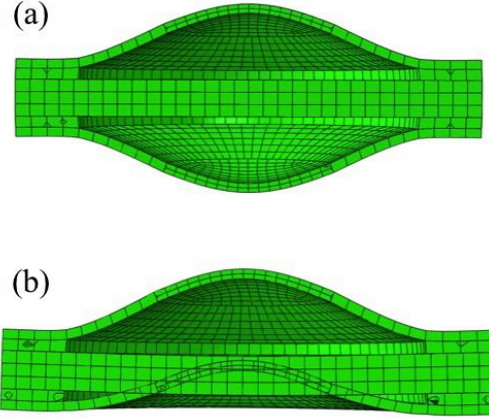
Figure 3.14: Mode shape of the (a) symmetric cavity resonant mode and (b) asymmetric mode of the cymbal transducer

From the impedance spectrum, the resonance and antiresonance frequencies of the cavity mode were measured to calculate the mechanical coupling factor k_{eff}. As mentioned previously, k_{eff} is an indicator of the amount of electrical energy that is transformed into mechanical energy, and is therefore related to the mechanical losses and efficiency of the device. The mechanical coupling factor can be calculated from the relationship between the frequencies of resonance, f_r, and antiresonance, f_a, given by the equation [150].

$$k_{eff} = \sqrt{\frac{f_a^2 - f_r^2}{f_a^2}}$$

(3.4.1)

The results of the impedance analysis measurements and the value of k_{eff} for the cymbal transducers with different end-cap materials are presented in Figure 3.15 and Figure 3.16.
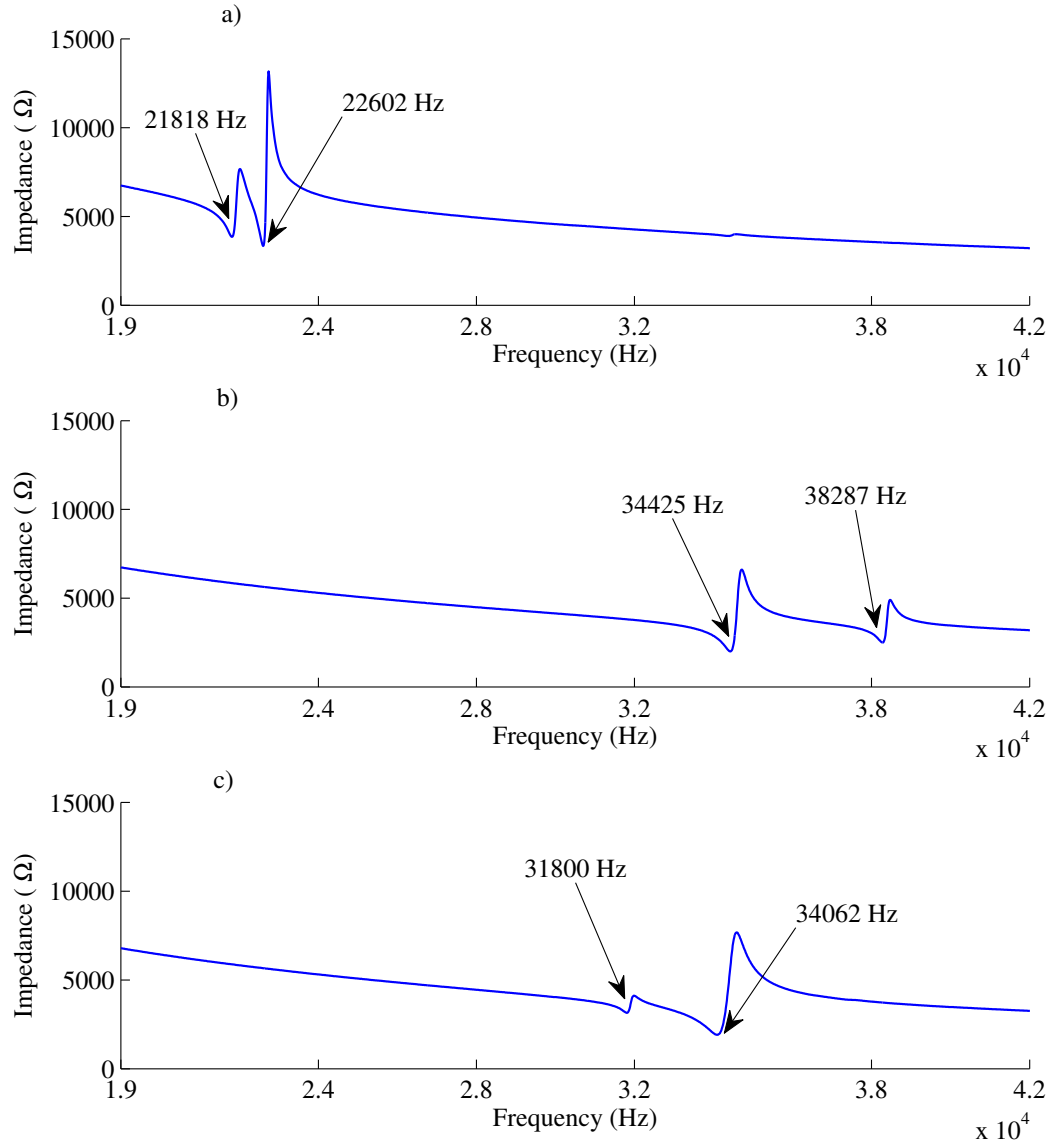
Figure 3.15: Electrical impedance spectra of the cymbal transducer with (a) brass end-caps, (b) steel end-caps and (c) titanium end-caps

The impedance analysis measurements show the existence of a double peak in the three transducers. Measurements of the end-cap geometries showed a high level of accuracy and symmetry, therefore the two resonance frequencies of each transducer are due to irregularities introduced during the fabrication process. Since all the end-caps were well aligned with the ceramic during the curing process, the cause of this asymmetry is mainly due to

nonuniformity in the epoxy layer. As mentioned previously, each resonant peak corresponds with a different resonant mode: symmetric cavity resonant mode and asymmetry mode. In the three transducers the symmetric cavity resonant mode coincides with the frequency peak with the lower impedance value. Since the electrical impedance can be related to the mechanical impedance of the transducer, this shows that the maximum energy generated by the transducer is, in the three cases, delivered at the symmetric cavity resonant mode, despite the different asymmetries presented in the transducers. In the case of the brass and titanium cymbal transducers the symmetric mode corresponds with the second peak, while in the case of the steel cymbal with the first. The orders of the frequencies of the cavity modes depends on parameters such as the dimension of the transducer, type of end-cap material and the level of asymmetry developed [143].
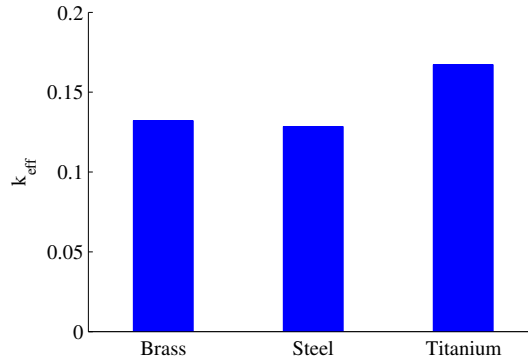
Figure 3.16: k_{eff} values for the cymbals with brass, steel and titanium end-caps

The results of the measurement of the k_{eff} parameter shows that the higher value obtained for the titanium cymbal transducer corresponds with a device with less mechanical losses, and therefore higher value of the quality factor, Q_m, and efficiency. In transducers with the same geometry, the mechanical losses differ depending on the material used. Relatively light alloys such as aluminium and titanium exhibit lower losses than heavier ones such as brass, steel and tungsten, therefore the results obtained are consistent with the values expected.

3.4.2 EMA of the cymbal transducer

Introduction to EMA

EMA is an experimental procedure to determine the modal parameters, natural frequencies, mode shapes and damping factors, of a vibrating structure. This experimental technique approximates the modal behaviour of real structures, which are continuous systems with

infinite DOFs, by means of a discretisation of the geometry which considers a finite number of DOFs, in order to accurately estimate the modal parameters.

Real structures can often be modelled as an assemblage of many single degree of freedom (SDOF) systems represented by the basic model shown in Figure 3.17. The differential equation of motion which governs this system is given by equation 3.4.2 [151].
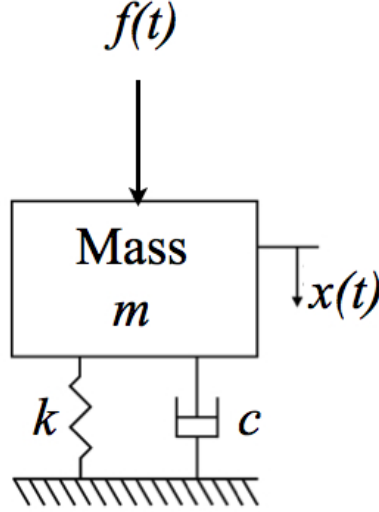
Figure 3.17: System with a single degree of freedom

$$m\ddot{x} + c\dot{x} + kx = f(t) \tag{3.4.2}$$

where $m\ddot{x}$ is the inertial force of the structure, $c\dot{x}$ is the damping force of the structure and kx is the stiffness of the structure, while $f(t)$ and $x(t)$ are the harmonic input force and displacement response quantities respectively of the structure.

The definition of the frequency response of a system can be established as the function that relates the input signal and the output signal of the system. This function defines the frequency behaviour of the system independently from the input signal. The frequency response function (FRF) is obtained by dividing the output signal by the input signal in the frequency domain. For that purpose, both signals, that are recorded in the time domain, are transformed into the frequency domain using a fast Fourier transform (FFT) algorithm.

$$f(\omega) \times H(\omega) = x(\omega)$$
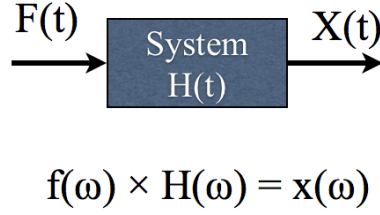
Figure 3.18: Relationship between the input and output signal in a system

With this definition, in the system with a SDOF the FRF could be defined in terms of the compliance of the system $\alpha(\omega)$, since it is the ratio between output displacement, $x(\omega)$, and the applied input harmonic force, $f(\omega)$ in the frequency domain. Solving the equation of motion of the system, the FRF $(H(\omega))$ becomes:

$$\alpha(\omega) = H(\omega) = \frac{x(\omega)}{f(\omega)} = \frac{1}{(k - \omega^2) + j(\omega c)} \qquad (3.4.3)$$

Depending on the output variable measured, it is possible to calculate the FRF of the system using the displacement $x(\omega)$, velocity $v(\omega)$ or acceleration response $a(\omega)$. Therefore the FRF and its inverse can be:

- $C = (d / F)$

- $M_b = (v / F)$

- $R_c = (a / F)$

- $D_s = (1 / C)$

- $Z_M = (1 / M_b)$

- $D_m = (1 / R_c)$

In EMA the real structure is sampled spatially with a grid of points, considering each point as a sub-system with a SDOF. When the structure is excited, the output response is recorded at each grid point to extract the corresponding FRF. Real structures have multiple number of DOFs, and multiple number of modes. However in the experimental process only a limited number of FRFs can be measure. The density of the grid of points must be sufficient in quantity and situated at the right locations to ensure that it is possible to identify every mode shape within the range of interest.

Excitation signals

Depend on the excitation method, there are two different vibration measurement techniques: ambient and forced. The ambient vibration technique, commonly known as operational modal analysis (OMA) uses the ambient vibration of the structure as the input signal. Usually, the ambient vibration is measured in one fixed point on the structure that becomes the reference point. This method is used to study large structures such as bridges or buildings to yield the resonance frequencies and possible fractures or weak regions from the analysis of the measured signals.

The forced vibration technique uses an excitation signal, externally applied, to measure the structural response of the structure. The input signal used to calculate the FRF can be from three main types: periodic, transient and random. The most representative signals within these three groups are the swept sine, impulse and noise signal respectively. The principal characteristic of these signals is that all frequencies, within the range of interest, are excited with the same level of energy. This is the principal requirement in order to obtain a correct FRF. The excitation force can be applied by a number of different mechanisms such as a hammer or an electromagnetic shaker [152].

The signals commonly used to excite ultrasonic systems for determining modal parameters are swept sine and true random. The true random signal must be used in combination with spectrum averaging in order to remove the possible noise generated in the structure. On the other hand, since the true random signal is a non-periodic signal, a special time domain window is used during the sampling process for the calculation of the FFT.

Boundary conditions

The structure can be subjected to different boundary conditions which are either free or grounded conditions. The selection of the boundary conditions in EMA will affect significantly the outcome of the experiment. Under real experimental conditions, the state of free boundary conditions is approximated by supporting or suspending the structure by soft elastic material, such as soft spring or elastic strings, in order not to affect significantly the stiffness and thus the modes of vibration of the structure [152].

In the case of the cymbal transducer, which weighs only few grams, it is necessary to use unrestrained supports. For that purpose, the device was suspended by the two wires connected to each end-cap. Since the small diameter, 0.213mm, of the wires do not introduce a significative variation on the stiffness of the structure, the cymbal transducer is free to

vibrate without restrictions, as shown in Figure 3.19.
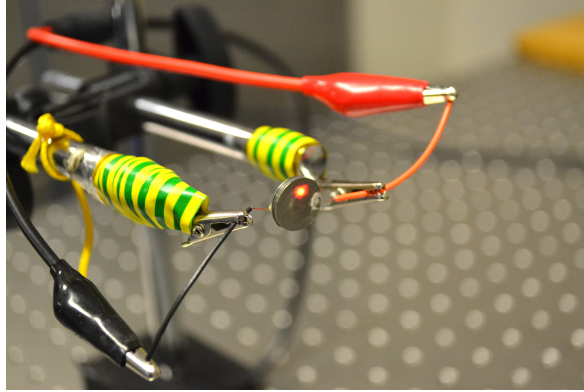
Figure 3.19: Cymbal transducer suspended by the wires

Measurement devices

There exists two different methods to measure the response of the structure at each point of the selected grid, using contact or non-contact devices. Contact devices such as force transducers, accelerometers and impedance heads, need to be attached firmly to the structure in order to measure the output signal. The attachment of the measurement device results in the addition of a mass loading to the structure at each point and will also introduce damping and stiffness errors. These errors are particularly significant for small structures.

Non-contact methods include laser Doppler vibrometers (LDV), ultra-high speed cameras and speckle interferometers. The principal advantage of these optical devices over contact devices is that they are non-invasive, therefore there is not an alteration of the mechanical properties of the structure. These instruments are employed for the measurement of ultrasonic devices due to the small dimensions of the devices and the high frequency range of the vibration modes [152].

Signal processing

The process of extraction and display of the FRF of the measured data is realised by a spectrum analyser that digitises and transforms the time domain signal to the frequency domain using the FFT method.

Prior to digitising the analogue signal, they are conveniently filtered to avoid aliasing of high frequency signals into the range of frequency of interest when processed by the FFT. This process is followed by the digitising of the filtered signal by an analogue to digital converter (A-D). During the process of digitising, the signal is sampled for a discrete number

of n-values per period of time, T. The sampling rate must be selected carefully to cover the frequency range of interest. Therefore, the higher the frequency the higher the number of samples required per period of time.

The spectrum analyser transforms the sampled signal from the time domain to the frequency domain using the FFT. This process is calculated over a discrete period of time, therefore problems can appear when processing random signals which are non-periodic. These problems, known as leakage, causes distortion of the results in the frequency spectrum when one single frequency can be related to multiple frequencies. To reduce this effect the signals are sampled using special time domain windows that are weighting functions. These functions generate a periodicity on the randomly sampled signal, allowing the spectrum analyser to calculate the FFT. There exist different windowing functions available to discretise the time domain signals such as rectangular, Hanning and exponential. For steady state periodic and random signals, the Hanning window is preferred [153].

When windows functions are used to discretise the signal sequentially, part of the data, generally situated at the boundary between windows, can be ignored, creating the possibility that important data is omitted during the analysis. In order to overcome this problem, an overlapping technique is used while the window function is applied to start sampling before the previous record has finished, thus avoiding any loss or discontinuity of data. However, overlapping can alter the statistical properties of the collected data as it is possible for data points from one record to appear in the following record. This can be solved using a data averaging process. In the averaging process a number of individual records will be compared and averaged according to a specific technique such as peak hold, exponential or linear. This ensures that the results obtained are statistically reliable and removes random noise from the signals. The EMA realised in the present work utilised a sample frequency of the spectrum analyser of 204.8kHz and 51200 spectral lines, giving a resolution of 1.56Hz over a frequency range of 0-80kHz [153].

Once the response at each point of the grid is measured and its FRF is calculated, the EMA of the whole structure provides a set of FRFs, three per point with a 3D LDV. To calculate the modal parameters from the measurement data, the FRFs are fitted using a curve-fitting process creating a single FRF function. This process is realised using specialist modal analysis software. For this thesis the software used was MEScopeVES, Vibrant Technology Inc.

Experimental setup

The setup of the experiment is shown in Figure 3.20. The cymbal transducer was excited using a random excitation signal, generated by the data acquisition hardware Data Physics Quattro DP240 and amplified by a power amplifier, QSC Audio RMX 4050HD. The level of the signal was selected in order to obtain an acceptable signal to noise ratio and obtain a clear FRF. The vibration velocity response from a grid of measurement points over the cymbal transducer was measured by using a 3D laser Doppler vibrometer, Polytec CLV 3000. This laser vibrometer measures three vibrational response components, two in plane and one out of plane of the structure surface. Therefore for each point of the grid three FRFs were calculated.
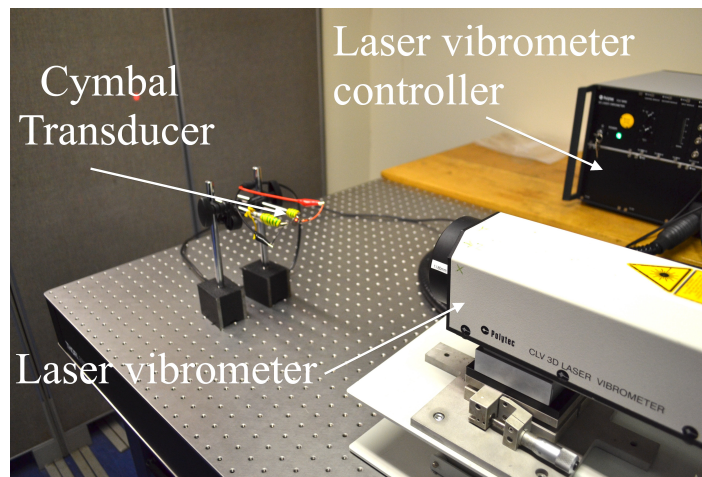
Figure 3.20: Experimental setup of the EMA

The FRFs were calculated and recorded using the Data acquisition software, SignalCalc 240 from Data Physics Corp. [153]. This software also controls the data acquisition hardware Data Physics Quattro, selecting the type of excitation signal, spectral resolution and sample rate. The calculated FRFs were exported to the modal extraction software MEScopeVES, Vibrant Technology Inc, for the curve fitting process and extraction of the mode shapes.

FEA and EMA comparison of the cymbal transducer

The mode shapes calculated from experimental data from the curve fitting process for the cymbal transducers with brass, steel and titanium end-caps are shown in Figure 3.21, Figure 3.22 and Figure 3.23.

(a) EMA: 23115 Hz

(b) FEA: 22244 Hz

(c) EMA: 22017 Hz

(d) FEA: 22966 Hz
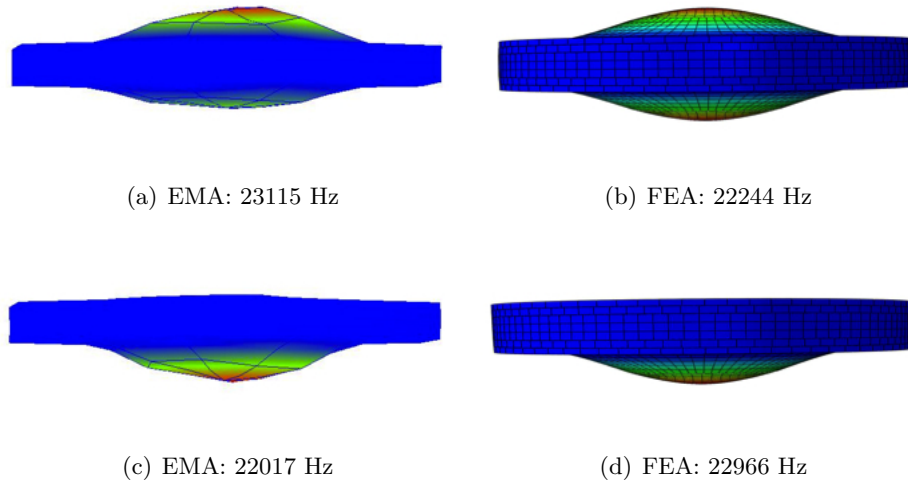
Figure 3.21: Mode shapes from (a), (c) EMA and (b), (d) FEA of the cymbal transducer with brass end-caps for the (a), (b) cavity mode and (c), (d) asymmetric mode

(a) EMA: 34560 Hz

(b) FEA: 31323 Hz

(c) EMA: 38317 Hz

(d) FEA: 32590 Hz
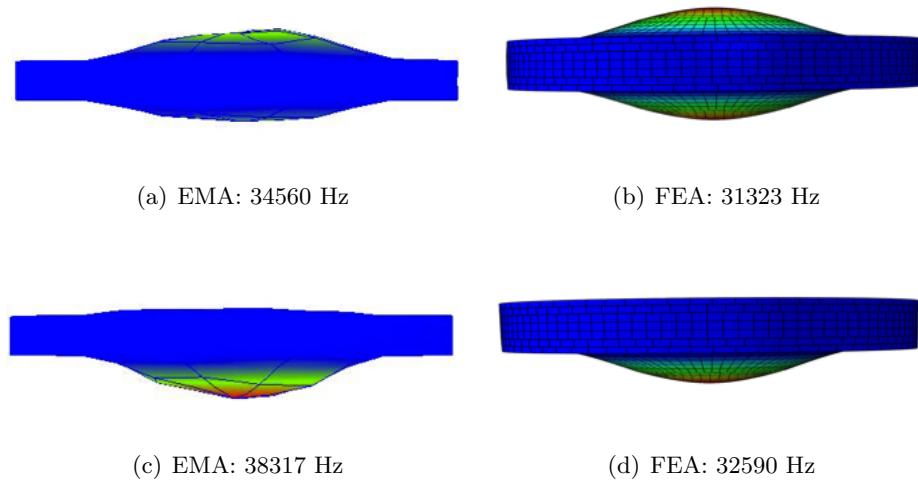
Figure 3.22: Mode shapes from (a), (c) EMA and (b), (d) FEA of the cymbal transducer with steel end-caps for the (a), (b) cavity mode and (c), (d) asymmetric mode

(a) EMA: 35235 Hz · (b) FEA: 34622 Hz

(c) EMA: 31900 Hz · (d) FEA: 34715 Hz
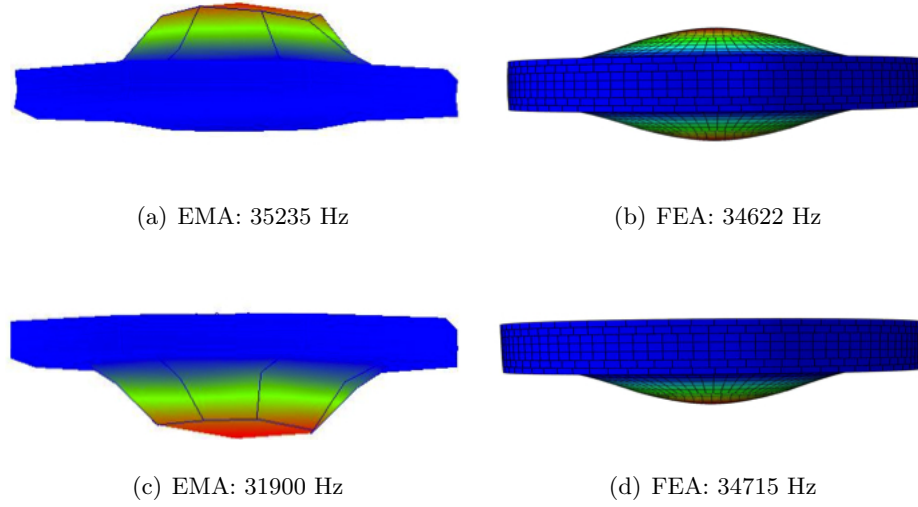
Figure 3.23: Mode shapes from (a), (c) EMA and (b), (d) FEA of the cymbal transducer with titanium end-caps for the (a), (b) cavity mode and (c), (d) asymmetric mode

The EMA mode shapes of the three cymbal transducers show that for each mode of vibration a different end-cap has the dominant motion. Therefore, the asymmetry introduced in the model means that each end-cap has its own resonance frequency. There exists a significant difference in the correlation of the resonance frequencies between the experimental and FE findings. The three cymbal transducers show a measured resonance frequency of the cavity mode that is higher than for the FE model. This can be due to in part to the epoxy deposited in the flange of the end-cap moving into the interior of the cavity, thus reducing the "effective" cavity diameter, and therefore increasing the resonance frequency. The maximum difference in estimating the resonance frequency of the cavity mode appears in the steel cymbal transducer, with a difference of 9.36 %. In the case of the asymmetric mode the differences are higher than those obtained for the cavity mode for the three transducers, reaching 14.9 % for the steel cymbal. In transducers with asymmetry between the end-caps, the difference between the resonance frequency of the cavity mode and asymmetric mode depends on the level of asymmetry introduced. The greater the asymmetry between end-caps the greater the separation of the frequencies.

The main problem in modelling cymbal transducers is the asymmetry introduced during the fabrication process. Since the epoxy layer is totally covered by the end-caps, it is not possible to observe if the deposition was only on the flange of the end-cap, or if there was a leak into the cavity or bubbles in the epoxy, without destroying the transducer. Therefore, despite of the differences between the experimental and numerical analysis data, this suggests that the FE model assumptions as to material properties, interactions and boundaries were

accurate for the cavity mode.

3.4.3 Power harmonic analysis of the cymbal transducer

The harmonic characterisation of the transducer was performed using a frequency sweep method that excites the transducer within a narrow band around the first resonance frequency. This method excites the ultrasonic transducer at a specified frequency for a short period of time using a burst signal of a finite number of cycles with constant voltage. The length of the burst signal is selected to allows the transducer to reach steady state vibration, where the different parameters of, voltage, current, power and output displacement of the transducer are measured. Upward and downward frequency sweeps around the first resonance frequency are performed in order to obtain the harmonic response and identify possible non-linearities of the transducer response in the operation mode. These non-linearities appear as a hysteresis region between the upwards and downwards sweeps. To minimise temperature increases in the piezoceramic, that lead to a frequency shift effect between sweeps, a time delay between bursts was introduced. The setup of the experiment is shown in Figure 3.24.
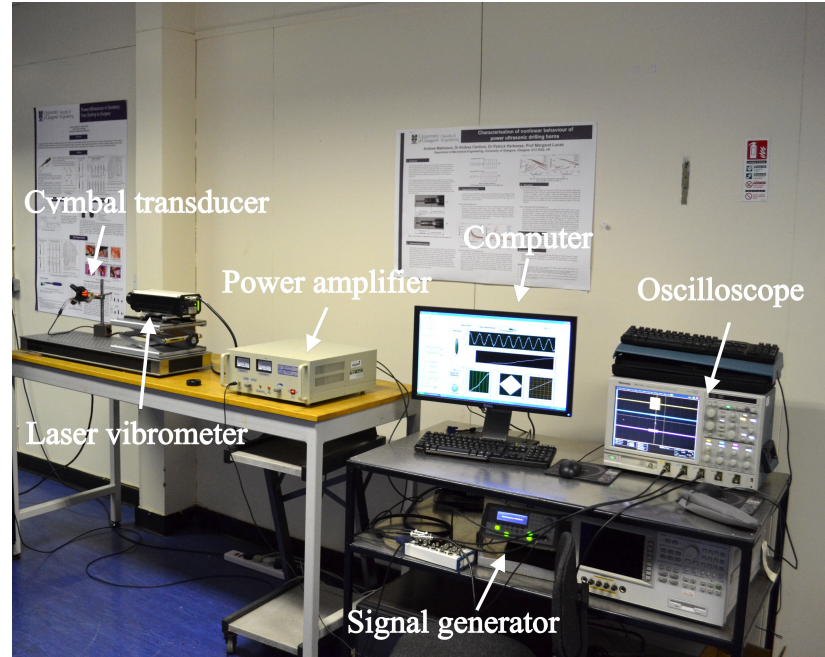
Figure 3.24: Experimental setup for the power harmonic analysis

For this experimental method [152], the burst signal, set up in a Labview program as a RMS voltage, is generated by a function generator, Agilent 33220A, and amplified by a power amplifier, ETS Solutions HFVA-62. The output velocity response of the transducer is measured using a 1D laser Doppler vibrometer, Polytec OFV3001. The input and output

signals are controlled and recorded using National Instruments data acquisition hardware controlled by the Labview program.

The Labview program allows for control of the number of cycles of the burst signal, usually set at a few thousand cycles to ensure that steady state vibration is reached without increasing the temperature of the piezoceramic. After the digitising of the signals, it is possible to omit the first few samples of the signals before analysis, as these correspond with the transient region. This guarantees that the different parameters are measured for steady state vibration. It is also possible to set the frequency range, level of voltage of the burst signal and the delay between bursts.

The measurement data of the cymbal transducers with different end-cap material and excitations levels from 3-15 V_{rms}, for output displacement and power consumed are shown in Figure 3.25, Figure 3.26, Figure 3.27, Figure 3.28, Figure 3.29 and Figure 3.30.
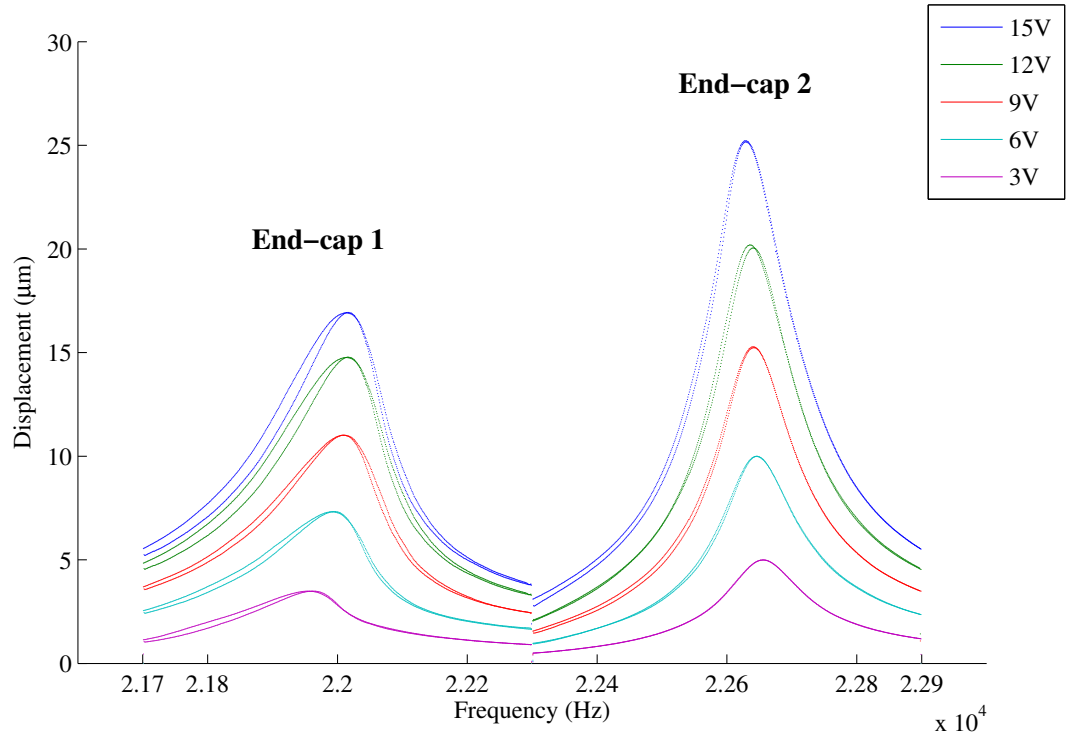
Figure 3.25: Experimental harmonic analysis data for cymbal transducer with brass end-caps
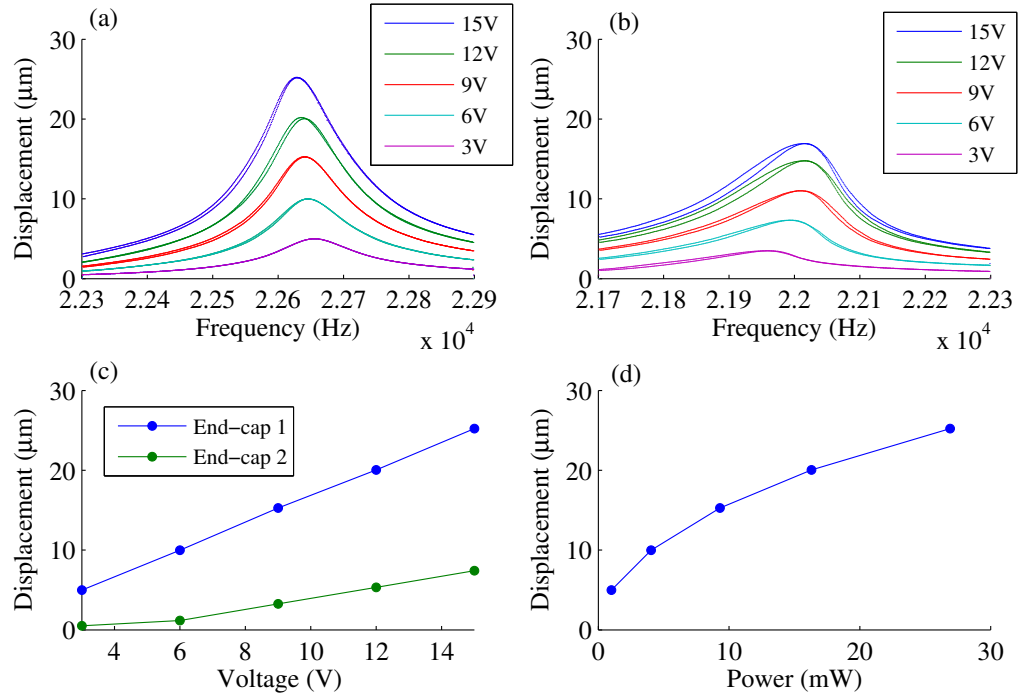
Figure 3.26: Experimental harmonic analysis data for cymbal transducer with brass end-caps. Vibration displacement response of (a) detail of end-cap 2 and (b) detail of end-cap 1, (c) vibration displacement of each end-cap at the cavity mode frequency and (d) power consumed at the cavity mode frequency *vs.* the maximum displacement generated
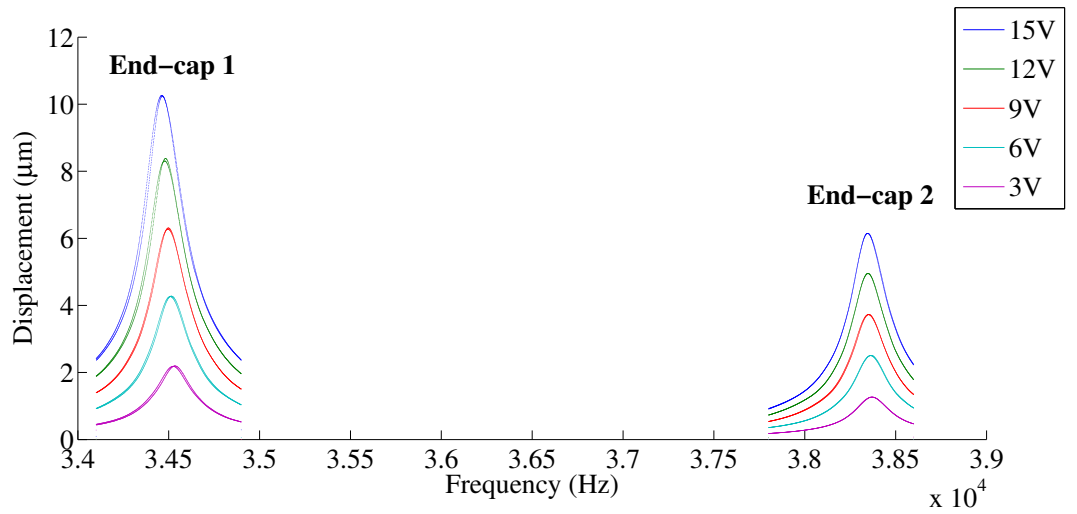
Figure 3.27: Experimental harmonic analysis data for cymbal transducer with steel end-caps
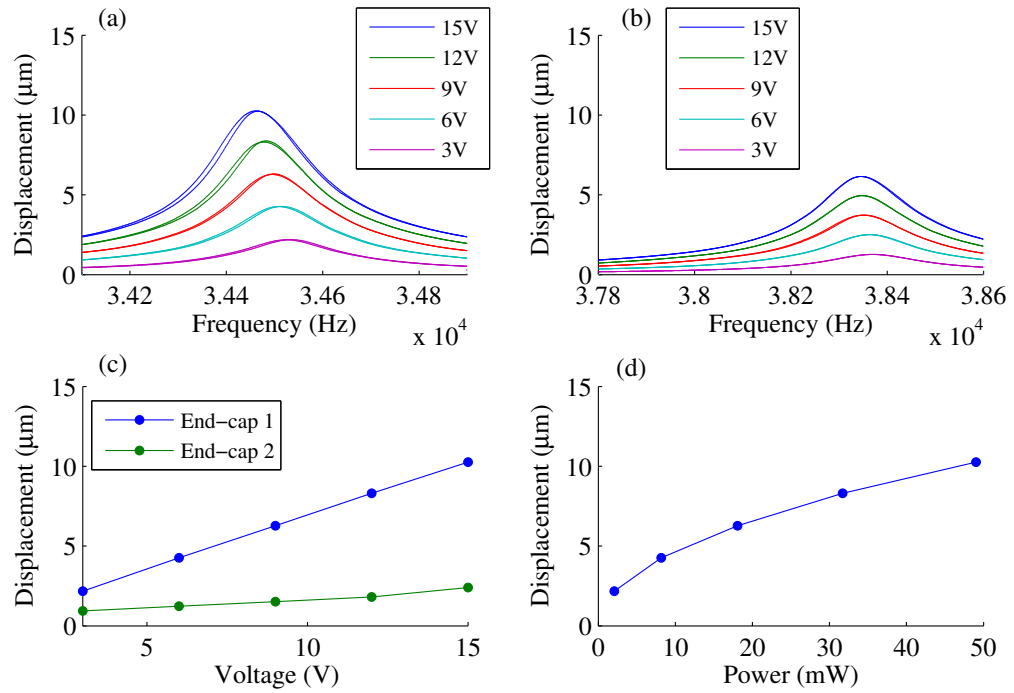
Figure 3.28: Experimental harmonic analysis data for cymbal transducer with steel end-caps. Vibration displacement response of (a) detail of end-cap 1 and (b) detail of end-cap 2, (c) vibration displacement of each end-cap at the cavity mode frequency and (d) power consumed at the cavity mode frequency *vs.* the maximum displacement generated
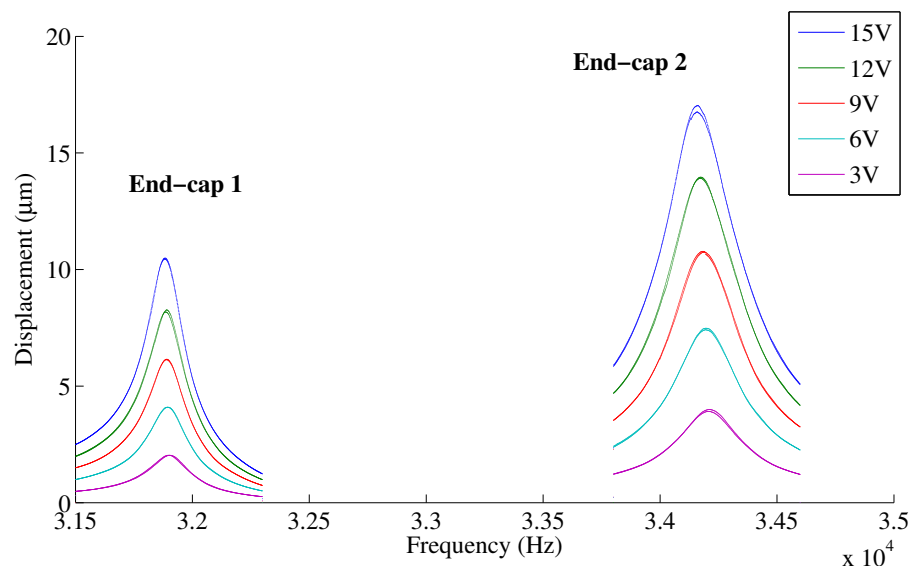
Figure 3.29: Experimental harmonic analysis data for cymbal transducer with titanium end-caps
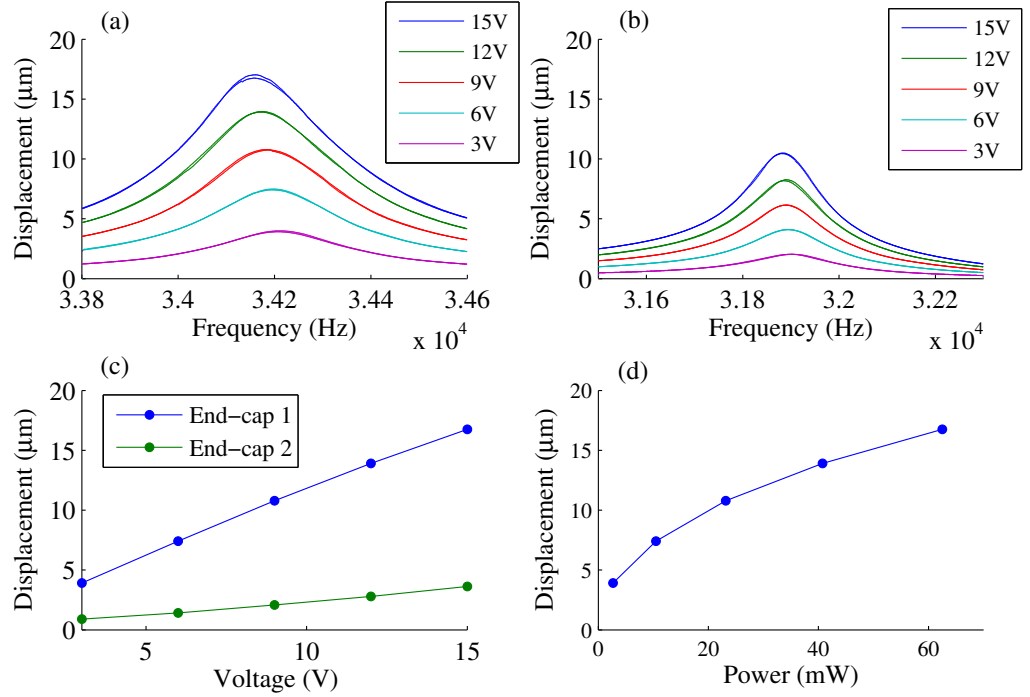
Figure 3.30: Experimental harmonic analysis data for cymbal transducer with titanium end-caps. Vibration displacement response of (a) detail of end-cap 2 and (b) detail of end-cap 1, (c) vibration displacement of each end-cap at the cavity mode frequency and (d) power consumed at the cavity mode frequency *vs.* the maximum displacement generated

From the results obtained it can be observed that, in the three cases, the maximum displacement corresponds to only one of the end-caps, of which has the dominant movement in the cavity mode. However, the difference in displacement between the end-caps at this tuned mode of vibration (considered the operational mode of the cymbal transducer), increases linearly with the level of excitation voltage. This difference in displacement between the end-caps can cause the appearance of bending motion associated with the cavity mode. This undesirable behaviour can considerably reduce the operational life of the transducer, especially when working at high input power levels, due to the degradation of the epoxy layer or the piezoceramic element.

The selection of the end-cap material has a significant influence on the maximum displacement reached. The Young's Modulus of the end-cap material is inversely proportional to the displacement generated by the transducer. In terms of power consumed, the brass cymbal transducer shows a higher efficiency than the steel and titanium one, as shown in

Figure 3.26, Figure 3.28 and Figure 3.30. For example, comparing the power consumed by the brass and steel cymbal to obtain a displacement of 10 μm, the steel cymbal consumes more than 10 times more power than the brass one.

In general a slight shifting of resonance frequency can be noted when the excitation level is increased. This can be related to a non-linear response of the transducer.

The maximum displacement measured experimentally at the cavity resonant mode frequency, and predicted from the FE model, for different levels of excitation, are shown in Figure 3.31.
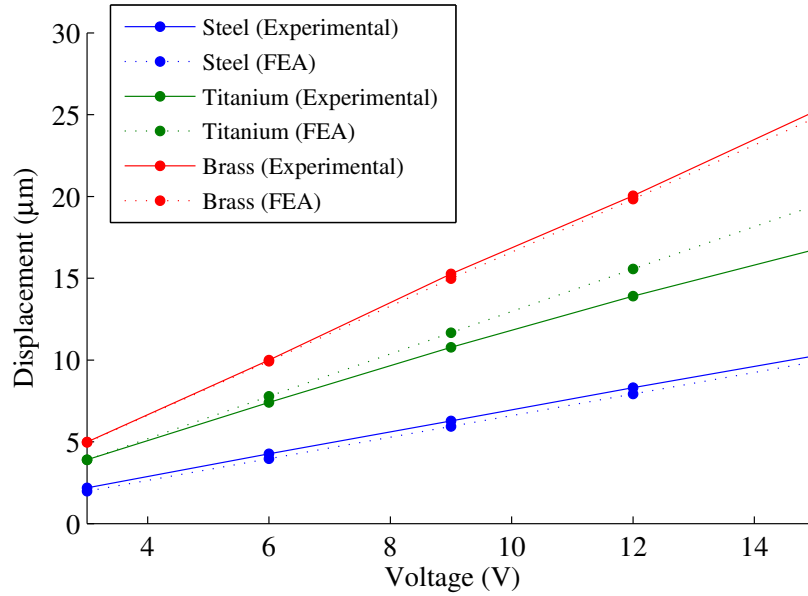
Figure 3.31: Experimental and predicted displacement at the cavity resonant mode frequency for the cymbal transducers with brass, steel and titanium end-caps

The linear dynamic behaviour of the different cymbal transducers was predicted by FEA by simulating different levels of potential difference across the piezoceramic discs in a steady state dynamic analysis step. In order to obtain accurate results in the numerical analysis, a value of global damping, defined in 3.3.13, was introduced in the model. The values of the mechanical quality factor, Q_m, were measured experimentally by using the half power bandwidth formula for frequency response.

There is good correlation between the predicted numerical results and the experimental data, particularly for the case of the brass and steel cymbal transducers.

3.4.4 Evaluation of the response of the cymbal transducer as an actuator

In general, previous research on the cymbal transducer acting as actuator have been focused on the characterisation of the device when subjected to an uniform load on all its surfaces, due to the pressure being applied by the medium in which is driven (usually water). The aim of this section is to study the response of the cymbal transducer as an actuator in air, when different masses are added to the end-caps. For that purpose, steel bars with different lengths were added to the top surface of each end-cap, simulating the action of a mechanical end-effector connected to the transducer, Figure 3.32.
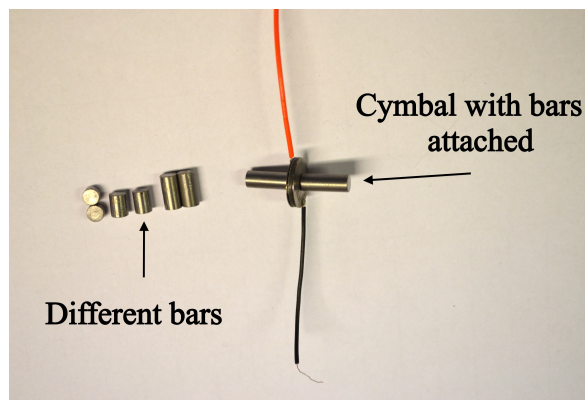
Figure 3.32: Metal bars coupled to the cymbal transducer

The length and mass of the bars are shown in Table 3.6. These bars are not tuned at the resonance frequency of the cymbal transducer, therefore they will act as rigid bodies. As a consequence, the resonance frequency of the device will be affected largely by the mass of the bar attached.

Bar	Longitude (mm)	Base diameter (mm)	Mass (g)
Bar 1	3.00	4.50	0.39
Bar 2	6.00	4.50	0.74
Bar 3	9.00	4.50	1.14
Bar 4	12.00	4.50	1.48

Table 3.6: Dimensions and mass of the bars coupled to the cymbal transducers

Impedance analysis measurements were implemented for each cymbal transducer with different bars, to calculate the change in the cavity resonance frequency and the k_{eff} parameter. The results are presented in Tables 3.7 and 3.8 Figure 3.33.

Bar length (mm)	Frequency (Hz) brass	Frequency (Hz) steel	Frequency (Hz) titanium
none	21818	34425	34062
3.00	8975	17415	11420
6.00	7438	13230	8475
9.00	5442	11375	6610
12.00	5054	9817	5453

Table 3.7: Variation of the resonance frequency of the cymbals with different masses added

Bar length (mm)	k_{eff} brass	k_{eff} steel	k_{eff} titanium
none	0,132	0,167	0,167
3.00	0,223	0,191	0,193
6.00	0,227	0,198	0,213
9.00	0,232	0,178	0,193
12.00	0,217	0,18	0,210

Table 3.8: Variation of the k_{eff} of the cymbals with different masses added
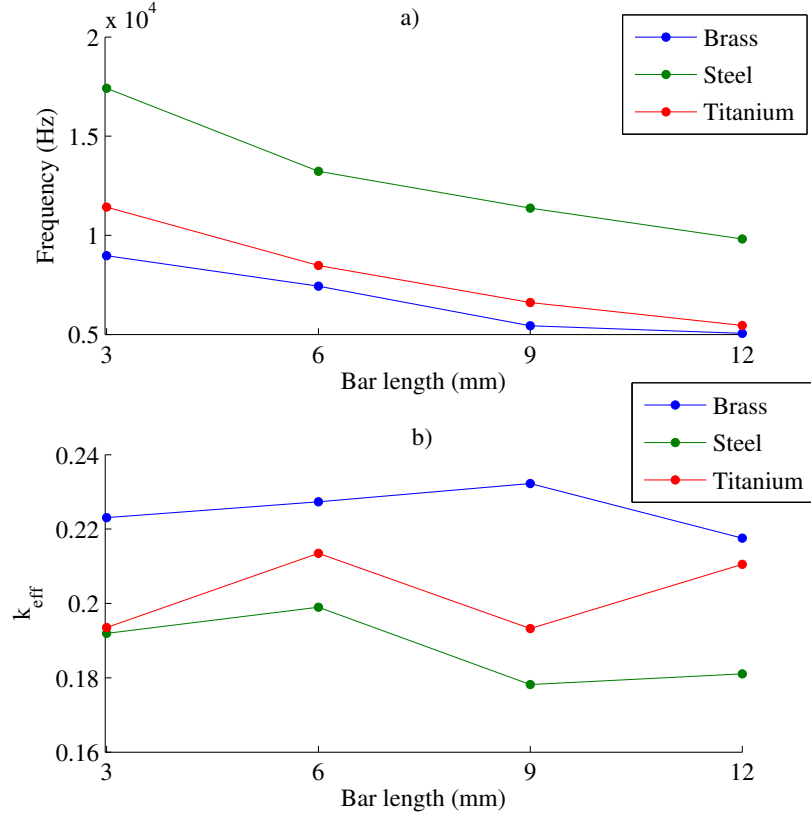
Figure 3.33: Variation of a) the resonance frequency and b) k_{eff} with different masses added

As expected incrementing the mass by adding a bar produces a reduction in the resonance frequency. From Figure 3.33 a) it can be observed that when the 3 mm bar is coupled to the end-cap, the resonance frequency of the cymbal transducer suffers a significant reduction. However, as the mass of the bar is increased, the resonance frequency does not change significantly. The reason for this behaviour is that after the rapid drop of the resonance frequency due to the addition of mass, subsequent increments in the stiffness compensate for the effect of the additional mass. On the other hand, due to the increasing stiffness of the transducer (especially in the epoxy layer), the mechanical losses of the device are reduced, as shown by the effect on the k_{eff} in Figure 3.33 (b) due to a better transmission of the motion from the piezoceramic to the end-caps.

This behaviour is especially important in applications where the insert coupled to the end-cap is not tuned to the frequency of the cymbal transducer. Since a variation of the geometry or mass of the insert does not introduce a significant variation in the resonance frequency of the device across a range of geometries and masses, and therefore in the cavity mode the design of the insert can be treated independent of the transducer.

The dynamic response of the transducers with different coupled bars was studied through power harmonic analysis. Since the cymbal transducers exhibit asymmetry of displacement of each end-cap, the output displacement for each cymbal plus bar combination was measured at the top centre of the bar, which was attached to the end-cap that showed the highest displacement at the cavity resonance frequency for an input voltage of 15V. The values of the displacement are show in Table 3.9 and Figure 3.34.

Bar length (mm)	Displacement (μm) brass	Displacement (μm) steel	Displacement (μm) titanium
none	25,21	10,26	16,76
3.00	2,75	1,72	1,49
6.00	3,18	1,74	1,25
9.00	2,87	1,71	1,35
12.00	2,86	1,76	1,15

Table 3.9: Variation of the displacement of the cymbals with different masses added
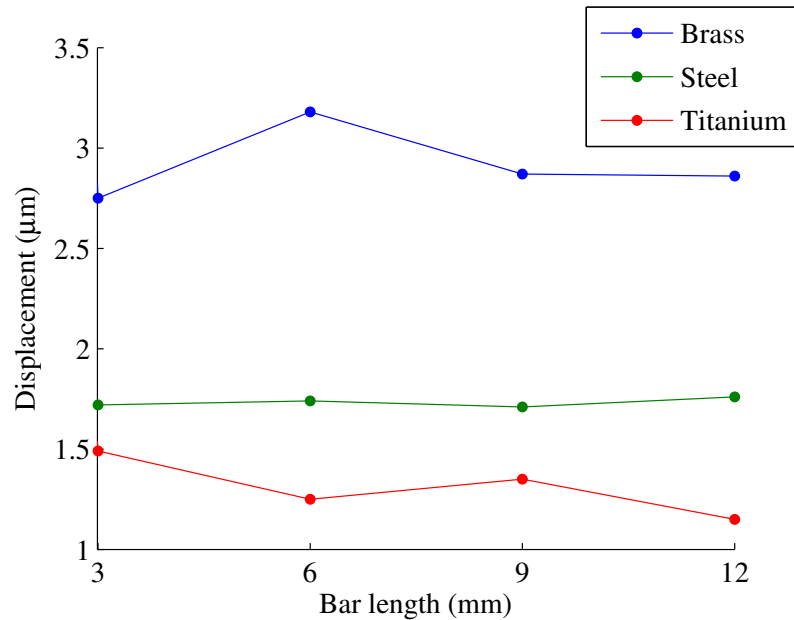
Figure 3.34: Vibration displacement with different masses added for an input voltage of 15V

As can be observed in Figure 3.34, after the initial reduction in displacement, the displacement of the cymbal transducer remains constant when the mass of the bar is increased. This can be explained by the combination of the flexural-axial movement of the end-cap. When the bar is connected directly to the top surface of the end-cap, the displacement of the

device exhibits a pronounced reduction because the motion of the end-cap, in particular the movement of the top surface, is constrained. However, each further increment of the mass of the bar does not introduce an additional constraint on the movement of the end-cap nor on the radial movement of the piezoceramic disc. Therefore the displacement generated in the axial direction is not further reduced, being quasi-independent of the coupled mass.

3.5 Summary

In this chapter the basic design of the cymbal transducer has been investigated. Material selection for the transducer and the assembly process have been discussed and the different numerical and experimental methods used for the characterisation of the modal and dynamic response of the transducers were defined.

The experimental results for the cymbal transducers have corroborated that the devices exhibit large displacements at low input voltage. There is a difference between the numerical and experimental data for the cavity mode frequency due to the appearance of asymmetries introduced during the fabrication process of the transducers. Due to these asymmetries the devices exhibits a non-symmetric motion at the resonant frequency of the cavity. This can cause the appearance of bending motions that can lead to the degradation of the transducer when working at high input power levels.

The characterisation of the cymbal transducer as an actuator has shown promising behaviour when different metal bars have been connected to the end-cap. Working in a non-resonant mode with the different metal bars connected (acting as rigid bodies), slight variations in the geometry of the bar do not introduce significant variation in the resonance frequency of the transducer. The displacement achieved remains constant, largely independent of the mass of the bar connected. This can be an advantage since the design of the coupled insert can be treated somewhat independently of the transducer.

In this chapter the basic design of the cymbal transducer has been investigated. Material selection for the transducer and the assembly process have been discussed and the different numerical and experimental methods used for the characterisation of the modal and dynamic response of the transducers were defined.

The experimental results the cymbal transducers have corroborated that the device exhibit large displacements at low input voltage. There is a difference between the numerical and experimental data for the cavity mode frequency. This is due to the appearance of asymmetries introduced during the fabrication process of the transducers. Due to these

asymmetries the devices exhibit a non-symmetric motion at resonant frequency of the cavity. This can cause the appearance of bending motions that can lead to the degradation of the transducer when working at high input power levels.

The characterisation of the cymbal transducer as an actuator has shown promising behaviour when different metal bars have been connected to the end-cap. Working in a non-resonant mode with the different metal bars connected (acting as rigid bodies), slight variations in the geometry of the bar does not introduce significant variation in the resonance frequency of the transducer. The displacement achieved remains constant, independent of the mass of the bar connected. This can suppose an advantage since the design of the insert coupled can be treated independent of the transducer.

Chapter 4

Cymbal transducer for high power applications

4.1 Introduction

The flextensional class V cymbal transducer has been widely adopted for low power ultrasonics applications, exhibiting high output displacement for low input energy, compared to a single ceramic, when used as an actuator. Despite its performance benefits, the original designs of cymbal transducers have inherent drawbacks for high power ultrasonics applications that require much higher output displacements. Asymmetries introduced during the fabrication process reduce the efficiency of the transducer, and degradation of the bonding layer between the end-caps and the electroactive material can alter the vibration response and ultimately lead to failure.

The two most critical features of the cymbal design, which directly influence the transducer performance, are the cavity dimensions and the thickness of the end-caps [139,154]. The geometry of the end-caps greatly affects the frequency response of the cymbal transducer and even small asymmetries in the epoxy layer or in the end-caps themselves can result in each metal end-cap exciting a different resonant frequency. Therefore, the vast majority of these devices exhibit a double resonance peak in the frequency response, as shown in the previous chapter. Although there are many low-power applications for this type of transducer, cymbals have remained largely undeveloped for high-power ultrasonic applications. One of the primary reasons for this is that the bonding material imposes a limit on the output displacement of the end-caps. For that reason, in order to obtain higher output power (generally high output acoustic power), designs have been focused on the development of

arrays of cymbal transducers. Previous studies have shown that when the device is driven at high power levels, degradation in the epoxy layer can occur due to high stress concentrations and this can significantly reduce the operating life of the device [144]. Depending on the quality of the mechanical coupling between the piezoceramic disc and the end-caps, which is a constraint dictated by the adhesion of the applied bonding agent, an amplitude limit exists after which the device loses functionality.

The displacement of the end-caps in a cymbal transducer is generated by the combination of a flexural and rotational motion. Due to its geometry and operational mode, there are consequently regions in the end-cap which are subjected to high stress. These areas are critically at the edge of the cavity, and therefore in regions of the epoxy layer in contact with the end-caps [144, 145], in form of a critical loading mode, cleavage. Figure 4.1 shows the displacement maxima of the expansion half-cycle as predicted by a finite element model run in Abaqus, and the resulting stress distribution on the surface of the end-caps when driven at the cavity resonance frequency.
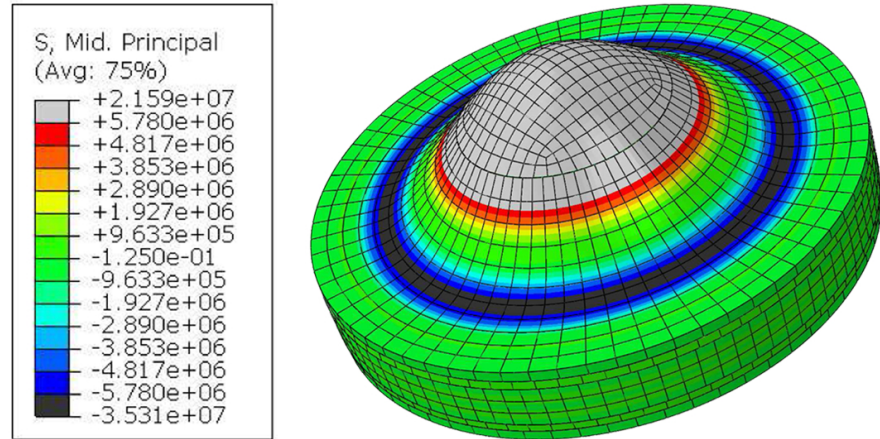
Figure 4.1: Stress (units: Pa) distribution in the end-cap when the cymbal is driven at the cavity resonance frequency

For high power applications, a cymbal transducer will operate in resonance, at the resonant frequency of the cavity mode of vibration. In resonance, the high displacement of the end-caps increases the stress at the inner edge of the adhesive bond layer. When this stress exceeds the tensile strength of the epoxy, failure occurs due to the appearance of micro cracks in the epoxy layer, leading to a loss of adhesion between the end-cap and the piezoceramic, often after only a small number of cycles [144]. This sharp rise in stress close to the cavity is predicted in the finite element model as shown in Figure 4.2, which plots the

axial stress component along the surface of the epoxy layer from the outer edge to the inner edge. This stress component has the highest magnitude due to the flextensional motion of the end-cap, which results in a moment on the edge of the epoxy layer. Since the epoxy is not a high strength adhesive suitable for high power applications, and its use is recommended in cymbals excited at frequencies away from resonance to avoid transducer failure, it is necessary to attempt to improve the mechanical coupling between the piezoceramic disc and the end-caps.
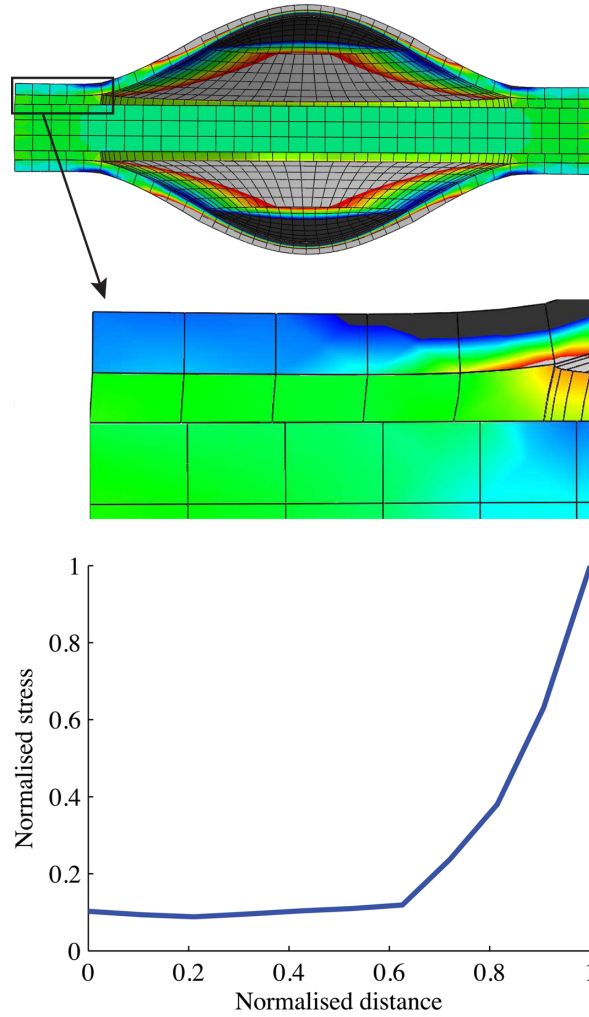
Figure 4.2: FE model prediction of the normalised stress distribution along the length of the epoxy layer at the cavity resonance mode

In this chapter, a new design of the cymbal transducer is proposed that delivers high output displacements. A comparison is presented between a cymbal based on the original design configuration and a new cymbal, to demonstrate the effects of input voltage levels on the dynamic characteristics and vibration response of the two different transducers.

The aim is to improve the mechanical coupling with the end-caps, thereby enhancing the operational capability of the device at higher voltages, allowing for excitation of higher output displacements by removing the problems associated with failure in the epoxy layer. This design is focused particularly on power ultrasonics applications such as miniature surgical devices, for example as drilling and cutting devices for orthopaedics procedures.

4.2 Limitations of the traditional design for high power applications

Cymbal transducers were first developed as low frequency, moderate-to-high power underwater projectors [115, 139] and subsequently as miniature flextensional devices, as hydrophones and microactuators. However, cymbal transducers were limited to shallow water applications, for example at depths of up to 200m, because the hydrostatic pressure experienced at greater depths would impart permanent deformations on the device end-caps. A new design was proposed to address this limitation, where the end-cap had a concave shape [155], and was named the double-dipper or concave cymbal transducer. In this new design, the end-caps are inverted, so that the radiating face is the concave face of the end-cap. On the other hand, since the convex shape of the end-caps are facing each other, this transducer must be driven by a piezoceramic ring with the same inner diameter as the cavity diameter of the end-caps, as shown in Figure 4.3. This concave configuration meant that the transducer could operate under higher pressures, albeit with reduced output displacement and lower frequency. This was one of the first attempts to enhance the design of the cymbal transducer for high power applications subjected to higher load conditions.
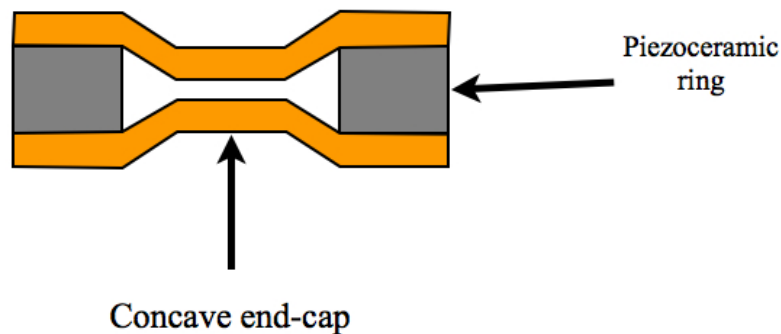
Figure 4.3: Schematic of the double dipper cymbal transducer

The simplicity of fabrication of the cymbal transducer allows for tailoring of different resonant frequencies in a single device by introducing small differences between the end-caps [154]. However, this sensitivity to changes in geometric dimensions of the end-caps was found to be a significant drawback in many applications where high efficiency was required. Irregularities introduced in the fabrication of cymbal transducers, such as asymmetries in the epoxy layer and end-cap dimensions, create a double resonance, characterised by a double-peak in the measured frequency response [143, 154, 156]. In these non-symmetric cymbal transducers, a proportion of the energy from the resonance cavity mode is transferred to the asymmetric mode, and this effect appears in approximately 80% of assembled transducers. This loss of energy in the cavity resonance mode entails a reduction in the Q_m of the device. Several studies have therefore focused on improving symmetry. A screen-printing method was proposed to improve the deposition of the epoxy layer [143], however this only improved the percentage of single-peak devices to approximately 35%. An alternative approach, proposed by Ochoa et al. [156], involves tuning one of the end-caps to the same resonance frequency as the other by adding a small mass to the top of the end-cap. Since the addition of a mass on the end-cap produces a reduction on the resonance frequency, this method only can tune both end-caps at the lower resonance frequency.

As mentioned previously, when a cymbal transducer is working at the resonance frequency of the cavity mode, high stress concentrations appear at the inner edge of the epoxy layer adjacent to the cavity, imposing a limit on the achievable maximum output displacement of the device [144]. Subsequent studies attempted to reduce the stress in the epoxy layer by introducing slots in the end-caps in order to release tension. In 2004 Ke et al. [157] proposed a new cymbal transducer where the end caps have multiple radial slots, as shown in Figure 4.4 (a). The radial slots in the cymbal end caps release the tangential stresses generated due to the flextensional motion at the resonance frequency of the cavity mode, thus increasing effective force transfer from the ceramic to the cap. A similar design was proposed by Yuan et al. [158]. In this case, the end-cap was designed with a single circumferential slot placed just above the bonding region adjacent to the cavity of the end-cap. The circumferential slotted cymbal transducer is shown in Figure 4.4 (b) .
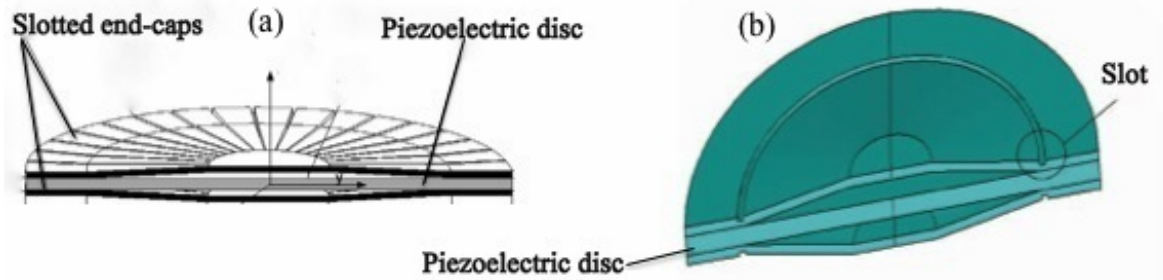
Figure 4.4: (a) Cymbal transducer with multiple radial slots, extracted from [157], (b) cymbal transducer with a single circumferential slot, extracted from [158]

These transducers exhibit higher output displacements with a considerable reduction of stress in the epoxy layer. However the slots decrease the fundamental resonance frequency of the cymbal transducer, that is inversely proportional to the number of slots introduced. Another important drawback involves the reduction in the structural stiffness of the end-caps. Therefore the maximum load that can be applied to the transducer before imparting permanent deformation of the end-cap shape is significantly reduced. Cymbal transducers generally exhibit high Q_m but low efficiency, due to being small in size compared to their wavelength at resonance when acting as sound projectors, generally in underwater applications [58]. Therefore, in order to achieve a desirable directivity and high output acoustic power, cymbals are commonly incorporated into array formations. Another configuration, which allows for excitation of higher displacement while avoiding failure of the bonding layer, involves fabrication of multi-stacked cymbals coupled in series [60], as shown in Figure 4.5. This configuration results in a low resonance frequency, dependent on the number of coupled devices. However, by simply stacking actuators in series, the strain in the actuation direction is not improved my more than around 2-3%. Other studies have also investigated the capability of transducer arrays to obtain larger output displacements. One such example utilises Class IV transducers with hierarchical cellular structures in order to obtain a significant improvement in the total displacement [159]. The principal problem with these types of configurations is the complexity of fabricating transducers with the same resonance frequency in order to resonate in phase. However when cymbal transducers are coupled in series, each transducer experiences a different load condition on its end-caps, so that each end-cap will resonate at a different frequency. Therefore, the number of resonant modes near to the main axial-longitudinal mode is increased, decreasing the efficiency of the
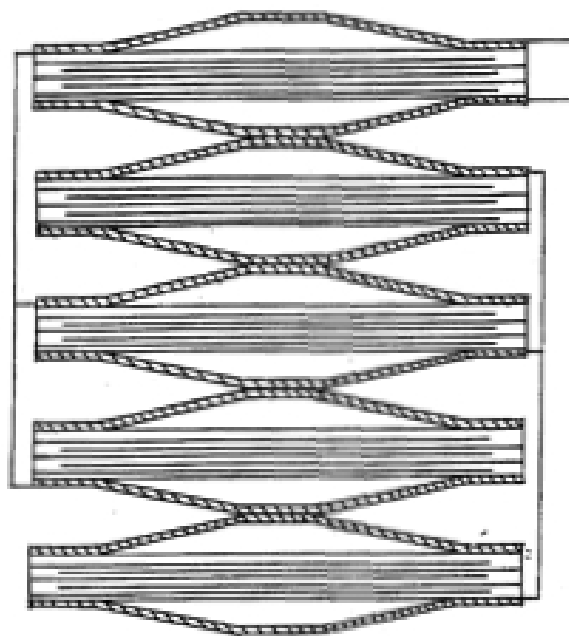
transducer.

Figure 4.5: Schematic of cymbal transducers coupled in series, extracted from [60]

4.3   New design of cymbal transducer for high power ultrasonics

One of the most recent studies regarding application of the cymbal transducer to higher power applications was the design propose by Lin in 2010 [160]. This improved design demonstrated that a modification to the coupling configuration resulted in a transducer which could be operated at higher power by incorporating a metal ring connected to the end-caps. This allowed for the necessary enhancements to the dynamic behaviour without significantly increasing the overall size of the device.

In this new cymbal design, compared with the original cymbal transducer design (OC), the electro-mechanical driver (the piezoceramic disc driving the radial vibration) is substituted by a combination of an inner piezoceramic ring coupled to an outer metal ring. The mechanical coupling between the piezoceramic disc and the metal ring can be performed by means of two different methods [160]. For the first method, a metal ring with a smaller inner radius than the piezoceramic disc is used. The metal ring radius is then expanded by heating, the piezoceramic disc is placed inside, and then the ring is cooled quickly to produce a strong mechanical coupling. The piezoceramic disc is now pre-stressed in the radial direction. For

the second method, a metal ring with a larger radius than the piezoceramic disc is used and the disc and ring are bonded by an epoxy layer. The metal end-caps are then connected directly to the metal ring through several screws. Since there is no epoxy layer between the metal end-cap and the piezoceramic disc, the mechanical coupling strength can be as high as the application requires. For this improved cymbal structure, the radial motion of the piezoceramic disc is transformed into a flextensional motion of the end-cap through two different mechanical couplings. The new cymbal design designed by Lin is shown in Figure 4.6 (b).
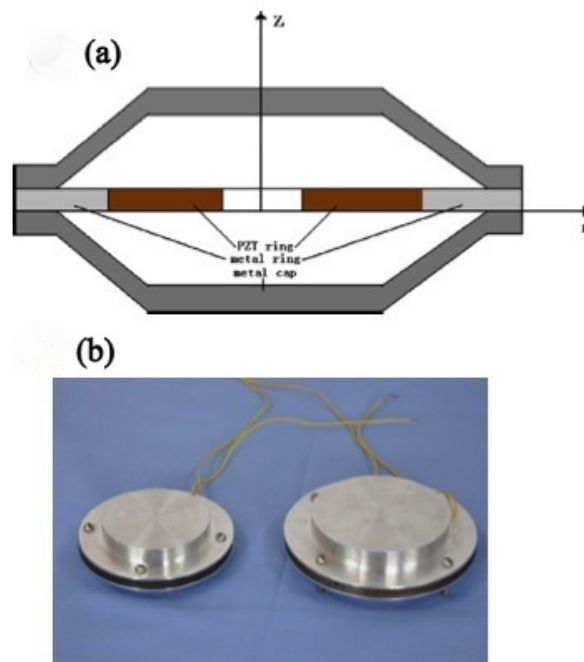
Figure 4.6: (a) Schematic and (b) photograph of the improved cymbal transducers designed by Lin, extracted from [160]

This cymbal transducer has a lower flexural vibration displacement compared with the OC, due to the piezoceramic disc being constrained by the metal ring. However, with this configuration the input power can be increased. Since there is now no epoxy layer between the end-caps and the piezoceramic disc, it is possible to drive the transducer at higher voltages to excite higher displacement amplitudes without compromising performance of the device. Therefore this transducer is the focus for high power ultrasonics applications.

4.3.1 Cymbal design for increased end-cap displacement amplitude

The new design of the cymbal transducer proposed by Lin solves some of the problems of the OC for high power applications. However, this transducer has several drawbacks when compared with the OC with the same geometrical dimensions of the piezoceramic and the end-cap. As explained in the previous chapter, the cavity diameter of the end-cap is one of the parameters that has the most influence over the resonance frequency of the cavity mode of the transducer. In the absence of a direct bonded connection between the inner edge of the end-cap cavity and the piezoceramic, the effective cavity diameter is larger. Therefore in the case of the new design proposed by Lin, where the end-caps are attached exclusively to the metal ring by some screws, the resulting cymbal transducer will operate at a considerably lower resonant frequency than the OC. On the other hand, the most important parameter is the difference in input electric power needed to obtain the same output displacement. Due to the lower displacement produced by the new design the efficiency of the transducer is reduced compared with the OC.

In this chapter, a variation of the configuration created by Lin is proposed in order to design and characterise a new cymbal transducer (NC) specifically aimed at high power applications where the cymbal operates in resonance at the cavity mode frequency. Figure 4.7 shows a schematic of the basic configuration of the OC and NC. As well as the mechanical connection of the ring and end-caps via four metal bolts, an epoxy layer bonds the end-caps and the piezoceramic disc. The coupling between the ceramic disc and the metal ring is also achieved via an epoxy layer, to prevent any radial pre-stress acting on the ceramic, and thus enabling more effective transmission of the radial vibration movement from the piezoelectric disc to the metal ring. The coupling of the end-cap and metal ring via four bolts leads to a more rigid end-cap flange. Because of this, it is expected that the base edge of the cavity allows for a rotational movement, which should slightly reduce the stress transmitted to the epoxy layer. Although the improved mechanical coupling does not entirely solve the adhesion degradation problems that were shown to affect the OC, it does enable the transducer to be operated at considerably higher powers and higher displacements at approximately the same resonance frequency and output displacement as the OC with the same geometrical dimensions. The NC similarly operates with the piezoceramic disc poled in the thickness direction to generate a radial vibration which is transmitted to the metal ring, from which the radial movement is transformed into flextensional displacement of the end-caps.
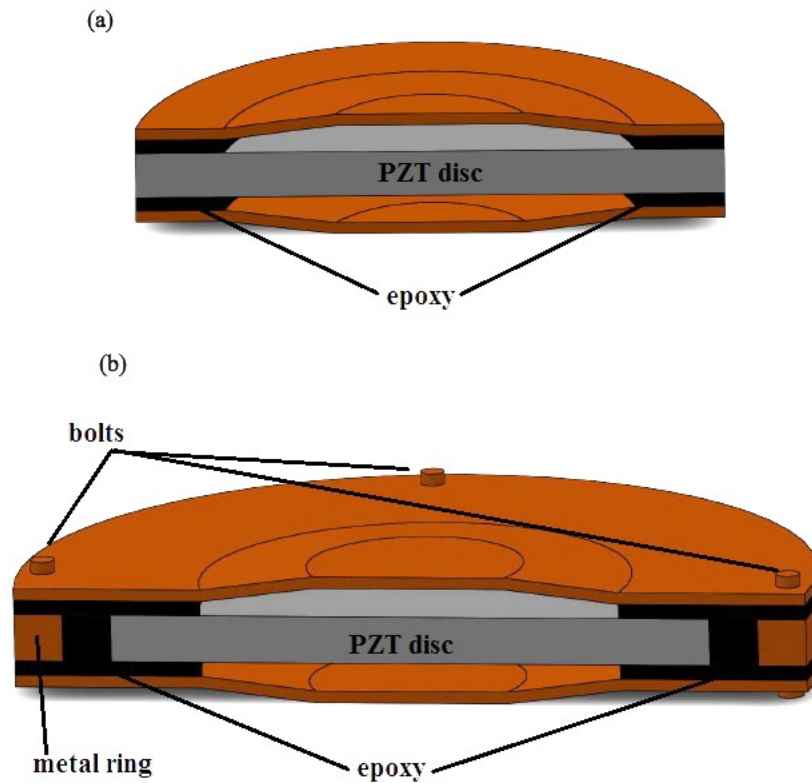
Figure 4.7: Schematics of the (a) original and (b) new cymbal transducer design

The mechanical coupling between the end-caps and the metal ring also protects the epoxy layer for the case of connection of different tool attachments to the top surface of the end-cap. Usually, in the configuration of ultrasonic transducer working as actuator, the external attachments are coupled with the transducer via a threaded stud, creating a strong mechanical coupling. The bolts, in the case of the NC, will prevent the degradation of the epoxy layer due to the tensions created during the coupling and de-coupling process of the external attachments. This is particularly important for those applications in which different types of attachments must be connected during a procedure, in order to perform different operations such as drilling, cutting or scaling, in a odontological process.

Another advantage of the NC is the improvement in control of the transducer during the assembly process. The use of screws means that the end-caps can be much more accurately aligned with the piezoceramic disc, after the deposition of the epoxy layer and during the curing process. This reduces asymmetries in the assembled transducer, reducing the likelihood that the transducer resonance frequency response will exhibit a double-peak.

In the NC the electrical leads are connected directly to the surface of the piezoceramic

disc. Since both metal end-caps are mechanically coupled with the metal ring through metal bolts, it is necessary to maintain the piezoceramic surface completely isolated in order to avoid an electrical short circuit. In comparison with the OC, where the end-caps are the electrodes of the transducer, the electrical connection is completely isolated inside the metal parts. In many applications of the OC, a layer of insulating epoxy is applied to the transducer to electrically isolate the device. This epoxy layer introduces damping, reducing both the resonance frequency and the displacement of the transducer. In the case of the NC, this problem is completely solved, therefore it is possible to drive the device in underwater applications or connected to different metal attachments without problems of a short circuit or malfunction of the transducer.

4.3.2 Comparison of the mechanical model of the end-cap for both designs

The configuration of the NC does not solve the adhesion degradation problems due to the flextensional motion of the end-caps. However, the aim of the coupling of the end-cap and metal ring via bolts is to create a more rigid end-cap flange. The cleavage loading mode, that appears in the epoxy layer adjacent to the cavity, is the combination of a rotation due to a moment generated at the cavity wall of the end-cap and an axial tension force, as was shown in Figure 3.1. In the ideal configuration of the cymbal transducer, at the edge of the cavity the movement generated by the end-cap should be a pure rotational motion, simulating a hinge. By creating a more rigid end-cap flange due to the bolts, it is expected that the base edge of the cavity allows for a rotational movement, reducing the axial tension force, which should reduce the stress transmitted to the epoxy layer.

There exist two different configurations to attach the end-caps with the metal ring using bolts, Figure 4.8. In the first configuration (configuration A), the head of the bolt has the same or smaller diameter than the thickness of the wall of the metal ring. In the second configuration (configuration B), the head of the bolt has larger diameter than the thickness of the wall of the metal ring, or some washers are used to increase the effective loading region. The effect on the stiffness of the flange of the end-cap will be different for each configuration.
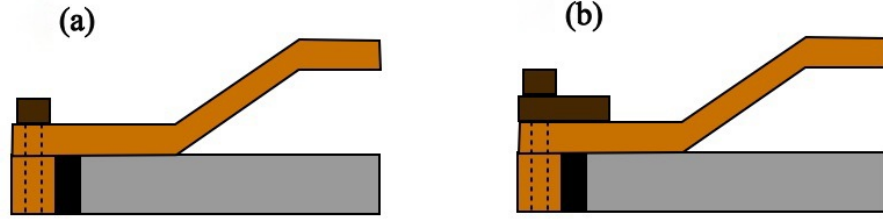
Figure 4.8: Different configurations of the mechanical coupling, (a) configuration A and (b) configuration B

In order to study the effect of the mechanical coupling between the end-cap and the metal ring on the force distribution in the end-cap, several mechanical analytical models have been created to analyse the two possible configurations. For these approximations, the radial movement of the ceramic is not taken into account, because it has been considered that both the end-cap and epoxy layer move simultaneously and, therefore, have the same radial movement. The aim of the analysis is to extract the tensile force generated in the cavity edge due to the movement of the wall of the cavity.

The mechanical analytical model of the end-cap of the OC can be simplified by a beam simply supported with a overhang. The section of the end-cap analysed is shown in Figure 4.9.
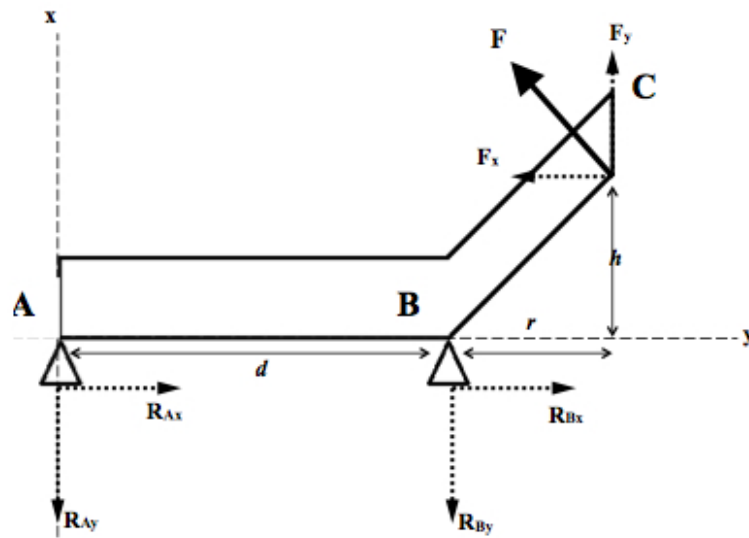
Figure 4.9: Mechanical model of the end-cap of the OC

In this model h is the cavity depth, D_c is the cavity diameter, D_a the apex diameter and $r = (D_c\text{-}D_a) \; / \; 2$.

At point B (edge of the cavity diameter) a rotational and tensile movement is registered. The equations of the equilibrium conditions are defined by:

$$\Sigma F_x = 0 \Rightarrow R_{Ax} + R_{Bx} - F_x = 0 \tag{4.3.1}$$

$$\Sigma F_y = 0 \Rightarrow F_y - R_{Ay} - R_{By} = 0 \tag{4.3.2}$$

$$\Sigma M_A = 0 \Rightarrow -R_{By}d + [F_{Cx}h + F_{Cy}(r + d)] = 0 \tag{4.3.3}$$

$$R_{By} = \frac{[F_{Cx}h + F_{Cy}(r + d)]}{d} \tag{4.3.4}$$

The mechanical analytical model for the end cap of the NC with the configuration A, can be represented by a cantilever beam with one simple support, as shown in Figure 4.10.
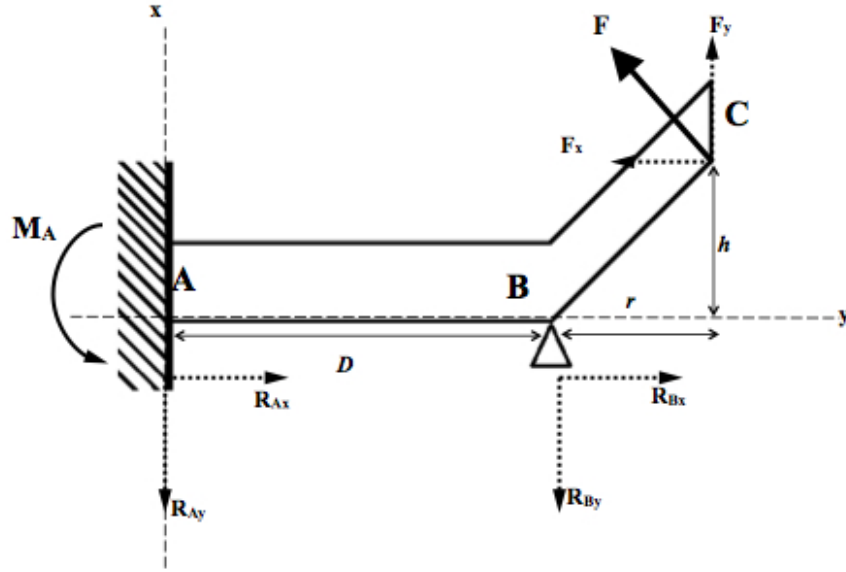
Figure 4.10: Mechanical model of the end-cap of the OC with configuration A

The equilibrium conditions are defined by Equations 4.3.1, 4.3.2 and:

$$\Sigma M_A = 0 \Rightarrow M_A - R_{By}D + [F_{Cx}h + F_{Cy}(r + D)] = 0 \tag{4.3.5}$$

$$R_{By} = \frac{M_A + [F_{Cx}h + F_{Cy}(r + D)]}{D} \tag{4.3.6}$$

where D is the distance between B and the inner edge of the metal ring.

The mechanical analytical model for the end cap of the NC with configuration B, is represented by a cantilever beam with one simple support, with an additional force applied next to point A, as shown in Figure 4.11.
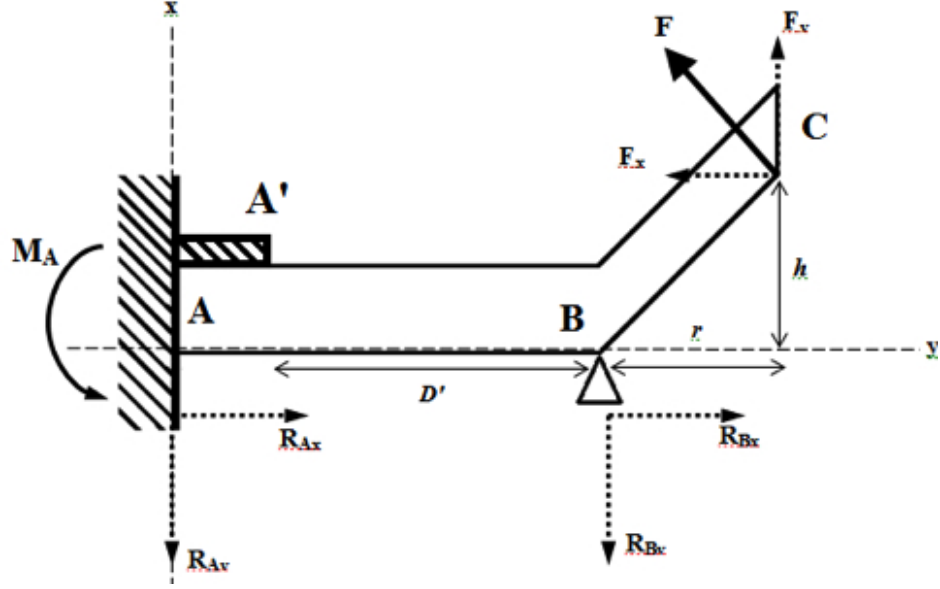
Figure 4.11: Mechanical model of the end-cap of the OC with the configuration B

The equilibrium conditions are defined by Equations 4.3.1, 4.3.2 and:

$$\Sigma M_{A'} = 0 \Rightarrow M_{A'} - R_{By}D' + [F_{Cx}h + F_{Cy}(r + D')] = 0 \qquad (4.3.7)$$

$$R_{By} = \frac{M_{A'} + [F_{Cx}h + F_{Cy}(r + D')]}{D'} \qquad (4.3.8)$$

where A' is the point of the edge of the head of the bolt or the washer. Therefore $D > D'$. In this model it is assumed that $M_A = M_{A'}$ since it is considered that the part of the end-cap under the washer is completely fixed and has not movement. The reaction force at the edge of the cavity, R_{By}, against the tensile force, F_y, in the NC is higher than in the OC, due to the action of the strong mechanical coupling between the end cap and the metal ring along with the epoxy. On the other hand, configuration B has higher R_{By} than configuration A, since R_{By} is inversely proportional to the dimension D, that is related to the diameter of the head of the bolt or washer.

Since the NC has a higher reaction force at the edge of the cavity, the motion of the end-cap at this point is expected to exhibit a more rotational movement reducing the axial tensional force, and therefore reducing the cleavage loading mode. This allows the end-cap to deliver higher displacements before incurring degradation of the epoxy layer. Between the

two configurations for the coupling of the end-cap analysed, configuration B offers a higher reaction force, therefore is the better option.

4.3.3 Transducer fabrication

End-cap manufacture

The method to produce the end-caps for the NC is the same as was explained in Chapter 3. Each cymbal end-cap was cut from a 0.25mm-thick brass or titanium alloy Ti-6-4 sheet. The cavity dimensions of the NC remains the same as the OC, in order to allow comparison of two transducers with a very similar cavity mode resonance frequency. It can be noticed that the dimensions of the end-caps for the NC allow for a metal ring, therefore the flange of the transducer is larger than in the case of the OC. Table 4.1 lists the dimensions of the end-caps used for both cymbal transducers, one based on the OC design and one based on the NC incorporating a metal ring. At the edge of the flange four holes were drilled around the circumference of the end-cap for the connection of the bolts. The end-cap for the NC is shown in Figure 4.12 .

Parameter	OC (mm)	NC (mm)
End-cap thickness	0.25	0.25
Total diameter	12.70	16.70
Base of the cavity diameter	9.00	9.00
Apex of the cavity diameter	4.50	4.50
Cavity depth	0.30	0.30

Table 4.1: Dimensions of the end-cap of the OC and the NC
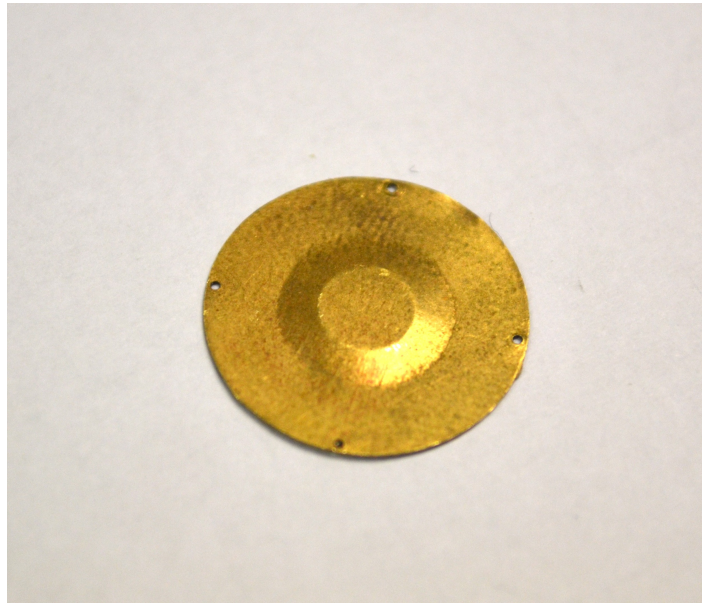
Figure 4.12: End-cap of the NC

In order to compare the response of the NC with different end-cap materials, two different devices were built made, one of brass and one of titanium with the same geometry dimensions.

Metal ring manufacture

Figure 4.13 shows a photo of the metal ring for the NC. The metal ring was designed to have an inner diameter 2 mm larger than the diameter of the piezoceramic disc. The thickness of the wall of the metal ring is 1 mm. This parameter has a significant influence on the displacement of the transducer, since when the ceramic expands radially, the movement is constrained by the metal ring. The wall thickness of the metal ring is inversely proportional to the radial displacement of the composite piezoceramic plus metal ring. The selection of the dimension of the wall thickness was based on the dimension of the diameter of the smallest suitable threaded bolt available commercially.
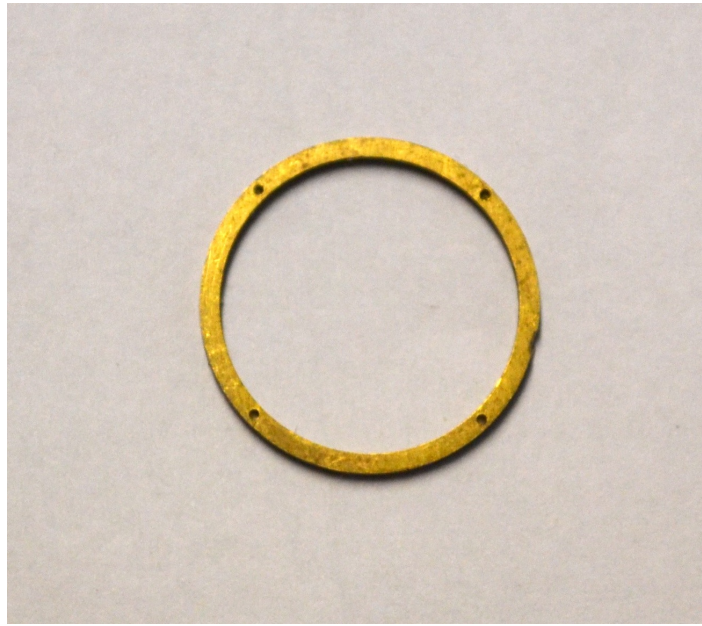
Figure 4.13: Metal ring utilised for the NC

The thickness of the ring was selected to be slightly larger than the thickness of the piezoceramic disc, for this work approximately 1.2 mm. This difference allows the piezoceramic disc, including the wires welded on its surface, to be placed perfectly centred in the metal ring.

Finally four holes were created around the circumference in order to allow connection with the end-caps using the bolts. The number of four holes was selected taken in account the work realised by Lin [160] for reasons of convenience. Since the piezoceramic is sealed in the metal parts, the electrical wires were welded to the surface of the ceramic through two holes on the metal ring, as shown in Figure 4.14 .
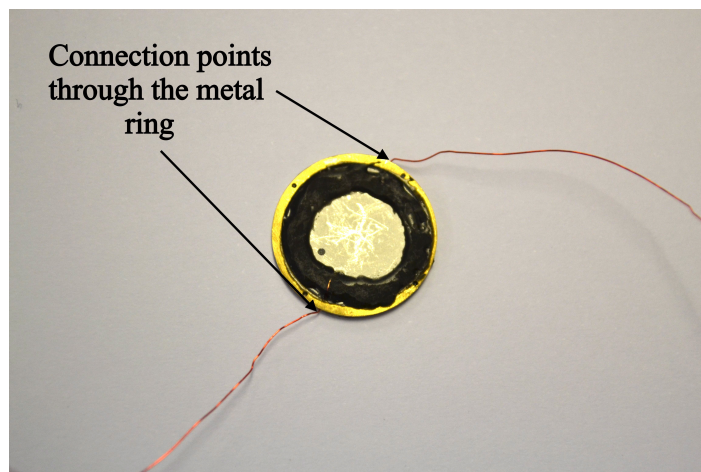
Figure 4.14: Piezoceramic disc placed into the metal ring

For each transducer, the metal rings were made with the same material as the end-caps, brass and titanium alloy Ti-6-4, in order to match impedances.

Cymbal transducer assembly

For the construction of the NC, hard PZT, PKI-402, piezoceramic discs were used. The dimensions of the piezoceramic disc were listed in Table 3.2. The electrical leads were welded directly on the surface of the ceramic and the wires were introduced into the lateral holes of the metal ring. The gap between the piezoceramic and the metal ring was then filled with epoxy resin covering also the electrical lead. The epoxy resin employed was the Eccobond insulating epoxy resin (Emerson & Cuming), at a ratio of three parts epoxy resin to one part resin hardener. After careful deposition of the epoxy, the metal ring with the piezoceramic was pressed between two sheets of PVC, in order to obtain alignment of the parts, and was left to cure at room temperature for 24 hours. Once the epoxy was cured, both faces of the ceramic were polished using a fine sand paper to remove the excess epoxy.

The end-caps were then bonded with the ceramic disc and metal ring using a layer of approximate 0.35 mm epoxy. The epoxy was deposited covering all the flange of the metal end-caps to avoid any direct contact with the surface of the ceramic. The correct alignment of the metal end-caps with the surface of the composite was performed through four bolts made with the same material of the metal parts. For this size of transducer, the selected threaded bolts and nuts have a head diameter of 0.50mm and thread diameter of 0.35mm. Once both end-caps were fixed using the bolts, the assembly was left to cure in a custom rig under pressure for 24 hours. The assembled NC is shown in Figure 4.15.
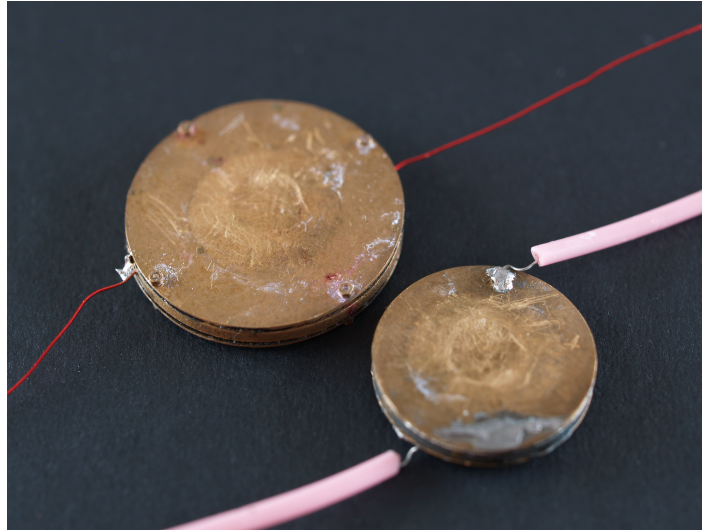
Figure 4.15: Assembled cymbal transducers based on OC (right) and NC (left) designs

4.4 Comparison of modal parameters and dynamic performance

Experiments were undertaken to characterise and compare the two cymbal transducer designs. Electrical impedance measurements were recorded for the purpose of quality verification of the device assembly, and also as a method of determining the level of symmetry of the transducer, a single-peak frequency response being an indicator of acceptable symmetry. A 1D laser Doppler vibrometer (LDV) measured the displacement amplitude response of the end-caps of both transducers for a range of input excitation voltage levels, and experimental modal analysis (EMA) was undertaken using a 3D LDV to measure the modal frequencies and mode shapes. These measurement techniques were explained in Chapter 3

The experimental results also allowed for validation of the numerical models created in Abaqus FEA software. For the finite element models, steady-state dynamic analysis was performed to predict the displacement amplitude of the end-caps under different input excitation voltages and to calculate the modal frequencies and mode shapes of the transducers.

4.4.1 Impedance analysis

The impedance spectra of the analysed transducers are shown in Figure 4.16 and Figure 4.17. The measurements give a clear indication of the improved level of symmetry achieved in the NC transducers analysed. In the transducers based on the OC design, a clear double-peak is present in the response spectrum in Figure 4.16 (a) and Figure 4.17 (a). As discussed in

Chaper 3, this indicates that the cymbal exhibits a double resonance, a symmetric (cavity) mode and an asymmetric mode characterised by out-of-phase and in-phase motion of the two end-caps respectively. Distinct to this behaviour, the NC transducers made of brass and titanium show a single resonance peak, indicating that at the resonance frequency of the cavity mode, the end-caps have out-of-phase motions and only the symmetric mode is excited.
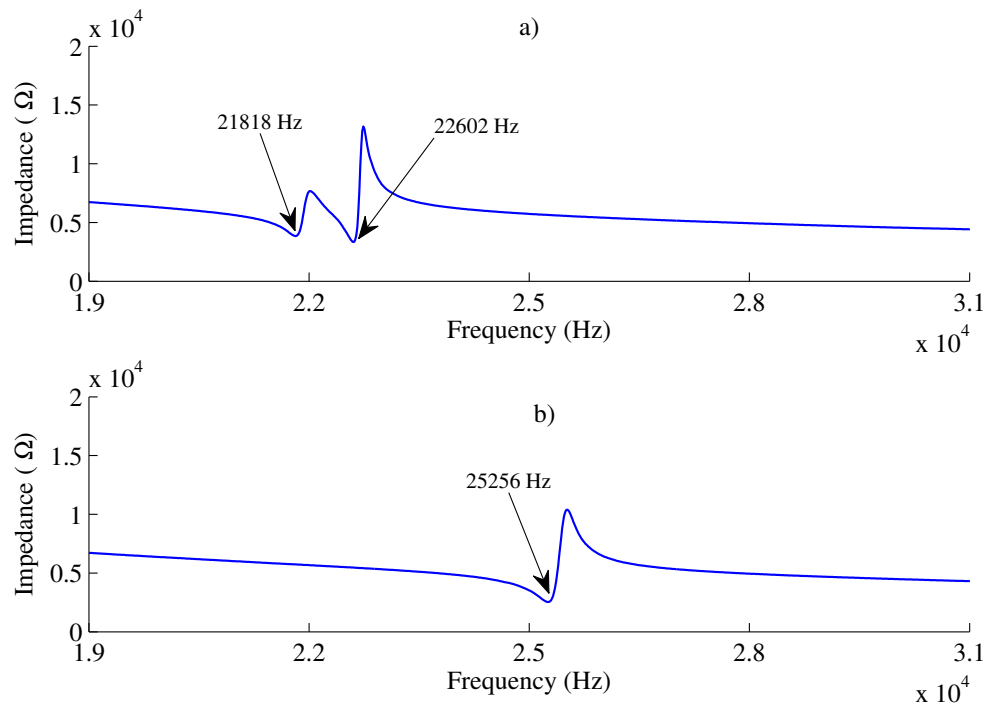
Figure 4.16: Impedance spectra of the (a) OC and (b) NC for brass end-caps
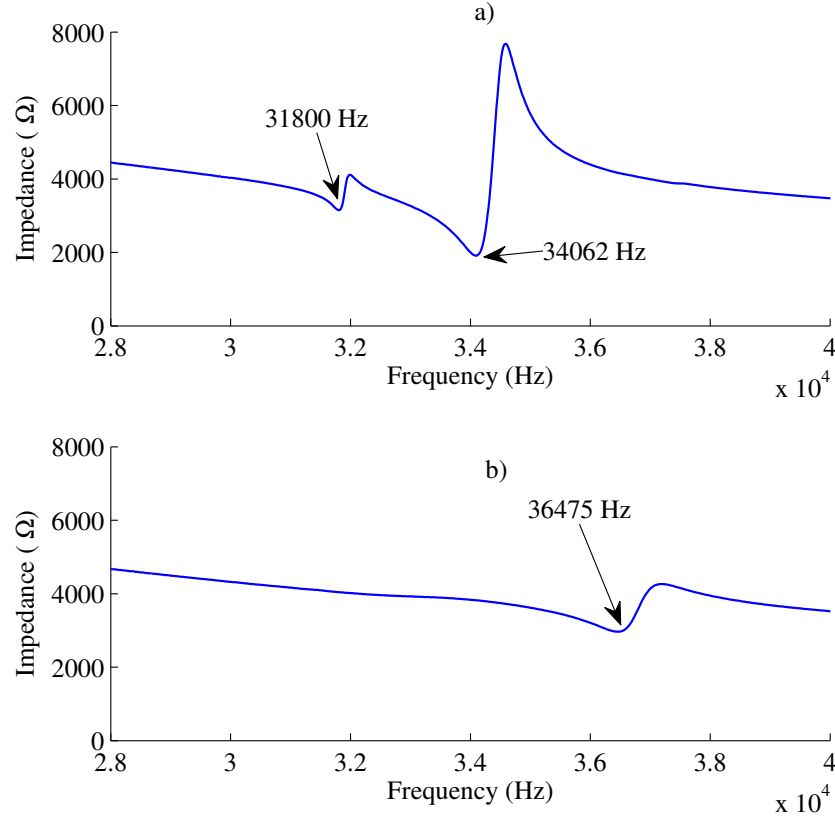
Figure 4.17: Impedance spectra of the (a) OC and (b) NC for titanium end-caps

For high power ultrasonics applications, transducers are designed to exhibit high levels of efficiency with minimum losses. As a result of the splitting of frequencies in the spectrum of the OC, part of the energy associated with the symmetric cavity mode is transferred to the asymmetric mode, therefore reducing the efficiency of the transducer. Additionally, the asymmetry also introduces bending responses in the piezoceramic disc resulting in undesirable stress that can reduce the operational life of the transducer, especially when operating at high power levels. The NC transducer solves this drawback, improving the fabrication process of the device in order to obtain a transducer where both end-caps vibrate at the same resonance frequency. During the curing process the bolts in the new cymbal transducer are used to help achieve improved symmetry through a controlled realignment of the end-caps and ceramic, simply by making slight adjustments to the different bolts.

Although the dimensions of the end-cap are the same as those of the OC, the resonance frequency of the NC in both cases is higher. This is due to the radial constraint introduced on the piezoceramic disc by the action of the metal ring. On the other hand it can be observed that the level of impedance at the resonance frequency of the NC is almost the same as for

the OC, however the level of impedance at the antiresonance frequency is lower.

4.4.2   Experimental modal analysis

An experimental modal analysis (EMA) was carried out using a 3D LDV and data acquisition hardware and software (DataPhysics SignalCalc, MEscopeVES). The mode shapes and associated frequencies from the EMA are shown alongside the corresponding results from the finite element analysis in Figure 4.18 and Figure 4.19.

(a) EMA: 25352 Hz   (b) FEA: 25215 Hz
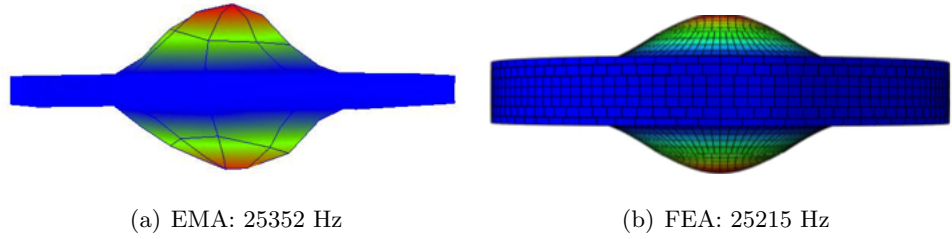
Figure 4.18: Mode shapes from (a) EMA and (b) FEA of the NC transducer with brass end-caps for the cavity mode

(a) EMA: 36330 Hz   (b) FEA: 36726 Hz
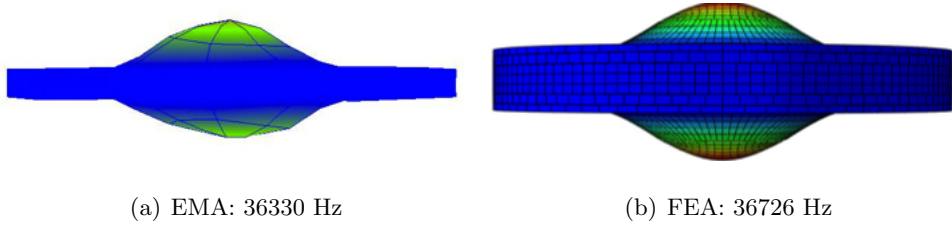
Figure 4.19: Mode shapes from (a) EMA and (b) FEA of the NC transducer with titanium end-caps for the cavity mode

Figures 4.18 and 4.19 show good correlation between the mode shapes and resonant frequencies predicted through FE models and obtained through experimental modal analysis of the brass and titanium NC. The percentage difference between the predicted and experimentally acquired resonant frequencies was found to be 0.54% and 1.07% for the brass NC and titanium NC, respectively. The high level of symmetry obtained due to improved control of the assembly process, reduces the appearance of internal irregularities and therefore the numerical model can be validated with high accuracy.

4.4.3   Power harmonic characterisation

The NCs with brass and titanium end-caps were driven over a range of voltage increments across a narrow frequency band centred at the resonance frequency of each device. The

transducers were excited through upwards and downwards frequency sweeps in order to observe any non-linearities in the displacement-frequency responses. A 1D LDV was used to measure the displacement amplitude response from the centre of each end-cap. To ensure that transducer heating was minimised for the duration of the experiment, the excitation was via a burst-sine wave with 2-4s intervals between bursts, with the interval selected depending on the voltage level. The resulting measured displacement amplitude responses of the two NCs are shown in Figure 4.20 and Figure 4.21. The results illustrate the maximum displacement response measured for each end-cap.
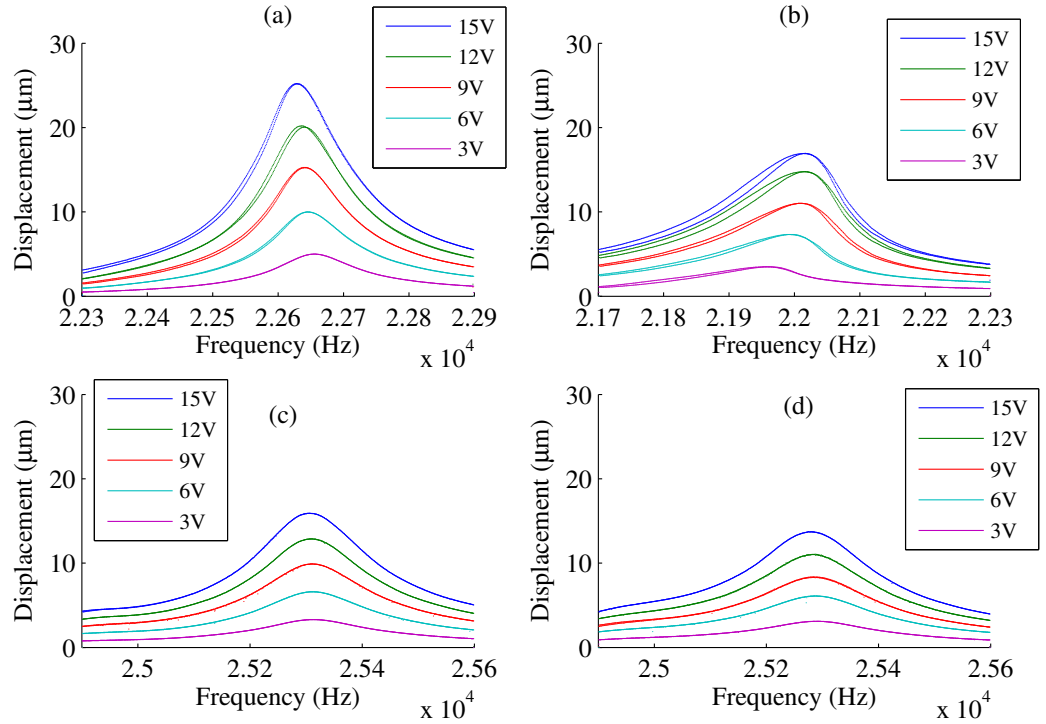
Figure 4.20: Vibration displacement response of the (a), (b) OC and (c), (d) NC, with brass end-caps, for each end-cap
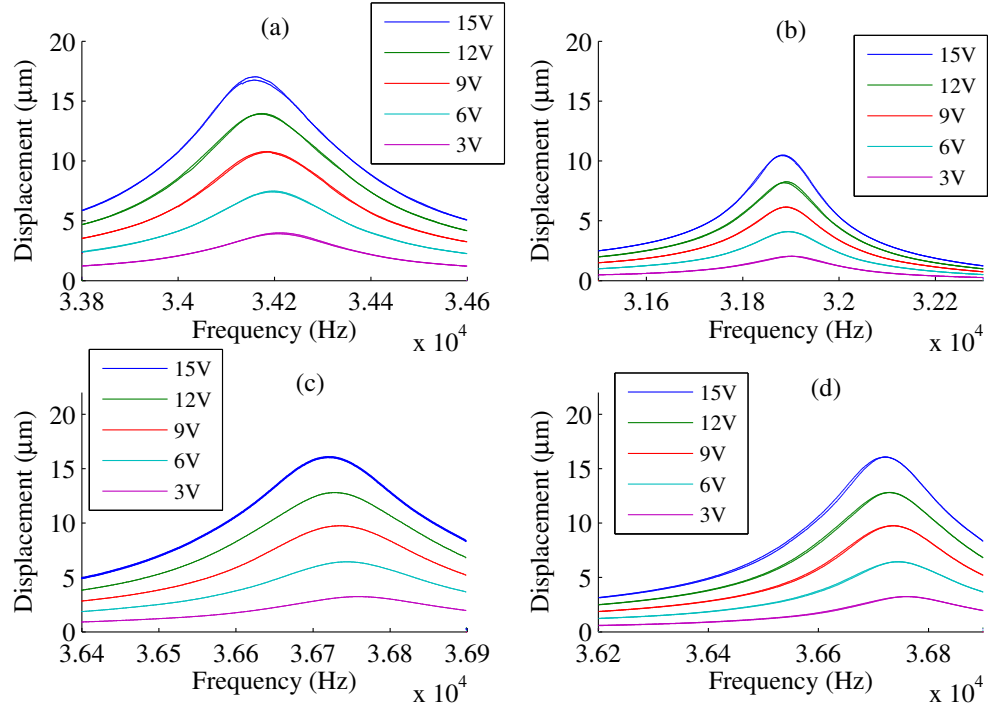
Figure 4.21: Vibration displacement response of the (a), (b) OC and (c), (d) NC, with titanium end-caps, for each end-cap

By comparing Figure 4.20 and Figure 4.21, it is possible to observe the result of improved symmetry in the fabricated NC, both from the excitation of a single mode (cavity mode) at 25.3 kHz in the case of the brass NC and 36.7 kHz for the titanium NC, and also from the more consistent displacement amplitudes measured on the two end-caps.

However, for the NC, the constraint of the metal ring results in a lower maximum achievable displacement amplitude at resonance (Figure 4.20 (c) and (d) and Figure 4.21 (c) and (d)) than for the OC (Figure 4.20 (a) and Figure 4.21 (a)) although the displacement are comparable to those of the second, less responsive, end-cap of the OC. In the NC configuration, the driver comprises both the piezoceramic disc and the metal ring, such that there are lower effective piezoelectric coefficients than for a piezoceramic disc driver alone. For a piezoceramic disc, the piezoelectric coefficient d_{33} is the strain in the polarization axis (i.e. perpendicular to the plane of the disc) per unit electric field applied in the axis of polarization, and the coefficient d_{31} is the strain in a direction perpendicular to the axis of polarization (i.e. in the plane of the disc) per unit electric field applied in the axis of polarization. The coefficient d_{33} is related to the displacement that the ceramic can attain in

the axial direction, and the coefficient d_{31} relates to the displacement in the radial direction. For high power ultrasonics applications, large values of piezoelectric coefficients are required. The axial and radial displacements of the drivers of the two configurations were therefore measured as an indicator of the difference between the d_{33} and d_{31} coefficients respectively for the two transducers. From these measurements the d_{33} for the brass NC is 13.4% lower than for the brass OC, whilst the d_{31} reduction is 38.1%. For the case of the titanium NC the reduction of the d_{33} is of 1.2% with respect to the titanium OC, and the d_{31} is 5.5% lower. The measured difference in axial displacement of the end-caps is 36.9% between the brass OC and brass NC while for the titanium devices it is 6.7%, where end-cap displacement is largely influenced by the d_{31} coefficient. These results mean that for high power ultrasonics devices the NC transducer needs to be driven at a higher input power than the corresponding original cymbal transducer to achieve the same displacement amplitude.

The degree of hysteresis in the displacement-frequency response is also an important measure of transducer performance, especially when accounting for mechanical losses. When part of the energy in the device is dissipated internally, there can appear regions of high stress, heat and electrical concentration in the piezoceramic that exhibit as non-linearities in the measured displacement, one consequence of which is hysteresis. The degree of hysteresis is defined as [61]:

$$\Delta H\% = \frac{100\Delta X}{X_{max}} \tag{4.4.1}$$

where X_{max} is the displacement at the location of maximum electric field, where the highest hysteresis region is generated, and ΔX is the difference in displacement between the paths of the upwards and downwards frequency sweeps at the half-maximum of the applied electric field. The degrees of hysteresis calculated from the data measured at the maximum voltage level used in this study for the OCs and NCs are recorded in Table 4.2.

Device	End-cap 1	End-cap 2
OC Brass	2.93%	4.19%
NC Brass	0.07%	0.12%
OC Titanium	0.09%	0.03%
NC Titanium	0.02%	0.06%

Table 4.2: Degree of hysteresis of the OC and the NC for brass and titanium end-caps, measured for 15V excitation level

Lower hysteresis is generally calculated for the NC design, in part due to the high level of symmetry achieved in its fabrication. The result is a transducer with a more linear response over the range of excitation voltages in this study, as evidenced by the highly symmetric response curves measured from both end-caps of the NC transducers (Figure 4.20 (c) and (d) and Figure 4.21 (c) and (d)) and the constant resonance frequency maintained in the measurements across the excitation voltage range.

4.4.4   Failure test

Through the same measurement methodology as described in the previous section, it was possible to determine the displacement amplitude achieved before failure of the transducers occurred. The two cymbal configurations were driven at increasing voltage levels and the results are shown in Figure 4.22.
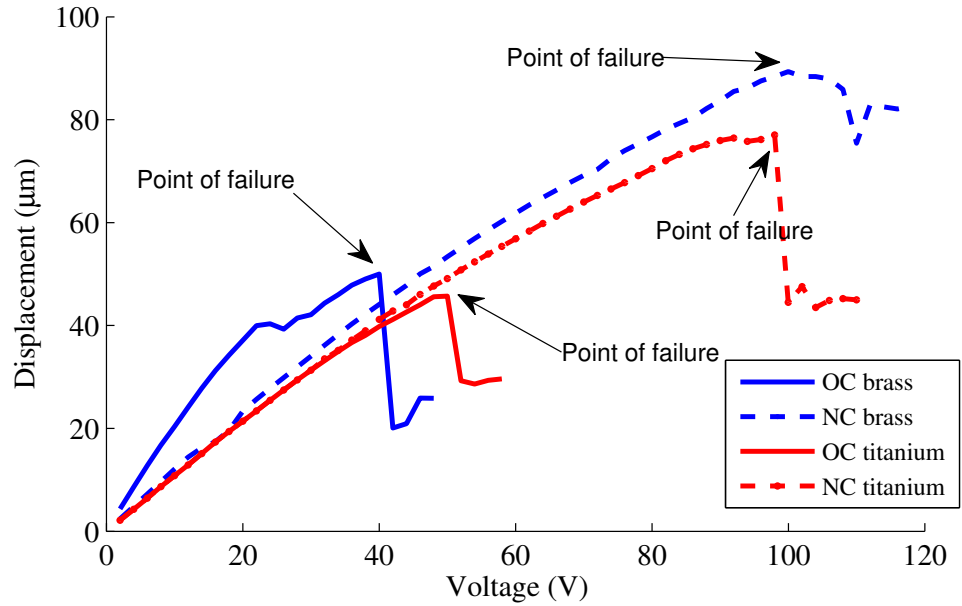
Figure 4.22: Displacement amplitude of the OC and NC for increased excitation voltage

For this experiment, the displacement obtained for each transducer at 40 V was used as a reference point to check the correct performance of the transducers. Beyond this reference point, the displacement was checked at every 4 V increase, to detect whether any internal failure had occurred that could affect the displacement. When the epoxy layer starts to lose adhesion, the displacement of the transducer exhibits an erratic response and subsequently the displacement of the transducer both at high and low input voltages suffer alterations. This failure is characterised by the appearance of micro-cracks in the epoxy layer in the vicinity

of the cavity, characteristic of a loss of adhesion between the end-cap and the piezoceramic disc.

The brass OC reached a displacement of 50 μm, above which the amplitude dropped due to failure of the bonding layer. In the case of the titanium OC the point of failure was reached at 45 μm. On the other hand, the brass NC reached a displacement of 89 μm before a sudden drop in displacement was measured and for the titanium NC the point of failure was observed at a displacement of 77 μm. The displacement difference between the brass OC and brass NC was 39 μm and 32 μm for the titanium OC and NC. This demonstrates the significant advantage of the new cymbal transducer, which can be driven at higher voltage levels to attain higher end-cap displacements through the improved mechanical coupling and symmetry of the device.

4.4.5 Evaluation of the response of the NC as actuator

To evaluate the NC as a transducer for high power ultrasonic applications, it is necessary to investigate its incorporation into a device for a typical application. For many high power applications, such as ultrasonic drilling or cutting, the transducer must be able to actuate an attached mass, such as a drill-bit or blade, and therefore a circular cylindrical bar was adopted in this study as a generic added mass. In order to maintain symmetry, equal masses were added to both end-caps. The addition of a mass introduces a force that constrain the motion transferred from the piezoceramic disc to the end-cap and therefore results in a lower axial displacement. It is therefore important to understand the effects of these constraints on the vibration displacement response of the NC configuration in which the mechanical motion is transmitted through three mechanical couplings instead the single mechanical coupling of the OC.

Experiments were conducted, using the same method as described in section 3.4.4, the bars used are listed in Table 3.6. Table 4.3 and Figure 4.23 show the displacement at resonance measured on the free end of each bar for an input voltage of 15V.

Bar length (mm)	Displacement OC brass (μm)	Displacement NC brass (μm)	Displacement OC titanium (μm)	Displacement NC titanium (μm)
none	25,21	15,90	16,76	16,02
3.00	2,75	2,64	1,49	1,19
6.00	3,18	3,44	1,25	1,18
9.00	2,87	3,42	1,35	1,53
12.00	2,86	3,26	1,15	1,51

Table 4.3: Vibration displacement of the OC and NC, with different masses added for an input voltage of 15V
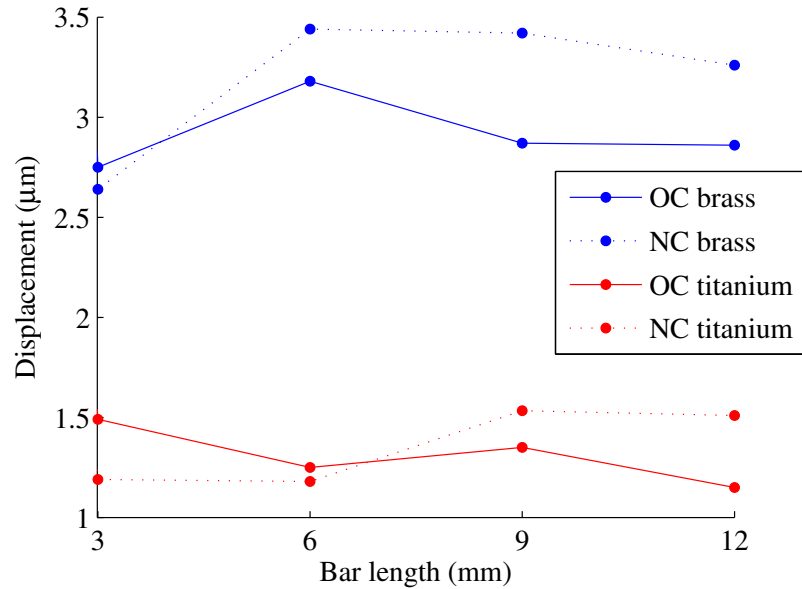
Figure 4.23: Vibration displacement of the OC and NC, with different masses added for an input voltage of 15V

It can be observed that, for both cymbal configurations, when a mass is added to the top surface of both end-caps, the displacement is significantly reduced compared to the end-cap displacements achieved with no added mass, as seen in Figure 4.20 and Figure 4.21. However, the length of the bar, and therefore size of the mass, has a negligible effect on the displacement and, for the range of added masses, the displacement is very similar for both configurations, despite the difference in the displacement between OCs and NCs when operating with no added mass. These results indicate that both transducers exhibit a similar response, despite the fact that the radial motion of the piezoceramic disc in the NC transducer is constrained

by the metal ring.

As explained previously, the mechanical coupling factor, k_{eff}, is an indicator of the amount of electrical energy transformed into mechanical energy, and is therefore related to the mechanical losses and efficiency of the device. The calculated mechanical coupling factors of the OC and NC are represented in Table 4.4 and Figure 4.24

Bar length (mm)	k_{eff} OC brass	k_{eff} NC brass	k_{eff} OC titanium	k_{eff} NC titanium
none	0,132	0,142	0,167	0,196
3.00	0,223	0,214	0,193	0,258
6.00	0,227	0,197	0,213	0,253
9.00	0,232	0,199	0,193	0,232
12.00	0,217	0,192	0,210	0,228

Table 4.4: Variation of the k_{eff} parameter of the OC and NC transducers, with different added mass
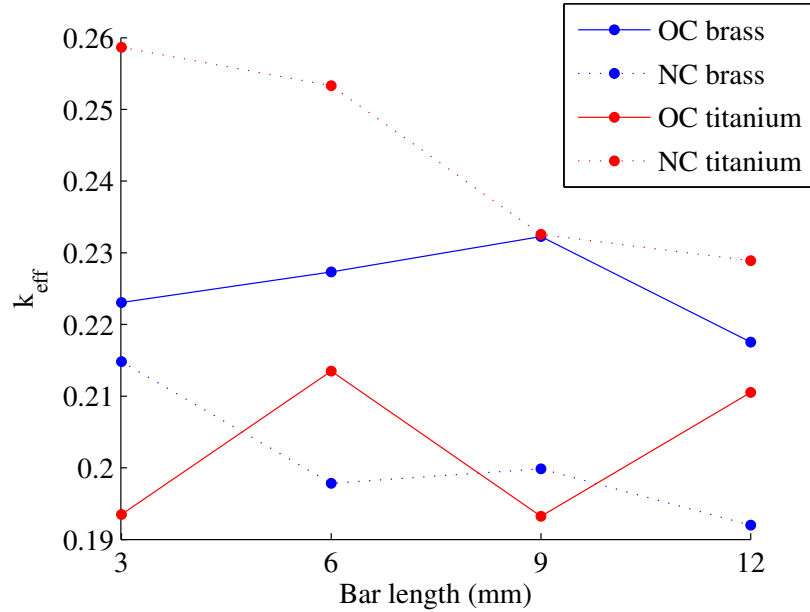
Figure 4.24: Variation of the k_{eff} parameter of the OC and NC transducers, with different added mass

In the case of the NC, higher mechanical losses might be expected as a result of the three different mechanical couplings influencing the motion of the piezoceramic disc and end-caps; epoxy layer, metal ring and fixing bolts. Additionally, it might be expected that the losses are increased for this transducer with increasing added mass to the end-caps as a result of the

additional load affecting all three couplings, rather than only the epoxy layer in the case of the OC. However, the results in Figure 4.24 exhibit similar behaviour for both transducers, indicating that the losses are not significantly increased for the new cymbal. The reason for this is that the added mass introduces an additional stress in the epoxy layer that increases the stiffness and therefore reduces the damping due to the high elasticity of the material. On the other hand, since the end-cap is attached directly to the driver (piezoceramic + metal ring) through bolts, there are a better transmission of the energy from the radial motion of the driver to the end-cap.

4.5 Summary

In this chapter an improved design of the OC, for high power applications, has been investigated. This NC incorporates a combination of a piezoceramic disc coupled with a metal ring as driver. The end-cap is attached to the metal ring through a few bolts and to the piezoceramic disc through an epoxy layer. The mechanical coupling of the end-caps with the driver enables the device to be driven at higher excitation levels and therefore higher displacements. A difference of more than 30 μm has been observed when comparing the operational displacement limit between the OC and the NC for different end-cap materials.

The experimental results have demonstrated that even though the new design incorporates additional components of threaded bolts and a metal ring, the device exhibits the same cavity resonance mode as the OC. The experimental results have also demonstrated that the performance of the new cymbal transducer preserves the advantages of the traditional design, including high axial displacement for small radial displacement of the disc and constancy of end-cap displacement with increasing added mass. A good correlation has been observed between the results predicted by the FE model and the measured experimental results. The improvement in the control of fabrication of the new transducer allows significantly improved symmetry to be attained, eliminating the double-peak in the cavity mode frequency response, and thereby improves the resonance performance of the transducer.

Chapter 5

Design of a novel ultrasonic cutting device

5.1 Introduction

Current commercial ultrasonic devices designed for bone cutting applications are based on a Langevin piezoelectric transducer. Langevin transducers incorporate a piezoceramic stack capable of delivering a few microns of vibration amplitude to the cutting blade, and therefore the transducer and the blade as a whole must be resonant to achieve the required ultrasonic displacement amplitude at the cutting tip, to perform the cut. This type of cutting device was first developed in 1945 by Balamuth [122] for dental applications. The original device comprised of an outer casing enclosing a magnetostrictive transducer which was connected to a mechanical amplifier, commonly known as horn. The horn could be welded or otherwise firmly secured at one end of the laminated stack of magnetostrictive material, creating a resonant transducer. The end part of the horn was provided with a threaded part for the connection of the cutting tip. During the process of cutting, an abrasive slurry was applied directly to the surface of the bone to assist the process. For that purpose a external flexible sheath was designed to enclose capillary tubing for delivery of the abrasive slurry to the work area. The flexible sheath was brought out of the casing through a suitable opening that also had the function of exhaust tubing for cooling the transducer.

The cutting tips were designed with specific curved shapes in order to perform a cutting movement with a combination of a longitudinal-flexural motion. The principal reasons for the design of these types of blades were to allow the surgeon better access to the zone to be treated and to provide blades capable of being used for cutting in more than one

direction. The whole device, including the cutting tip, was designed to a specific dimension to resonate at a particular frequency (usually around 30 kHz), however the blade itself also had a resonant frequency in the neighbourhood of this device resonant frequency in order to amplify the motion delivered by the Langevin transducer. One of the advantages of the design proposed by Balamuth was that due to the operational frequency, the cutting device could be implemented in a relatively short tool of less than 20 cm.

Although the first attempts to introduce ultrasonic technology in bone cutting procedures came from Catuna in 1952 [120] with his drilling device for dentistry, the main application of this technology was focused on oral prophylaxis procedures or dental scaling. During almost 50 years researchers have worked on the development of more efficient devices. The original magnetostrictive transducer was replaced with the more efficient and cheaper pre-stressed Langevin piezoelectric transducer, and the design of the vibrating tips was improved for a better adaptation of its performance to the different medical procedures. Despite the promising results obtained from different medical studies, comparing the use of traditional manual scaling methods with ultrasonic devices, it was not until 2001 when Mectron S.p.A. developed the Piezosurgery® device.

The device consist of a pre-stress sandwich transducer fabricated with a stack of 4 hard PZT rings coupled with a horn, with a threaded end for the connection of different inserts. Inside the body of the transducer, along the compression bolt, a cooling system is introduced to assist the cutting process, delivering a coolant directly to the inserts. This coolant has two different purposes, in the first place to cool and clean the cut zone and also to cool the transducer itself. Operating in a frequency range of 24 to 36kHz. The energy delivered from the piezoceramic stack to the cutting tip generates microvibrations in a range of 60-210 mm depending of the type of insert and the input power selected [94]. This cutting device has the ability to cut mineralized tissue without cutting neurovascular and other soft tissues, thereby maintaining a blood-free operating area, better visibility and greater precision, due to the the presence of cooling fluid. In Figure 5.1 Balamth's device and the Piezosurgery® device are shown.
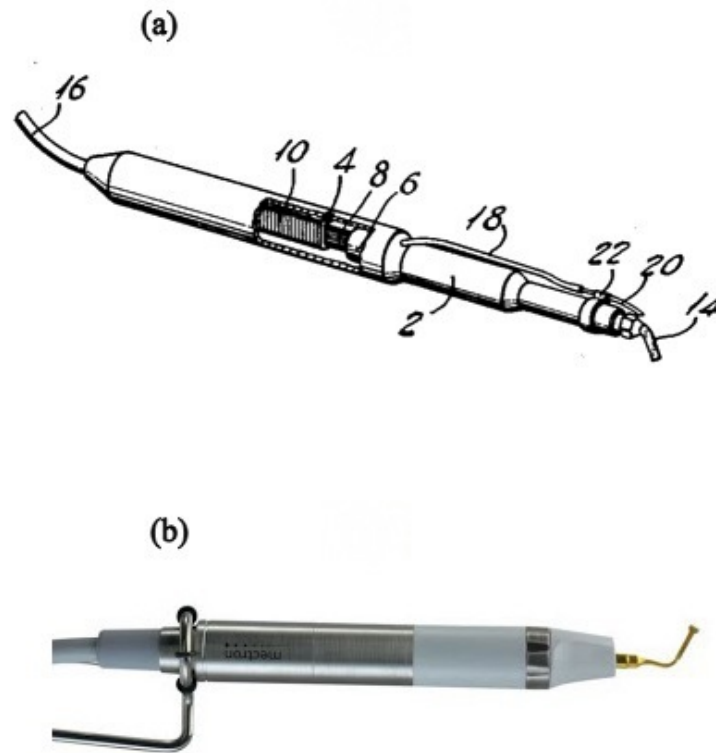
Figure 5.1: Ultrasonic cutting device design by (a) Balamuth in 1952 and (b) Piezosurgery$^{®}$ device developed by Mectron S.p.A. in 2001

The Piezosurgery$^{®}$ device was originally designed exclusively for oral prophylaxis procedures, with a broad variety of scaling vibrating inserts. However, during a sinus lifting procedure, surgeons reported successful dissection of hard tissue using the Piezosurgery$^{®}$ device with a scaling insert [94]. This led to the development of devices specifically designed for bone cutting. The first prototype designs, named as OT1 and OT2, were based on the original scaling insert, however to assist more effective cutting, the inserts incorporated two different cutting edge designs; the OT1 was developed with a diamond coated cutting edge and the OT2 with a plain cutting edge. The results of the different trials showed better performance in the OT2 due to its design with a cutting edge being similar to a traditional scalpel. Later modifications of the OT2 lead to the development of the OT6 insert. This insert has a doubly curved shank with a saw-like cutting edge which enabled larger vibrational amplitudes and deeper cutting with a reduction of the heat generated in the bone during the cutting process. Recently, in order to develop an insert able to produce deeper cuts, Metron

S.p.A. designed the OT7 insert with a longer insert. With this blade (see Figure 5.2) it is possible to perform dissections of small bones in a relatively short time.
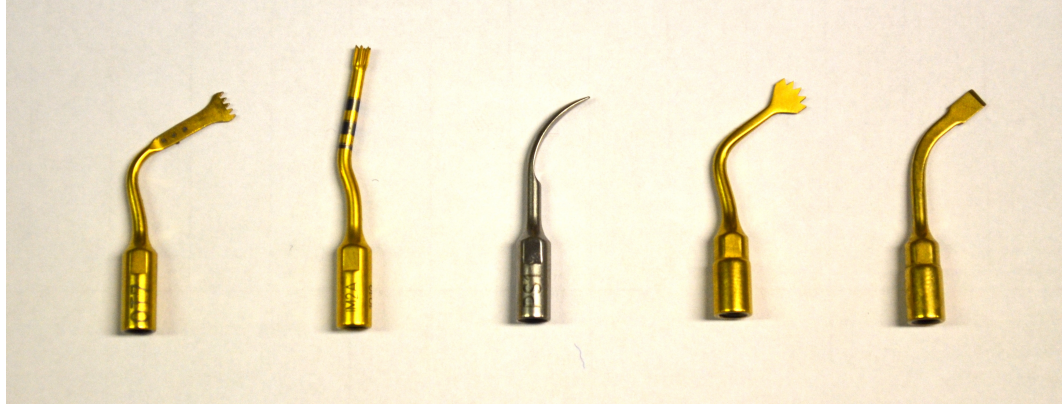
Figure 5.2: Inserts developed by Mectron for hard tissue. From left to the right: OT7, IM2A, PS1, OT6 and OT2

Despite the difference of nearly 50 years between Balamuth's device and the Piezosurgery® device, the basic design has remained the same. Although the actual commercial ultrasonic cutting device has demonstrated good performance, there exists an important drawback that is inherent to this type of transducer. Langevin transducers incorporate a piezoceramic stack capable of delivering a few microns of vibration amplitude, and therefore the transducer and the insert as a whole must be resonant to achieve the required ultrasonic displacement amplitude at the cutting tip. The cutting blade itself incorporates high amplitude gain, which can lead to very high stresses, and the design of the blade geometry is somewhat restricted by the requirement for resonance. Small variations in the geometry of the blade can produce a device that does not resonate at the desired frequency or, in the worst case, the blade itself can break if another resonant mode is excited.

In this chapter, a new prototype ultrasonic cutting device for bone surgery is introduced based on the NC transducer, for use in power ultrasonic applications, which removes many of the geometrical restrictions on the cutting tip of the device. When a mass is connected directly to the top surface of the metal end-caps of the transducer, the resonance frequency of the device does not experiment a significant variation when the mass is slightly modified. On the other hand the displacement amplitude is almost independent to changes on the mass coupled, as is the k_{eff} parameter, which is related to the losses of the device. The enormous benefit of this technology is, therefore, that the cutting blade design can focus more closely on delivering the best interaction between the blade and bone to provide a highly accurate cut. Also, due

to the displacement amplification generated by flextensional transducers, it is not necessary to use more than a single piezoceramic element to deliverer the desired vibration amplitude. Therefore, devices can be miniaturised to allow for delicate orthopaedic procedures involving minimal access surgery. The results show how the prototype based on the NC transducer can excite sufficiently high vibration displacement amplitude at lower driving voltages, by optimising the cymbal end-caps and geometry through finite element modelling supported with experimental vibration characterisation. Preliminary trials of the resulting prototype ultrasonic bone cutting device, which operates near to 25 kHz, are presented to illustrate the success of this novel device design.

5.2 Prototype ultrasonic device based on a NC transducer

The cymbal transducer is ideally a symmetrical transducer where both end-caps deliver the same energy in opposite directions at the resonance frequency of the cavity mode. For an ultrasonic cutting device it is necessary to maximise the energy delivered to the vibrating blade, therefore creating a non-symmetric transducer along the axial direction. In the case of the Langevin transducer the metal front and back masses on either side of the stack of ceramics are made of metals of different density and dimension, increasing the vibration amplitude towards the front. However the most important parameter when designing a non-symmetric transducer is the distribution of the mechanical stress when working at resonance. When different asymmetries are introduced in the model this stress distribution changes, and the piezoelectric element, as well as, the other mechanical parts are subjected to a non-uniform stress distribution that could cause of the degradation, and in the worst case, the failure of the device if this stress exceeds the tensile stress of the materials. Also, this non-uniform stress can cause a reduction of the efficiency in the transducer due to undesirable mechanical losses generated.

In the cymbal transducer the higher levels of stress are concentrated in the piezoceramic. However, due to the symmetry of the transducer, the stress distribution is uniform in the whole volume of the piezoceramic, except in the area situated below the epoxy layer at the edge of the cavity, where the maximum level of stress is located, when working at the resonance frequency of the cavity mode. The symmetry of a cymbal transducer keeps the ceramic driver in a pure radial (d_{31}) mode when the transducer is tuned at the resonance frequency of the cavity mode. The absence of one of the metal end-cap in a cymbal transducer, that corresponds with the most basic configuration of the transducer with a single radiating

face, introduces a non-uniform stress distribution on the piezoceramic. This distribution shows a gradient of stress in the piezoceramic that produces the appearence of bending stresses [144]. At high power levels, these undesirable bending stresses in the piezoceramic can lead to damage to the driver itself or the epoxy bonding agent, with a consequent loss of performance

Based on the NC configuration, a novel prototype (PNC) for a high power ultrasonic transducer with a single radiating face is proposed. This device has only one end-cap and a back-shell where the piezoceramic disc is placed bonded with insulating epoxy resin. The metal end-cap is attached directly to the back shell using bolts and to the piezoceramic disc with an epoxy layer. A schematic of the PNC is shown in Figure 5.3. The design of the whole transducer is optimised to transfer the radial movement of the piezoelectric disc directly to the metal end-cap, so that at the resonant mode the device exhibits a pure axial movement, consistent with the cavity mode of the symmetric cymbal transducer. The back-shell of the PNC was designed, through FEA, to keep the ceramic motion uniform, avoiding a significant bending, in order to transmit the maximal energy from the radial movement of the ceramic to the end-cap. The operational mode of the PNC compared with the symmetric and non-symmetric NC modes are shown in Figure 5.4, the red rectangular sections represent the bars attached to the transducers.
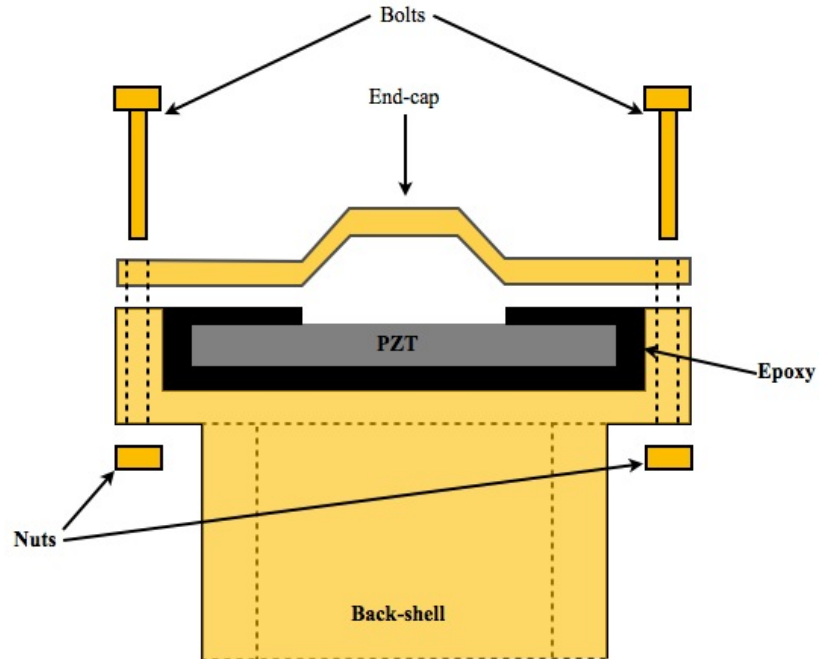
Figure 5.3: Schematic of the PNC
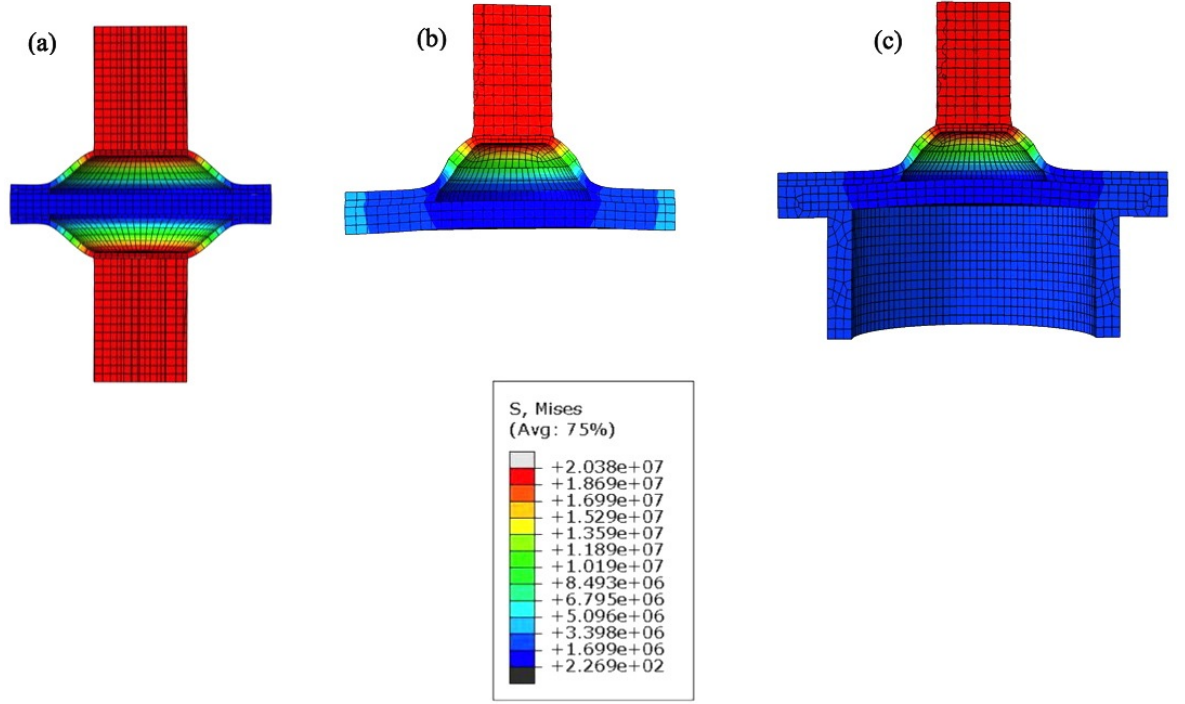
Figure 5.4: Operational stress distribution in (a) NC transducer, (b) non-symmetric NC transducer and (c) the PNC. Units in Pa

The back-shell of the PNC has 3 different parts, Figure 5.5 (a). Part A is a metal ring similar to the metal ring used for the NC configuration. The metal end-cap is attached directly to this ring through few bolts. Part B is a sheet that join the metal ring with the back cylinder (part C). The thickness of the part B, that join both cylinders, has a strong influence on the correct transmission of energy from the piezoceramic to the metal end-cap. Therefore this parameter is optimised to eliminate, as far as possible, undesirable bending of the transducer during operation. Different FEA models have shown that the best configuration is where the thickness of B is equal to the thickness of the end-cap. Part C, the back cylinder, has a double function; to create a rigid support for the piezoceramic and provide a support area to hold the PNC with minimum interference on the operational mode. Additionally, the cylinder length is designed to provide balance to the mass added to the end-cap. The majority of cutting tips designed for ultrasonic cutting in bone surgery exhibit a combination of longitudinal-flexural motion in order to perform the cut. This movement will generate a moment on the end-cap. Therefore, in order to minimise the appearance of bending motion in the transducers, associated with the operational mode, the mass and

volume of the back-shell is selected to compensate for the additional moment and eliminate bending stresses.
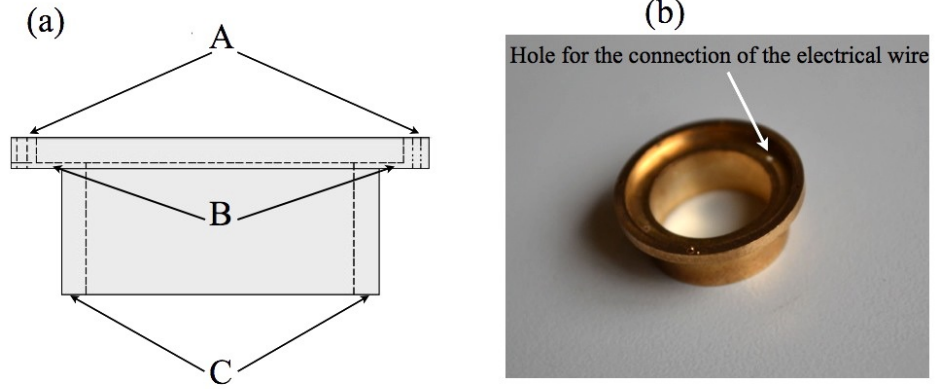
Figure 5.5: (a) Schematic and (b) photo of back shell of the PNC

The piezoceramic disc is placed in the back-shell and fixed with non-conductive epoxy, to ensure that the electrodes do not have contact with the metallic back-shell. The electrical leads are welded directly to the surfaces of the piezoceramic disc and brought out through a hole placed in the back-shell, as shown in Figure 5.5 (b). Once the epoxy that cover the piezoceramic disc is cured, the surface is sanded with a fine grain sand paper to remove the excess epoxy and the end-cap is fixed.

With OC and NC transducers, the resonance frequency and displacement of the PNC is controlled by the geometry of the end-cap. Therefore with the same dimensions and material the behaviour of the PNC should be similar to its predecessors. Therefore the reason for using brass for the metallic parts was for allowing comparation with the OC and NC.

5.2.1   Dynamic and modal characterisation of the PNC

The fabricated PNC was designed and built using brass as the material for the end-cap and the back-shell. In order to compare the performance of the PNC with the OC and NC, the geometry of the end-cap was selected to be the same, listed in Table 4.1. The piezoceramic disc was a hard PZT, PKI-402, with the dimensions as listed in Table 3.2. The dimensions of the back-shell are shown in Figure 5.6.
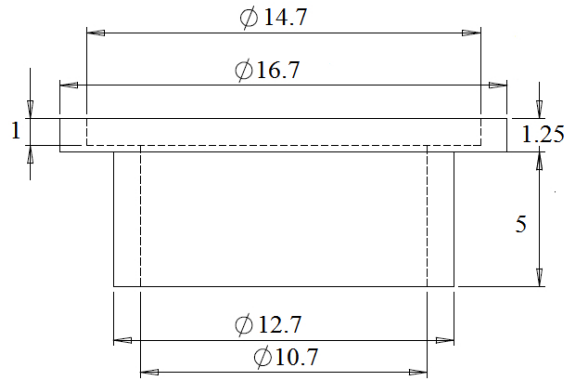
Figure 5.6: Dimensions of the back-shell for the brass PNC. Units in mm

Electrical impedance and modal characterisation of the PNC

The experimental data of the electrical impedance spectrum, comparing the OC, NC and PNC are presented in Figure 5.7.
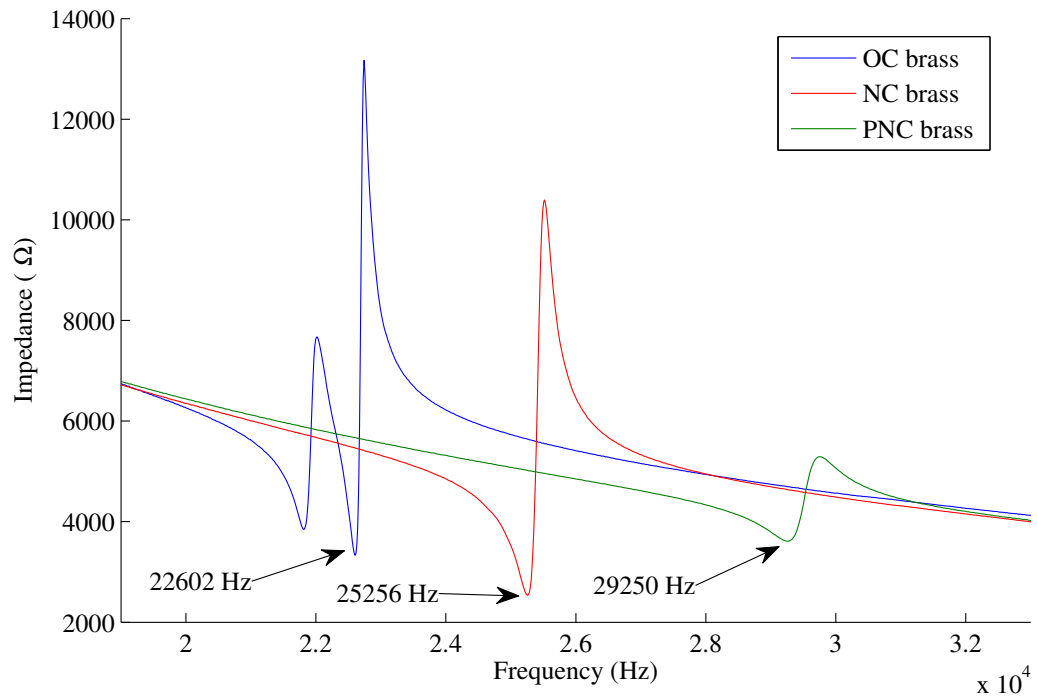
Figure 5.7: Impedance spectra of the brass OC, NC and PNC

The results indicate that for the PNC a single peak, similar to the NC transducer, is excited. The resonance frequency, that corresponds with the resonance frequency of the cavity

mode, occurs at a higher frequency due to the back-shell constraint on the piezoceramic disc. The back-shell constitutes a stiffer constraint than the metal ring of the NC configuration. The level of impedance for the resonant frequency of the cavity mode for the three devices differs less than 1 KΩ. However as occurred for the NC transducer, the level at the anti-resonance frequency is significantly reduced. Therefore, the amount of power required to drive the PNC at the anti-resonance frequency is significantly higher.

The estimation of the modal parameters of the PNC was implemented by EMA from a grid of measurement points, as explained in Chapter 3. The extracted resonance frequencies and mode shapes of the PNC for the resonance frequency of the cavity mode from EMA and FEA data are shown in Figure 5.8. The PNC was supported by the bottom at the back-shell using a small clamp. The influence of the clamp over the performance can be considered negligible, therefore the PNC was tested under free boundary conditions.

(a) EMA: 29987 Hz   (b) FEA: 29231 Hz
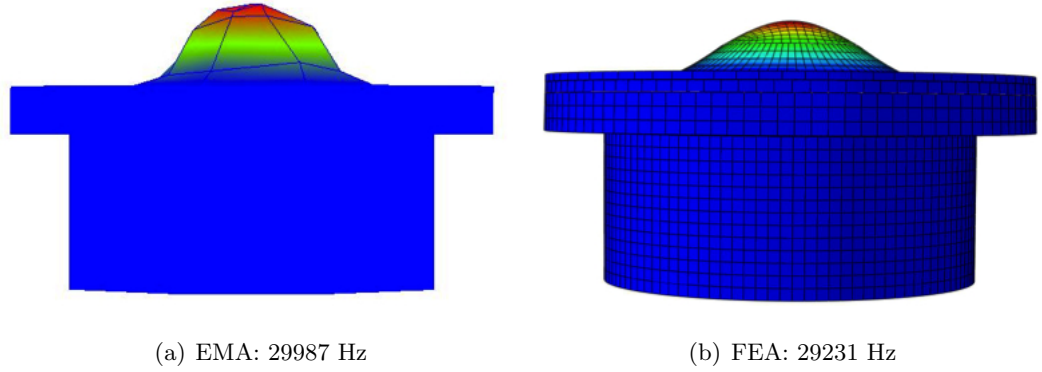
Figure 5.8: Mode shapes from (a) EMA and (b) FEA of the PNC for the cavity mode

Figure 5.8 shows good correlation between the mode shape and resonant frequency predicted through FE models and obtained through experimental modal analysis of the PNC. The mode shape of the cavity mode shows that the radial movement generated by the piezoceramic disc is transferred directly to the end-cap, without the appearance of undesirable bending.

Power harmonic characterisation of the PNC

The technique of frequency sweep excitation using a burst signal was used to experimentally characterise the vibration response of the PNC. The measured displacement was recorded at the top surface of the end-cap at different levels of excitation voltage. The results of the experiment are shown in Figure 5.9.
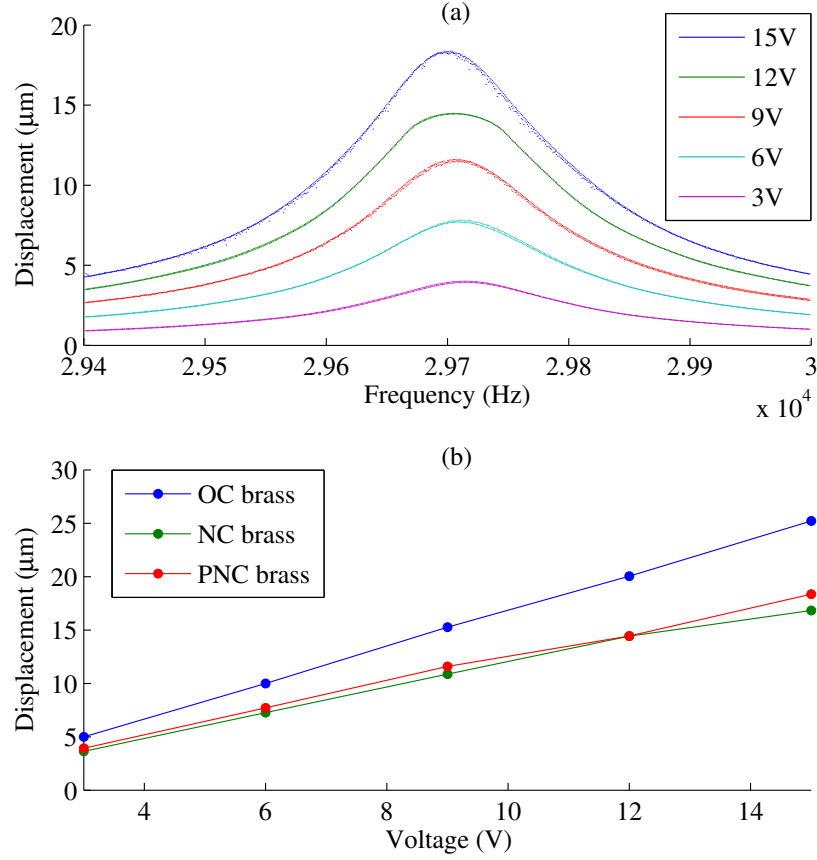
Figure 5.9: (a) Vibration response of the PNC and (b) comparison of the maximum displacement of the cavity mode for the OC, NC and PNC

The vibration response measured shows a linear response of the transducer, Figure 5.9 (a) for the range of excitation voltage levels. In this case there is no significant shift of frequency as input voltage is increased and there is consequently a reduced level of hysteresis of 0.04%. The slightly difference on the resonance frequency compared with the frequency obtained with the impedance analysis and the EMA, is due to the excitation of the PNC with different input voltage levels for each analysis. From Figure 5.9 (b), it can be observed that the displacement generated by the PNC is similar to that obtained for the NC. This demonstrates that the back-shell, that substitutes one of the end-caps, does not introduce an additional constrain on the radial movement of the ceramic.

5.3   Ultrasonic cutting device

The design procedure employed for the development the ultrasonic cutting device, was similar to that used for the design of the PNC. FEA was used first to model the initial design, predict its modal parameters, and estimate the linear response amplitudes for different levels of excitation. The cutting device was designed to operate at a resonance frequency (resonant mode of the cavity) nominally at 25.5 kHz (this frequency can slightly vary depending on the type of insert coupled). The displacement was tailored by end-cap geometry to be around 30 μm for an input voltage of 300 V in the axial direction.

As discussed in the previous section, when a mass (in this case a vibrating tip) is coupled to the PNC and it is not resonant with the transducer, the final resonance frequency is significantly reduced from that of the cymbal. Therefore, in order to design a cutting device whose operational frequency is around 25.5 kHz, the resonance frequency of the PNC must be higher to compensate for this decrease once the different inserts are connected.

The end-cap of the cutting device incorporates a threaded stud on the top surface for the connection of different inserts, as shown in Figure 5.10. The end-cap with the threaded stud was made from a solid metal bar using a thread mill machine. In order to increment the tolerance of the machined parts, and hence, improve the accuracy of the prototype, the dimensions of the transducer were increased. The dimensions for the end-cap are listed in Table 5.1 and for the back-shell in Figure 5.11. The piezoceramic disc used for the cutting device was PIC181 from PI ceramics with the dimensions shown in Table 3.2.
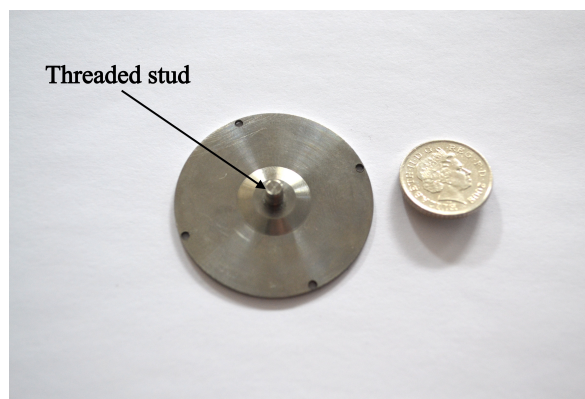
Figure 5.10: End-cap of the cutting device

Parameter	Dimension (mm)
End-cap thickness	1.1
Total diameter	33.0
Base of the cavity diameter	11.0
Apex of the cavity diameter	6.0
Cavity depth	1.0
Diameter of the threaded stud	3.50
Length of the threaded stud	5.00

Table 5.1: Dimensions of the end-cap
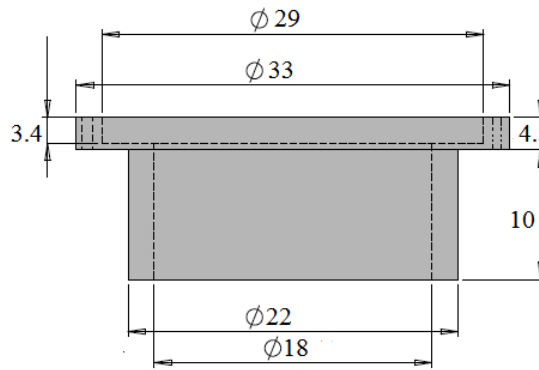
Figure 5.11: Geometry of the back-shell. Units in mm

The end-cap and back-shell were manufactured from Titanium alloy Ti-6-4. In the design of transducers for high power ultrasonics applications, the selection of the material is determined by two important parameters. One of these parameters is the mechanical Q, which is related to losses. The quality factor differs from material to material, relatively light alloys such as aluminium and titanium exhibit lower losses and higher Q than heavier ones such as tungsten. The other parameter is stress. Under operational conditions ultrasonic components experience cyclical stresses which are dependent on the component shape, vibration amplitude and material properties (such as Young's modulus). The value of limiting strain is the threshold above which acoustic attenuation rapidly increases due to changes within the material, and the maximum stress is the threshold before critical failure. Titanium has a high tensile stress (maximum stress) around 200 MPa, which is the maximum stress that can be exerted in the material before the risk of failure. For this reason titanium alloys are often

employed for the design of transducer, horns, and blades for high power applications. The cutting device without insert, and with the OT7 connected is shown in Figure 5.12.

(a)
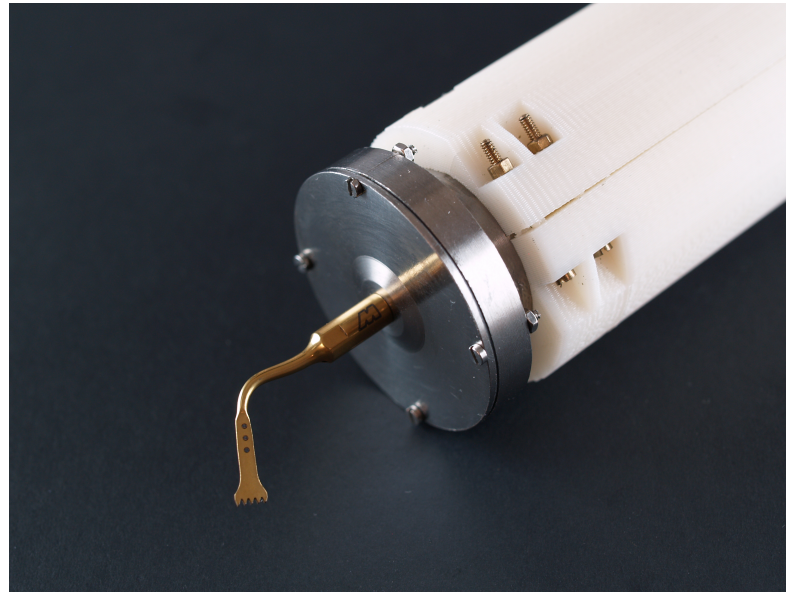
(b)

Figure 5.12: Ultrasonic cutting device (a) without insert (b) with the OT7 insert

In order to provide a support for the cutting device and facilitate handling by a surgeon, the device was housed in a plastic case, which also incorporates an electrical BNC connector to facilitate the connection with the power source. Experimentally was proved that coupling the plastic case to the back-shell of the PNC does not affect the resonance frequency nor the displacement of the transducer.

5.3.1   Experimental characterisation of the cutting device

The experimental characterisation of the cutting device was divided in two different procedures. The first procedure was the characterisation of the cutting device under free vibration conditions. For that purpose the response of the cutting device without any insert connected, and then with different inserts connected was analysed. The second procedure was the characterisation of the cutting device cutting different materials. For these experiments, the OT7 insert was used, since is the insert that offer a better cutting action.

Impedance analysis

The results of the impedance analysis of the device without insert and with the OT7 insert connected are presented in Figure 5.13.
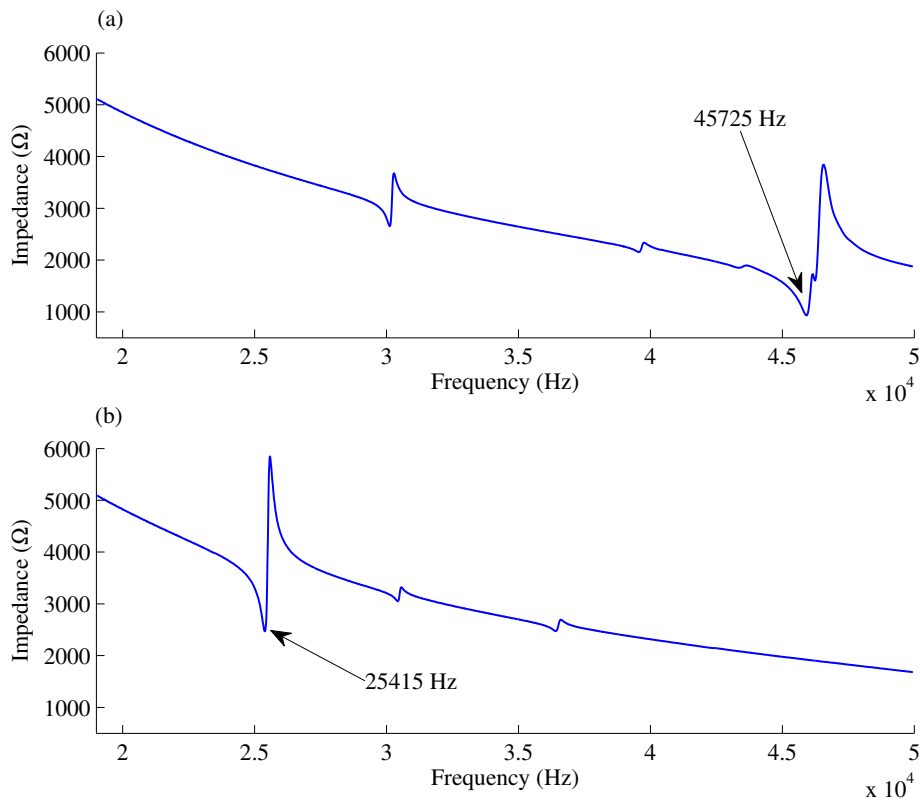
Figure 5.13: Impedance analysis of the cutting device. (a) without insert (b) with the OT7 insert

From the impedance spectra showed in Figure 5.13, it is possible to observe that the resonance frequency of the cavity mode for the cutting device without insert is tuned at about 20 kHz higher than the resonance frequency selected for the operational mode in order

to compensate for the reduction in frequency due to the addition of the mass of the inserts. The final operational frequency, when the OT7 insert is connected, of 25.4 kHz is a good correlation with the predicted resonance frequency during the design phase.

As mentioned previously, the commercial cutting devices are designed to work in a wide range of surgical procedures. Therefore they have to be able to support different types of inserts without losing performance. For that purpose, in order to analyse the variation on the impedance spectrum of the device, different inserts developed by Mectron S.p.A were connected. The characteristics of these inserts showed in Figure 5.2 are listed in Table 5.2.

Insert	Length in axial direction(mm)	Mass (g)	Application
OT7	30.68 ± 0.01	1.02 ± 0.01	Osteotomy
IM2A	36.35 ± 0.01	1.21 ± 0.01	implant site preparation
PS1	28.85 ± 0.01	0.96 ± 0.01	root scaling
OT6	30.77 ± 0.01	1.31 ± 0.01	Osteotomy of large bone
OT2	30.16 ± 0.01	1.22 ± 0.01	micrometric osteotomy (about 1 mm)

Table 5.2: Different inserts connected to the cutting device
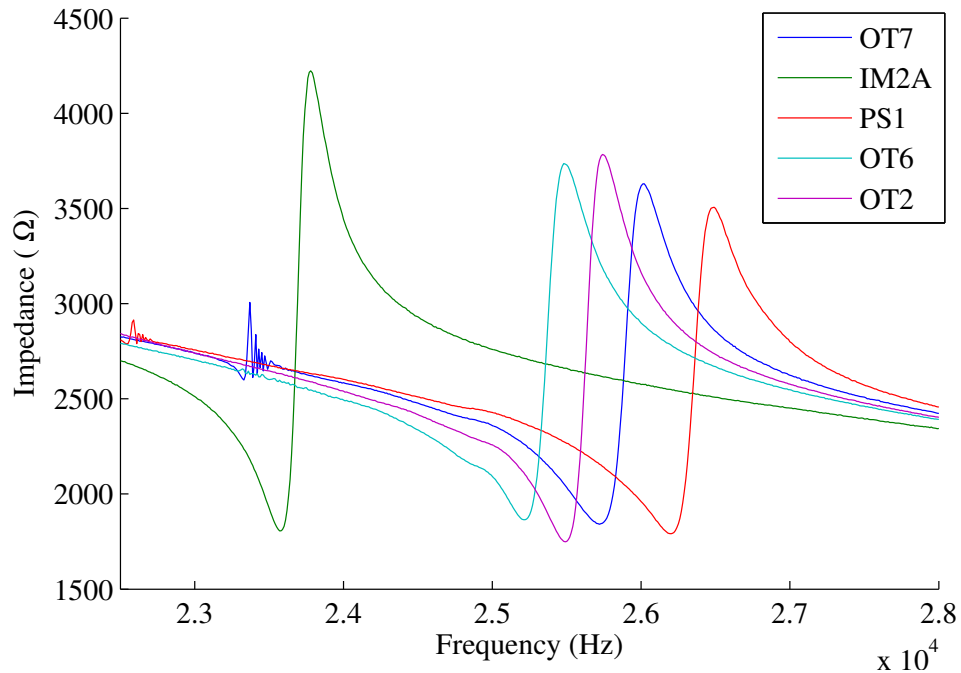
Figure 5.14: Impedance spectra of the cutting device with different inserts

Figure 5.14, shows the variation of the resonance frequency of the cavity mode when

different inserts are connected to the cutting device. As it can be seen, the resonance frequency does not suffer significant changes when the shape and mass of the insert is modified. A variation in mass of 36.43 % only entails a variation of 10.26 % on the resonance frequency. On the other hand, the levels of impedance for the resonance and anti-resonance frequencies remain similar, showing a high degree of independence of the operational frequency from the geometry of the vibrating tip.

A change in the resonance frequency of the cutting device with the OT7 insert, compared with the results analysed in the previous section, occurred after the first time the cutting device was driven at high input power levels. The altered resonant frequency was then permanent. This effect is also noticed in the development of other ultrasonic transducers, such as the Langevin transducer, and is produced due to a readjustment of the different parts when the first operational procedure is finished. In the case of the ultrasonic cutting device based on the PNC, this variation is influenced by permanent changes in the physical properties of the epoxy layer. After this first variation, the resonance frequency does not suffers other changes and is independent of the input power selected. This behaviour was reported as 'normal' by Mectron since it happens in other tools developed by the company. Although the causes are not well-known one possible reason can be the re-adjust of the different parts when subjected to a high input power.

Modal analysis

The dynamic behaviour of the two assemblies, without and with the OT7 insert, was studied through a combination of finite element and experimental modal analysis in order to find the natural frequency and mode shape of the cutting device, Figure 5.15. Good correlation can be seen between the mode shapes of the FE predictions and the EMA results with a difference between the resonance frequencies for the cutting device without insert and the cutting device with the OT7 being 1.92% and 0.44 % respectively.

(a) EMA: 46170 Hz   (b) FEA: 45282 Hz

(c) EMA: 25842 Hz   (d) FEA: 25727 Hz
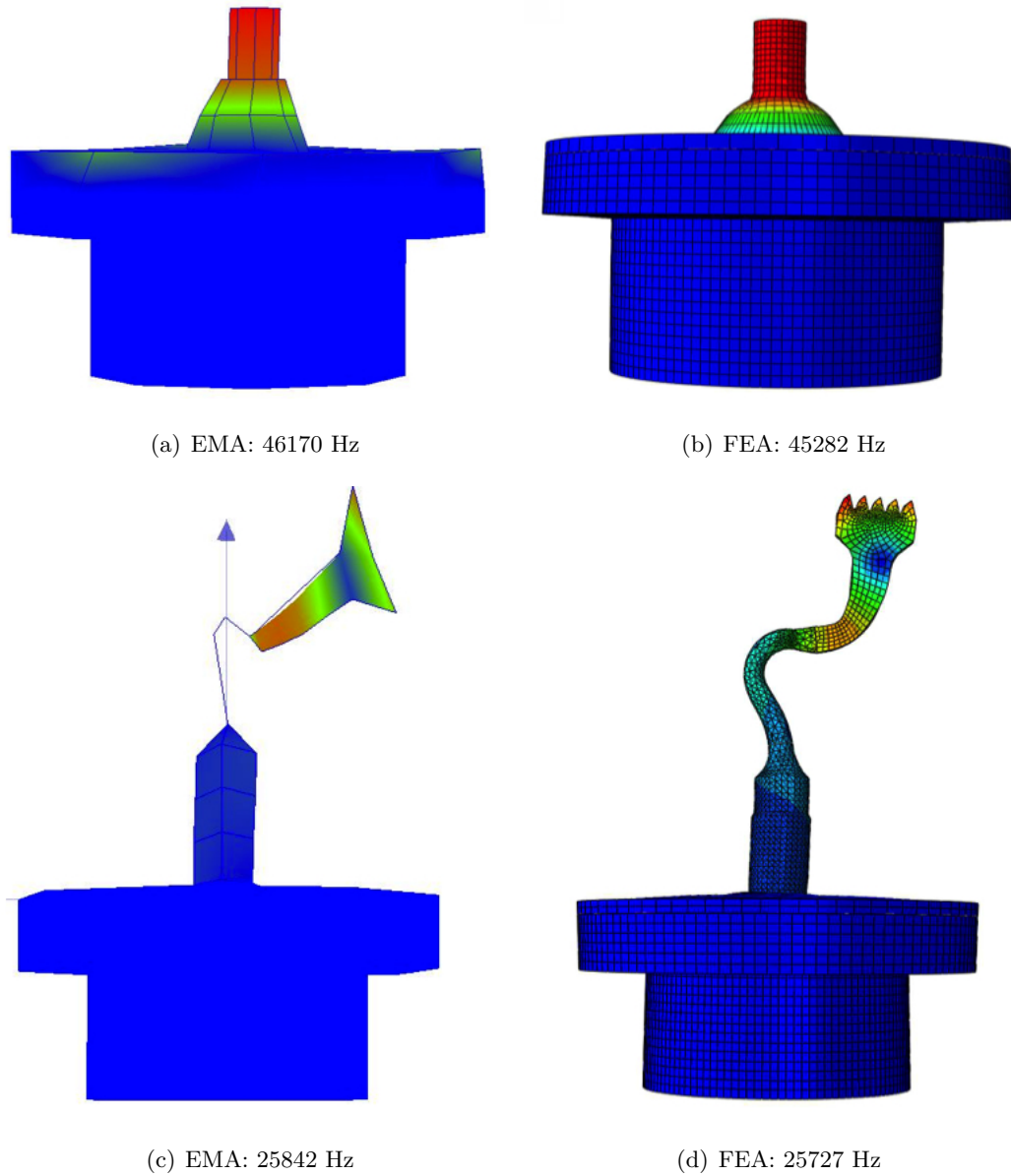
Figure 5.15: Mode shapes from (a) EMA and (b) FEA of the cutting devie without insert and (c) EMA and (d) FEA for the cutting device with the OT7 insert

Power harmonic characterisation

The cutting device without any insert underwent harmonic characterisation. The vibration response measurements were recorded from the free end of the threaded stud of the end-cap, Figure 5.16.
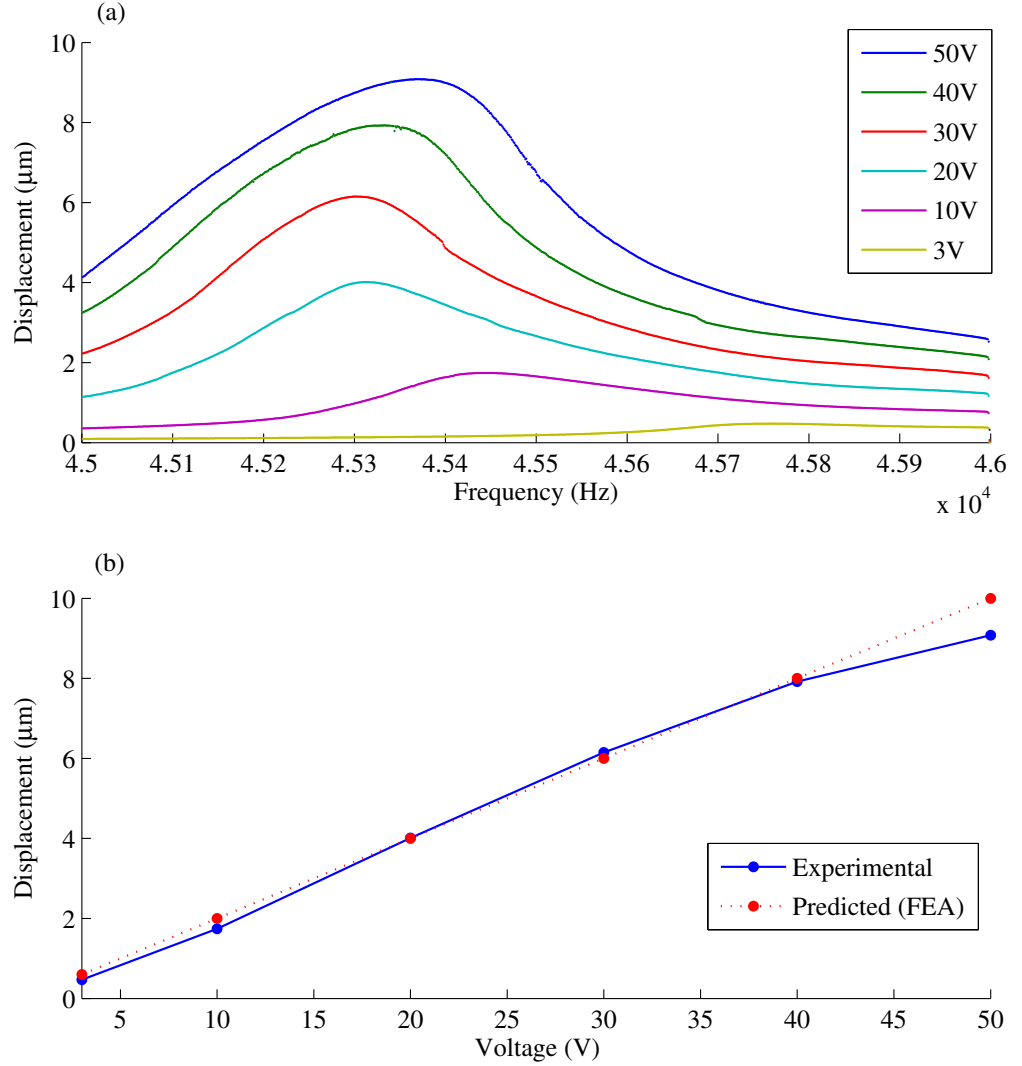
Figure 5.16: Vibration characterisation of the cutting device without insert. (a) Vibration displacement response and (b) vibration displacement at the cavity mode frequency

In Figure 5.16 a slight shifting of resonance frequency can be noted when the excitation levels are increased. The shift starts with a softening effect (reduction of the resonance frequency) then continues with a hardening effect (increase of the resonance frequency) for higher input voltage levels. This can be principally related to the temperature increase within piezoceramic disc that alters their properties, generating a non-linear effect. The vibration displacement shows a linear trend with voltage (Figure 5.16 (b)), and there exists a good correlation with the predicted displacements calculated from the FE model developed in

Abaqus.

The vibration response of the cutting device with the OT7 insert connected was measured in the axial direction for different input powers. Due to the high input voltage levels reached for these experiments, the signal generator was connected directly to a power amplifier with a constant gain that showed accurate information about the power consumed by the cutting device, but not the voltage, for that reason the experiments of the device with the OT7 insert were related with the input power. Due to the difficult nature of acquiring measurements from the insert cutting end, since the motion is a combination of a flexural and axial movement, the response was recorded from the base of the insert. This displacement provides information of the displacement generated by the end-cap, Figure 5.17 (a). Subsequently, with the same input powers, different cuts were produced in a biomechanical test block that simulates the properties of bone, made of solid rigid polyurethane foam, Figure 5.17 (b) and Figure 5.18. Each cut was performed during a period of time of 5 seconds applying the same loading force. For that, the transducer was handled using the weight of the transducer as the only loading force, avoiding any additional force by the hand.
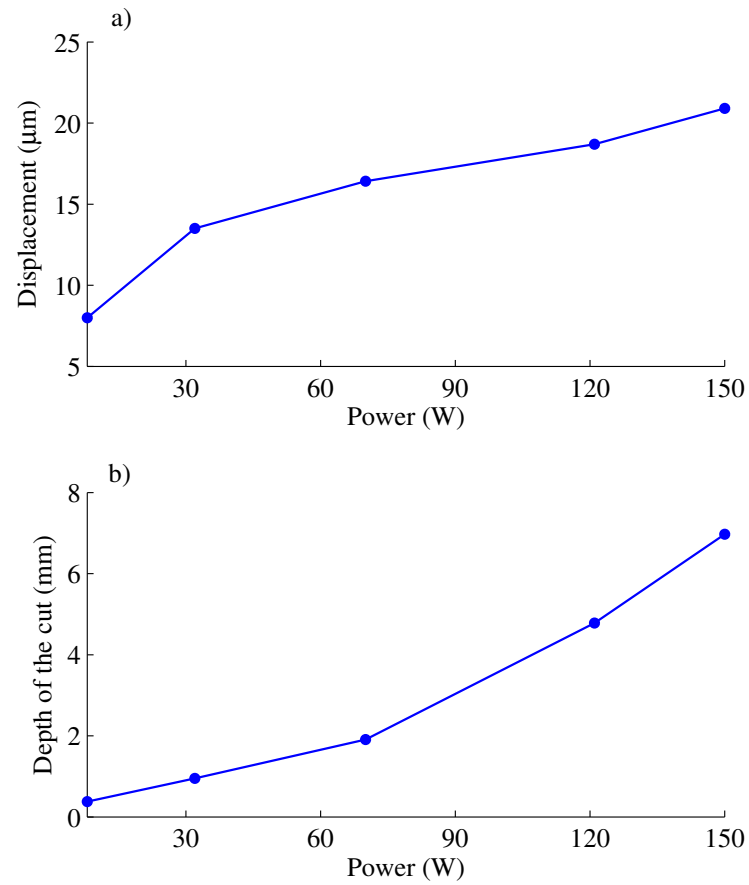
Figure 5.17: Vibration characterisation of the cutting device with OT7 for different input power levels. (a) Relationship between the input power vs. axial displacement at the base of the OT7 insert and (b) relationship between the input power vs. the depth of the cut for 5s of cutting action
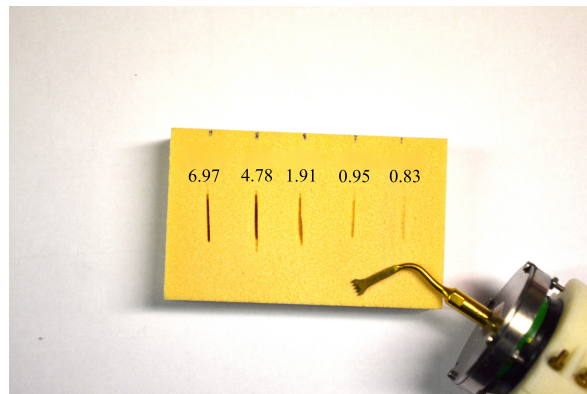
Figure 5.18: Cuts performed on the biomechanical test block for different input power levels. Depths of the cuts measured in mm

In Figure 5.17 (b) it can be observed that there exist a significant increase in the depth of cut when the power of the device increases from 70W to 120W that corresponds with a cut of 1.91 and 4.78 mm respectively. In terms of axial displacement at the base of insert, this difference corresponds with a change in the displacement from 17 to 19 μm. The axial motion at the base of the insert is amplified by the flexural motion of the cutting tip, therefore a small increment of the axial displacement results in a large increase in the cutting motion of the tip.

Studies carried out by Mectron S.p.A. have demonstrated that for an efficient cut using the OT7 insert, the axial displacement at the base of the insert must be 15 μm or higher. In the case of the cutting device based on the PNC to reach this displacement a minimum input power of 50W is required.

Experiments with real bones

These experiments were realised in collaboration with the Department of Orthopaedic Surgery at the University of Edinburgh. The aim of the study is to compare the cutting performance of different traditional surgical tools for bone cutting, bone burs and saws, with the ultrasonic device. Ultrasonic devices used in osteotomy have shown to have advantages such as high precision, less damage to both soft and hard tissues, less damage to close delicate structures, and quicker recovery times than traditional instruments such as bone burs and bone saws.

Bone burs and saws used macrometric rotations and oscillations to dissect hard tissue, but these can easily damage soft tissue. Additionally, during the cutting process, high temperatures are generated in the zone of the cut due to the friction between the blade with the bone, resulting in osteonecrosis (bone cell death) as result of tissue heating.

For the experiment, 6 rat femurs were cut in two different locations using the ultrasonic cutting device with the OT7 insert. Two different operational conditions were analysed; cutting without coolant, and with a coolant liquid applied directly to the zone of cut. Subsequently a histological study was carried out by the researches in Edinburgh to analyse the number of live and dead cells in the zone of the cut. In Figure 5.19 (a) and (b) it is possible to observe the procedure of cutting without and with coolant respectively and (c) a thermal image, and in Figure 5.19 (d) a detail of the section of the bone after being cut.
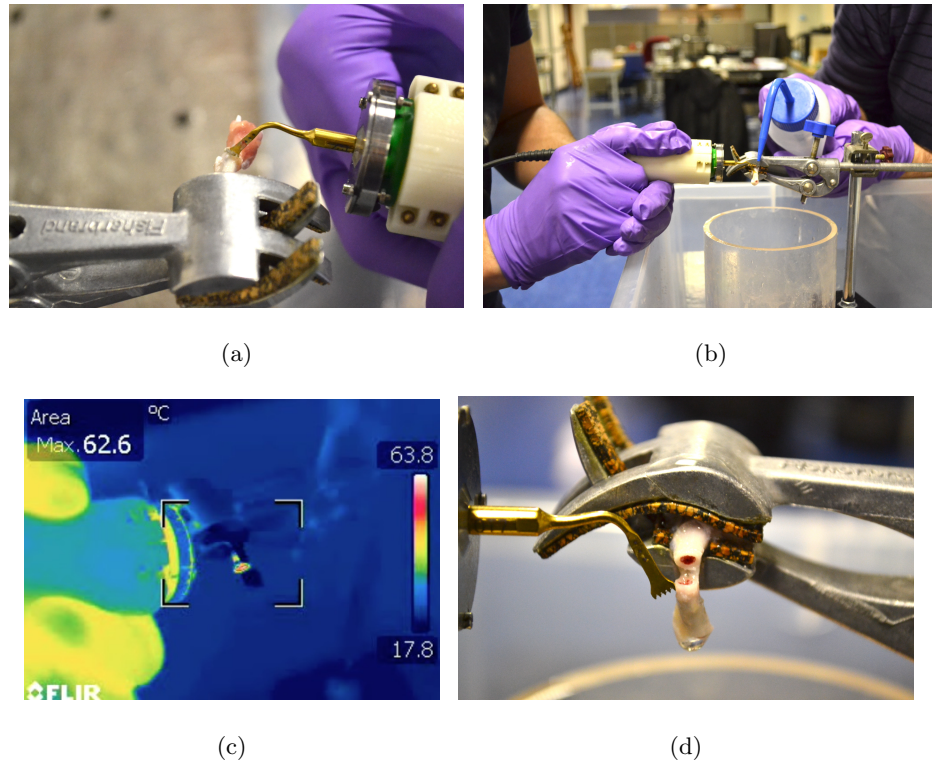
Figure 5.19: Experimental setup of the rat bone cutting procedure. (a) cut without coolant, (b) with coolant, (c) thermal image of the cut procedure and (d) detail of the bone cut

In the histological analysis each section of the bone cut using the ultrasonic device was divided in zones of 50 μm from the cut surface to the interior of the bone. In each zone, the bone cells, classified as live or dead, were counted and compared for statistical significance by an ANOVA. In Figure 5.20 the percentage of live cells in each zone for both operation conditions, with and without coolant, are shown.
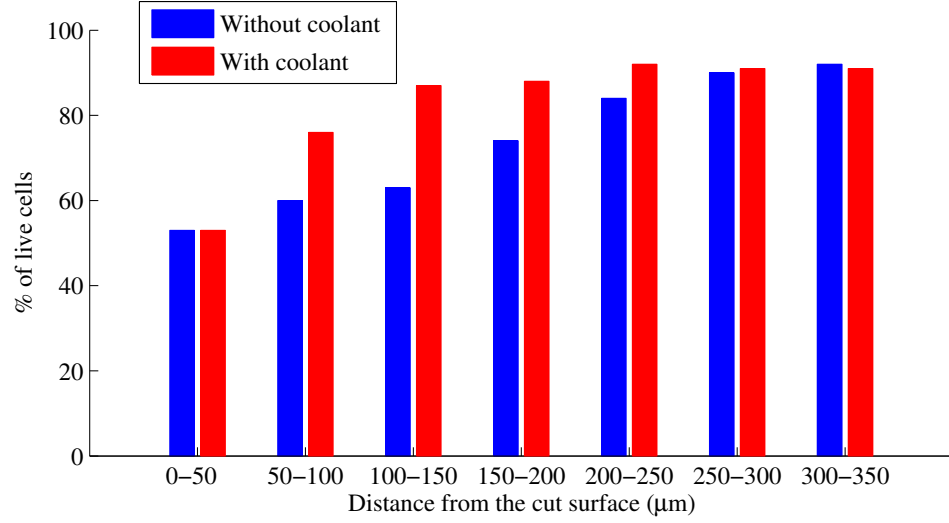
Figure 5.20: Histological analysis of the cut bones divided in zones of 50 μm

As can be observed in Figure 5.20, the results show that more than 50 % of the cells in the nearest zone of the cut surface, up to 50 μm, are alive. In this zone the use of coolant does not introduce a improvement, however there exist a significant difference between the configurations when analysing zones between 50 - 250 μm, since the use of a coolant increases the number of live cells by more than 20 %. This difference is negligible when the zone analysed is further than 250 μm away from the cut surface. The fact that there are more live cells than dead cells in the surroundings of the cut surface, compared with traditional saws that exhibit a lower percent (in many cases lower than 30%), enhances the healing time of the bone. The use of a coolant improves the number of live cells further, therefore its use is highly recommended.

For reason of time, the histological results of the traditional tools are not available at the moment of the submission of this thesis. The final comparative study will be published in a journal paper in collaboration with the researchers of the Department of Orthopaedic Surgery at the University of Edinburgh.

5.4 Summary

In this chapter a prototype for high power applications (PNC) based on the NC design has been investigated. The device is consist of a single metal end-cap coupled to a back-shell where the piezoceramic disc is placed. Therefore, the energy generated in the piezoceramic disc is delivered directly to the end-cap, creating a single radiating face. The design of the back-shell was developed through FEA, in order to optimise the transfer of energy from

the piezoceramic disc to the end-cap, without introducing bending in the resonant mode of vibration.

For the design of the cutting device, the metal end-cap incorporates a threaded stud to allow the connection of different cutting inserts. The modal and dynamic characterisations of the cutting device have shown a good correlation between the predicted values of frequency, displacement and mode shapes using the FEA, and experimental results. For the characterisation of the device under real operational conditions, several experiments were undertaken in collaboration with the Department of Orthopaedic Surgery of the University of Edinburgh. The results obtained have demonstrated promising performance of the device, realising precise cuts in animal bones using a commercial cutting blade designed by Mectron S.p.A.

Chapter 6

Conclusions and Future work

The work presented in this thesis has focused on the development of a novel miniaturised ultrasonic cutting device for high precision minimal access orthopaedic surgical procedures based on the class V flextensional cymbal transducer. Through investigating a structural modification of the original cymbal transducer (OC), creating a non-symmetric transducer optimised for delivering the energy generated in the piezoceramic element in a single axial direction, a new prototype of ultrasonic transducer (PNC) for high power applications has been developed. This device incorporates a threaded stud for the attachment of different vibrating cutting inserts, so that it is possible to perform different surgical procedures.

The actual commercial ultrasonic cutting devices for bone surgery are based on the ultrasonic cutting device developed by Balamuth in 1945. This was comprised of a Langevin transducer, which incorporated a piezoceramic stack coupled to a horn which provided a threaded connection for attaching the cutting tips. During more than 50 years researchers have been working on modifications of the original design in order to improve the efficiency of the transducer. However, due to the nature of the Langevin transducer, there are important inherent drawbacks that have not yet been resolved. In order to deliver the required ultrasonic amplitude to the cutting tip, the whole transducer must be resonant, therefore the design of the vibrating blade is somewhat restricted by the requirement for resonance. On the other hand, the blade itself incorporates high amplitude gain, which can lead to very high stresses. In this thesis a new point of view is offered by redesigning the ultrasonic cutting device based on a different type of ultrasonic transducer, a flextensional transducer.

6.1 Characterisation of the cymbal transducer

6.1.1 Summary

In Chapter 3, the performance of the OC was studied for three different types of end-cap materials. The process of design and analysis of the different devices, started with the creation of a finite element (FE) model of the transducers. This modelling stage is used to create, optimise and predict the performance of an initial design whilst experimental techniques, which consist of electrical impedance analysis, experimental modal analysis (EMA), and harmonic response analysis, are used to characterise the fabricated models and to validate and update the numerical models.

Despite the small dimensions of the transducer, high displacement levels are generated at relatively low input voltages. The enormous amplification factor enabled by the truncated conical shape end-caps, amplifies the small radial motion of the ceramic disc to achieve a much larger axial motion due to the flexural-axial movement of the end-cap. This amplification factor can be up to 45 times the axial displacement of a single piezoceramic disc. To evaluate the response of the OC working as actuator, different bars were couple directly to the top surface of the metal end-cap. In this configuration the masses added largely act like rigid bodies and they are not tuned to the resonance frequency of the cavity mode body of the OC.

6.1.2 New contribution to knowledge

- The 3D EMA realised for the OCs which exhibit a double resonant peak in the response spectrum, have demonstrated that the two peaks correspond with the cavity resonant mode and the asymmetric resonant mode.

- The analysis of the vibration response of the OCs has shown that for each of the two resonant modes, only one of the end-caps has dominant movement exhibiting a higher displacement. However the highest displacement is obtained at the cavity resonant mode when the end-caps of the OC move out-of-phase.

- When a mass is coupled to the cymbal transducer, the resonance frequency of the cavity mode is significantly reduced. The results have shown a slight convergence in the relationship between the weight of the mass added and the resonance frequency of the cavity mode, so that when weight of the mass added is increased the variation on the resonance frequency is reduced.

- The maximum displacement generated by the OC, recorded at the top surface of the different bars, was shown to be independent of the weight of the mass added. On the other hand, the mass added reduces the mechanical losses of the device, as shown by the effect on the k_{eff}.

6.1.3   Conclusions

- The appearance of a double resonant peak due to asymmetries introduced during the fabrication process of the transducers can cause bending motions that can lead to the degradation of the transducer when working at high input power levels. For that reason it is necessary to improve the mechanical coupling between the end-cap and the piezoceramic disc of the OC.

- The relationship between the resonance frequency of the OC with the weight of the mass coupled to the end-cap is especially important in applications where the insert coupled to the end-cap is not tuned to the frequency of the cymbal transducer. Since a variation of the geometry or mass of the insert does not introduce a significant variation in the resonance frequency of the device across a range of geometries and masses, the design of the insert can be treated independent of the transducer. In ultrasonic cutting applications the design of the cutting insert can therefore be focused on obtaining the best interaction with the material in which the insert will be applied.

6.2   Design of the cymbal transducer for high power applications

6.2.1   Summary

The OC has been widely adopted for low power ultrasonics applications. However, it presents important drawbacks for high power ultrasonics applications that require much higher output displacements. Asymmetries introduced during the fabrication process reduce the efficiency of the transducer. These asymmetries can be recognised by the appearance of a double resonance peak in the frequency response of the transducer. On the other hand, due to the flexural-axial movement of the end-cap, there are regions in the end-cap which are subjected to high stress. These areas are critically at the edge of the cavity, and therefore high stress is transmitted to regions of the epoxy layer in contact with the end-caps. When the OC is driven at high input voltages, the degradation of the bonding layer between the end-caps and

the electroactive material can alter the vibration response and ultimately lead to failure of the device. In order to solved these problems, in Chapter 4 a variation of a design first described by Lin in 2010 is proposed for high power ultrasonics applications. In comparison with the OC design, the driving element of this new cymbal design (NC) consists of a ceramic disc bonded to a metal ring. The end-cap, with a larger flange, is attached directly to the metal ring through some bolts and to the piezoceramic disc by means on an epoxy layer, enhancing the mechanical coupling and reducing the stress in the epoxy layer. Another advantage is the improvement in the control of the fabrication process of the transducer. The use of threaded bolts means that the end-caps can be much more accurately aligned with the piezoceramic disc. This reduces asymmetries in the assembled transducer, reducing the likelihood that the transducer resonance frequency response will exhibit a double-peak, that occurs in the majority of the OCs fabricated.

The experimental characterisation of the NC shows a good correlation between the FE model and the experimental results. This is due to the high level of symmetry obtained due to an improved control of the assembly process. In the two NCs assembled, a response spectrum with a single peak was measured. The response of the NC is similar to that obtained for the OC with the same end-cap material. However, when driving at high input voltages, the NCs show a significant superiority. The difference in the maximum displacement reached for the NCs before degradation of the epoxy layer was in both cases more than 30 μm compared with the OCs. Both the increased displacement amplitude capability and improved symmetry of this NC configuration mean that it is better suited to applications in high power ultrasonics than the OC.

6.2.2   New contribution to knowledge

- The development of the NC, introducing an additional mechanical coupling between the end-cap and the piezoceramic disc, improves the fabrication process of the transducer. The control of the asymmetry of the transducer results in a device with a single resonant peak in its response spectrum.

- The NC has shown similar response to that obtained for the OC when working as an actuator, however the maximum amplitude reached by the NC is significantly higher due to the action of the additional mechanical coupling, improving its response at high input power.

6.2.3 Conclusions

- The possibility of driving the NC at high input power without losing performance makes this transducer a promising device for high power ultrasonic applications where a high level of displacement is required.

- Due to the symmetry of the NC it is necessary to develop a modification of the transducer to obtain a single radiating face in order to use this transducer in applications such as ultrasonic cutting where the transducer has to deliver the mechanical motion to a vibrating insert.

6.3 Design of a novel ultrasonic cutting device

6.3.1 Summary

Based on the NC configuration a prototype (PNC) for high power ultrasonics applications was proposed. The PNC constituted a variation of the NC in which one end-cap is removed and substituted by a back-shell. The main problem for designing a non-symmetrical NC transducer is the appearance of undesirable bending modes associated with the resonant mode of the cavity, that can cause degradation of the device when operating at high power levels. For that reason the design of the back-shell was the result a careful study by FE modelling, in order to optimise the transfer of energy from the piezoceramic disc to the end-cap, without introducing additional bending motion. The dynamic characterisation of the PNC shows a good correlation with the results predicted by the FE model. The results obtained from the experimental analysis demonstrate that the performance of the PNC, that is a non-symetric transducer, is similar to that obtained for the NC.

For the design of the cutting device, introduced in Chapter 5, an end-cap which incorporates a threaded stud for the connection of different cutting tips was developed. The resonance frequency of the transducer was selected significantly higher than the final operational resonance frequency in order to compensate for the reduction in the resonance frequency when the cutting insert (mass) is coupled to the device.

This cutting device has shown a stable resonance frequency when different types of insert have been connected. Therefore, for slight changes on the geometry of the inserts the operational resonance frequency remains almost independent.

Initial lab based trials, in collaboration with the Department of Orthopaedic Surgery of the University of Edinburgh, have demonstrated promising performance of the device,

realising precise cuts in rat bones using a commercial cutting blade designed by Mectron S.p.A.

6.3.2 New contribution to knowledge

- The PNC constitutes a new transducer based on the NC where the action of the back-shell, which substitutes for one of the end-caps, allows the device to deliver the motion generated by the piezoceramic disc in a single direction. The design of the back-shell was tailored to reduce the bending on the ceramic disc, due to the lack of symmetry of the new transducer, in order to prevent failure of the transducer when driving at high input power.

- The back-shell does not introduce an additional constraint to the radial motion of the ceramic, therefore the displacement of the PNC is comparable to that obtained for the NC.

- The connection of different commercial cutting inserts, designed by Mectron S.p.A., does not modify significantly the resonance frequency of the transducer, which incorporates a threaded stud on the top surface of the end-cap to allow the optimal connection of the vibrating tips.

6.3.3 Conclusions

- This cutting device has shown a stable resonance frequency when different types of insert have been connected. Therefore, for significant changes in the geometry of the inserts the operational resonance frequency remains almost independent. The enormous benefit of incorporating the PNC for ultrasonic bone surgery is that, since the cutting blade itself does not have to be tuned to be resonant with the transducer, the blade design can focus more closely on delivering the best interaction with bone to provide a highly accurate cut.

- The first experiments have demonstrated the capability of this cutting device to cut in moderately different materials using commercial cutting inserts. This device, as opposed to the Langevin based cutting devices, uses only a single piezoceramic disc as the driver, however it is able to generate the necessary displacement to perform cuts.

- Initial lab based trials, in collaboration with the Department of Orthopaedic Surgery of the University of Edinburgh, have demonstrated promising performance of the device.

More than 50 % of cells located near the cut surface of rat bones cut using the ultrasonic cutting device are alive. This high number of live cells implies that there will be a reduction in the healing time of the bone, and therefore the risk of possible complications that can affect the total recovery of the tissue is reduced.

6.4   Future works

In this thesis a new ultrasonic cutting device has been developed using a flextensional transducer, originally designed for low power ultrasonics applications, instead of the widely known Langevin transducer. The development of an efficient transducer able to operate at high power levels, that removes much of the drawbacks presented in the actual Langevin transducer, offers a new vision for the development of ultrasonic transducers for high power ultrasonic applications. Although there exist many lines of investigation on which this new transducer can be studied, the following works are proposed as of interest for complementing the work presented in his thesis.

6.4.1   Miniaturisation of the PNC and design of a cooling system

Although good correlation was achieved between the FE model and the experimental results for the PNC designed, a complete loss of performance appeared when the size of the transducer was reduced. The tolerances achieved during the fabrication process and the assembly of the transducer fell short of those required for a miniature transducer design. For that reason, for the miniaturisation of the PNC it is necessary to improve (and automate) both the manufacturing process of the different parts and the assembly process.

As discussed in the literature review, it has been widely demonstrated that the irrigation of the work area using a coolant agent during the cutting process improves the efficiency of the cutting action of the blade by cleaning the cut zone. Additionally, the coolant reduces the heat generation due to the friction between the cutting tip and the bone, hence reducing the risk of necrosis of the neighbouring tissues. For that reason an improved design of the PNC, that incorporates a cooling system in the posterior face of the top surface of the end-cap, was developed. The cooling system would connect to a silicon tube, introduced through the back-shell of the transducer, to the threaded stud through an internal canal. The cooling solution would be then directed through the instrument and expelled, cooling both the tip and treatment area.

Tests of a miniaturised PNC incorporating this cooling system did not exhibit satisfactory

performance due to the mentioned lack of accuracy during the manufacturing and assembly process.

6.4.2 Improvement of the mechanical coupling of the PNC

Although the NC increases the displacement capability of the OC, the design does not solve completely the problem of the degradation of the epoxy layer due to high stress concentrations in the vicinity of the cavity. Also, the physical properties of the epoxy are sensitive to changes in the environmental conditions in which the transducer is used. Therefore, the frequency and displacement characteristics of the transducer can be altered due to changes, for example, in the temperature or humidity. For that reason it is proposed that coupling the metal end-cap with the piezoceramic disc using ultrasonic welding might provide a better design solution. By removing the epoxy layer the problem of the degradation of the mechanical coupling between the piezoceramic and the end-cap would be solved. Other option could be to solder directly the end-cap and the ceramic, with special care on the control of the temperature to avoid reaching the Curie temperature of the piezoceramic.

6.4.3 Connection of various NC in series

It has been demonstrated that a single NC can achieve large displacements with a relative low input power. However, for industrial ultrasonic applications such as ultrasonic drilling, a large displacement has to be in combination with large generative forces. Since the NC is constituted by a single ceramic and two thin end-caps, the generated force will not be high enough for this kind of application. For that reason the connection in series of several NCs would increase greatly not only the displacement generated, but also the generative force produced and this might further widen the applicability of this transducer technology in high power ultrasonics.

Appendix A

List of Publications

Journal papers

- F. Bejarano, A. Feeney, M. Lucas, A cymbal transducer for power ultrasonics applications, Sensors and Actuators A: Physical, Vol. 210, Pages 182189, 2014

Conference papers

- M. Lucas, F. Bejarano, An ultrasonic orthopedic surgical device based on a cymbal transducer, Proceedings of the 2013 International Congress on Ultrasonics (ICU 2013), pp.185-190, 2013

- F. Bejarano, A. Feeney, M Lucas, Vibration characterisation of cymbal transducers for power ultrasonic applications, MPSVA Conference, Institute of Physics, Journal of Physics: Conference Series 382 (2012) 012063, 2012

- F. Bejarano, A. Feeney, M. Lucas, Optimisation of a cymbal transducer for its use as driver of a high-power ultrasonic cutting device for bone surgery, 41st UIA Symposium, 2012

- A. Feeney, F. Bejarano, M. Lucas, Dynamic characterisation of cymbal transducers for power ultrasonics applications, 41st UIA Symposium, 2012

- F. Bejarano, M. Lucas, Finite element modelling and design of cymbal transducers for power ultrasonics applications, IEEE International Ultrasonics Symposium, pp.1567 - 1570, 2011

References

[1] C. Dictionaries, *Collins Paperback Dictionary & Thesaurus.* Collins, 2011.

[2] S. Middelhoek and A. Hoogerwerf, "Smart sensors: when and where?," *Sensors and Actuators*, vol. 8, no. 1, pp. 39 – 48, 1985.

[3] R. C. Rosenberg, *Introduction to Physical System Dynamics (McGraw-Hill series in mechanical engineering).* Mcgraw-Hill College, 1983.

[4] I. J. Busch-Vishniac, *Electromechanical Sensors and Actuators (Mechanical Engineering Series).* Springer, 1999.

[5] J. L. Pons, *Emerging Actuator Technologies: A Micromechatronic Approach.* Wiley, 2005.

[6] A. Rich, "Thermo-mechanical transducer," Feb. 27 1968. US Patent 3,371,309.

[7] R. Venditti, J. S. H. Lee, Y. Sun, and D. Li, "An in-plane, bi-directional electrothermal mems actuator," *Journal of Micromechanics and Microengineering*, vol. 16, no. 10, pp. 2067–2070, 2006.

[8] J. Khazaai and H. Qu, "Electro-thermal mems switch with latching mechanism: Design and characterization," *IEEE Sensors Journal*, vol. 12, no. 9, pp. 2830–2838, 2012.

[9] C. Cobb, N. LeComte, S. Nott, and S. Strobel, "Electrothermal sensor apparatus," Aug. 18 1992. US Patent 5,140,394.

[10] J. Yang, G. Lau, C. Tan, N. Chong, B. Thubthimthong, and Z. He, "An electro-thermal micro-actuator based on polymer composite for application to dual-stage positioning systems of hard disk drives," *Sensors and Actuators A: Physical*, vol. 187, pp. 98 – 104, 2012.

[11] S. W. Meeks and R. W. Timme, "Rare earth iron magnetostrictive underwater sound transducer," *The Journal of the Acoustical Society of America*, vol. 62, no. 5, pp. 1158–1164, 1977.

[12] D. McClements, "Advances in the application of ultrasound in food analysis and processing," *Trends in Food Science & Technology*, vol. 6, no. 9, pp. 293 – 299, 1995.

[13] J. G. Juarez, "Macrosonics: Phenomena, transducers and applications," *Revista de acstica*, 2002.

[14] A. A. Pilla, M. A. Mont, P. R. Nasser, S. A. Khan, M. Figueiredo, J. J. Kaufman, and R. S. Siffert, "Non-invasive low-intensity pulsed ultrasound accelerates bone healing in the rabbit," *J Orthop Trauma*, vol. 4, no. 3, pp. 246–253, 1990.

[15] M. Lucas, A. Cardoni, E. McCulloch, G. Hunter, and A. MacBeath, "Applications of power ultrasonics in engineering," *Applied Mechanics and Materials*, vol. 13-14, pp. 11–20, 2008.

[16] A. Shoh, "Industrial applications of ultrasound - a review I. high-power ultrasound," *Sonics and Ultrasonics, IEEE Transactions on*, vol. 22, no. 2, pp. 60–70, 1975.

[17] A. Olabi and A. Grunwald, "Design and application of magnetostrictive materials," *Materials & Design*, vol. 29, no. 2, pp. 469 – 483, 2008.

[18] F. Claeyssen, N. Lhermet, R. L. Letty, and P. Bouchilloux, "Actuators, transducers and motors based on giant magnetostrictive materials," *Journal of Alloys and Compounds*, vol. 258, no. 1-2, pp. 61 – 73, 1997.

[19] R. Sathishkumar, A. Vimalajuliet, and J. Prasath, "Terfenol D: A high power giant magnetostrictive material for submarine mapping," *International Journal of Engineering Science and Technology*, vol. 2, pp. 7165–7170, 2010.

[20] K. Ullakko, J. K. Huang, C. Kantner, R. OHandley, and V. V. Kokorin, "Large magnetic-field-induced strains in Ni_2MnGa single crystals," *Applied Physics Letters*, vol. 69, no. 13, pp. 1966–1968, 1996.

[21] J. Pons, E. Cesari, C. Segu, F. Masdeu, and R. Santamarta, "Ferromagnetic shape memory alloys: Alternatives to Ni-Mn-Ga," *Materials Science and Engineering: A*, vol. 481-482, pp. 57 – 65, 2008.

[22] K. Uchino, *Ferroelectric Devices 2nd Edition*. CRC Press, 2011.

[23] R. E. Newnham, *Properties of Materials: Anisotropy, Symmetry, Structure*. Oxford University Press, USA, 2005.

[24] A. S. Bhalla, R. Guo, and R. Roy, "The perovskite structure-a review of its role in ceramic science and technology," *Material Research Innovations*, vol. 4, no. 1, pp. 3–26, 2000.

[25] A. J. Moulson and J. M. Herbert, *Electroceramics: Materials, Properties, Applications*. Wiley, 2003.

[26] B. Jaffe, W. Cook, and H. Jaffe, *Piezoelectric ceramics*. Academic Press, 1971.

[27] F. IEEE Ultrasonics, F. C. S. G. on Sonics, Ultrasonics, A. N. S. Institute, I. of Electrical, and E. Engineers, *IEEE Standard Definitions of Primary Ferroelectric Terms*. ANSI/IEEE Std, The Institute of Electrical and Electronics Engineers, 1986.

[28] N. Setter, *ABC of Piezoelectricity and Piezoelectric Materials. Piezoelectric Materials in Devices: Extended Reviews on Current and Emerging Piezoelectric Materials, Technology, and Applications*. N. Setter, 2002.

[29] H. Jaffe and D. Berlincourt, "Piezoelectric transducer materials," *Proceedings of the IEEE*, vol. 53, no. 10, pp. 1372–1386, 1965.

[30] J. G. Juarez, "Piezoelectric ceramics and ultrasonic transducers," *Journal of Physics E: Scientific Instruments*, vol. 22, no. 10, p. 804, 1989.

[31] D. Damjanovic, "Ferroelectric, dielectric and piezoelectric properties of ferroelectric thin films and ceramics," *Reports on Progress in Physics*, vol. 61, no. 9, p. 1267, 1998.

[32] A. N. S. Institute, F. IEEE Ultrasonics, F. C. S. S. Committee, I. of Electrical, and E. Engineers, *IEEE Standard on Piezoelectricity: An American National Standard*. ANSI/IEEE, The Institute of Electrical and Electronics Engineers, 1988.

[33] N. Meyer and M. Jrgensen, "Acoustoelectric effects in piezoelectric semiconductors with main emphasis on cds and zno," *Advances in Solid State Physics*, vol. 10, pp. 21–124, 1970.

[34] S. Zhang and T. Shrout, "Relaxor-PT single crystals: observations and developments," *IEEE Trans Ultrason Ferroelectr Freq Control*, vol. 57, pp. 2138–2146, Oct 2010.

[35] S. Zhang and F. Li, "High performance ferroelectric relaxor-PbTiO$_3$ single crystals: Status and perspective," *Journal of Applied Physics*, vol. 111, no. 3, pp. 031301–031301– 50, 2012.

[36] S. Zhang, F. Li, J. Luo, R. Sahul, and T. Shrout, "Relaxor-PbTiO$_3$ single crystals for various applications," *Ultrasonics, Ferroelectrics and Frequency Control, IEEE Transactions on*, vol. 60, no. 8, pp. 1572–1580, 2013.

[37] P. Langevin, 1920. French Patent 502913 - 505703.

[38] P. Langevin, 1924. French Patent 575435.

[39] E. Neppiras, "The pre-stressed piezoelectric sandwich transducer," in *Ultrasonics International conference proceedings*, pp. 295–302, 1973.

[40] J. G. Juarez, "Macrosonics: Phenomena, transducers and applications," *Forum Acusticum Sevilla. Keynote Lectures: KL-05*, vol. 33, pp. 36–42, 2002.

[41] H. B. Miller, "Origin of the 33-driven ceramic ring-stack transducer," *The Journal of the Acoustical Society of America*, vol. 86, no. 4, pp. 1602–1603, 1989.

[42] F. Arnold and S. Mhlen, "The mechanical pre-stressing in ultrasonic piezotransducers," *Ultrasonics*, vol. 39, no. 1, pp. 7 – 11, 2001.

[43] L. Merkulov, "Design of ultrasonic concentrators," *Soviet Physical Acoustics*, vol. 3, pp. 230–238, 1957.

[44] L. Merkulov and A. Kharitonov, "Theory and analysis of sectional sconcentrators," *Soviet Physical Acoustics*, vol. 5, pp. 183–190, 1959.

[45] L. Shuyu and Z. Fucheng, "Study of vibrational characteristics for piezoelectric sandwich ultrasonic transducers," *Ultrasonics*, vol. 32, no. 1, pp. 39 – 42, 1994.

[46] J.-N. Decarpigny, B. Hamonic, and J. Wilson, O.B., "The design of low frequency underwater acoustic projectors: present status and future trends," *Oceanic Engineering, IEEE Journal of*, vol. 16, no. 1, pp. 107–122, 1991.

[47] R. S. Woollett, "Basic problems caused by depth and size constraints in low-frequency underwater transducers," *The Journal of the Acoustical Society of America*, vol. 68, no. 4, pp. 1031–1037, 1980.

[48] K. D. Rolt, "History of the flextensional electroacoustic transducer," *The Journal of the Acoustical Society of America*, vol. 87, no. 3, pp. 1340–1349, 1990.

[49] H. Hayes, "Sound generating and directing apparatus," Dec. 22 1936. US Patent 2,064,911.

[50] J. Toulis, "Flexural-extensional electro-mechanical transducer," Oct. 4 1966. US Patent 3,277,433.

[51] J. Toulis, "Flexural-extensional electro-mechanical transducer," Sept. 20 1966. US Patent 3,274,537.

[52] L. H. Royster, "The flextensional concept: A new approach to the design of underwater acoustic transducers," *Applied Acoustics*, vol. 3, no. 2, pp. 117 – 126, 1970.

[53] D. F. Jones and D. A. Christopher, "A broadband omnidirectional barrel-stave flextensional transducer," *The Journal of the Acoustical Society of America*, vol. 106, no. 2, pp. L13–L17, 1999.

[54] R. Abbot, "Broad band electroacoustic transducer," July 14 1959. US Patent 2,895,062.

[55] R. Newnham, Q. Xu, and S. Yoshikawa, "Transformed stress direction acoustic transducer," Mar. 12 1991. US Patent 4,999,819.

[56] Q. C. Xu, S. Yoshikawa, J. R. Belsick, and R. Newnham, "Piezoelectric composites with high sensitivity and high capacitance for use at high pressures," *Ultrasonics, Ferroelectrics and Frequency Control, IEEE Transactions on*, vol. 38, no. 6, pp. 634–639, 1991.

[57] K. Onitsuka, A. Dogan, J. F. Tressler, Q. Xu, S. Yoshikawa, and R. E. Newnham, "Metal-ceramic composite transducer, the 'moonie'," *Journal of Intelligent Material Systems and Structures*, vol. 6, no. 4, pp. 447–455, 1995.

[58] A. Dogan, K. Uchino, and R. E. Newnham, "Composite piezoelectric transducer with truncated conical endcaps "cymbal"," *Ultrasonics, Ferroelectrics and Frequency Control, IEEE Transactions on*, vol. 44, no. 3, pp. 597–605, 1997.

[59] K. Onitsuka, A. Dogan, Q. Xu, S. Yoshikawa, and R. E. Newnham, "Design optimization for metal-ceramic composite actuator, 'moonie'," *Ferroelectrics*, vol. 156, no. 1, pp. 37–42, 1994.

[60] A. Dogan and R. Newnham, "Metal-electroactive ceramic composite transducer," Mar. 1998. US Patent 5,729,077.

[61] J. Fernandez, A. Dogan, J. Fielding, K. Uchino, and R. Newnham, "Tailoring the performance of ceramic-metal piezocomposite actuators, 'cymbals'," *Sensors and Actuators A: Physical*, vol. 65, no. 2??3, pp. 228 – 237, 1998.

[62] C. Rubin, M. Bolander, J. P. Ryaby, and M. Hadjiargyrou, "The use of low-intensity ultrasound to accelerate the healing of fractures," *The Journal of Bone & Joint Surgery*, vol. 83, no. 2, pp. 259–259, 2001.

[63] K. N. Malizos, M. E. Hantes, V. Protopappas, and A. Papachristos, "Low-intensity pulsed ultrasound for bone healing: an overview," *Injury*, vol. 37 Suppl 1, pp. 56–62, Apr 2006.

[64] L. Claes and B. Willie, "The enhancement of bone regeneration by ultrasound," *Prog. Biophys. Mol. Biol.*, vol. 93, no. 1-3, pp. 384–398, 2007.

[65] T. El-Bialy, T. Royston, R. Magin, C. Evans, A.-M. Zaki, and L. Frizzell, "The effect of pulsed ultrasound on mandibular distraction," *Annals of Biomedical Engineering*, vol. 30, no. 10, pp. 1251–1261, 2002.

[66] T. El-Bialy, I. El-Shamy, and T. M. Graber, "Repair of orthodontically induced root resorption by ultrasound in humans," *Am J Orthod Dentofacial Orthop*, vol. 126, pp. 186–193, Aug 2004.

[67] G. ter Haar, "Therapeutic applications of ultrasound," *Prog. Biophys. Mol. Biol.*, vol. 93, no. 1-3, pp. 111–129, 2007.

[68] S. Sheikh, S. Pallagatti, B. Singh, N. Puri, R. Singh, and A. Kalucha, "Sonoporation, a redefined ultrasound modality as therapeutic aid: A review," *Journal of Clinical and Experimental Dentistry*, vol. 3, pp. 228–234, 2011.

[69] R. Rao and S. Nanda, "Sonophoresis: recent advancements and future trends," *J. Pharm. Pharmacol.*, vol. 61, pp. 689–705, Jun 2009.

[70] P. A. Dijkmans, L. J. Juffermans, R. J. Musters, A. van Wamel, F. J. ten Cate, W. van Gilst, C. A. Visser, N. de Jong, and O. Kamp, "Microbubbles and ultrasound: from diagnosis to therapy," *Eur J Echocardiogr*, vol. 5, pp. 245–256, Aug 2004.

[71] G. T. Clement, "Perspectives in clinical uses of high-intensity focused ultrasound," *Ultrasonics*, vol. 42, pp. 1087–1093, Aug 2004.

[72] K. D. Evans, B. Weiss, and M. Knopp, "High-intensity focused ultrasound (HIFU) for specific therapeutic treatments: A literature review," *Journal of Diagnostic Medical Sonography*, vol. 23, no. 6, pp. 319–327, 2007.

[73] T. J. Mason, "Therapeutic ultrasound an overview," *Ultrason Sonochem*, vol. 18, pp. 847–852, Jul 2011.

[74] E. J. Linebarger, D. R. Hardten, G. K. Shah, and R. L. Lindstrom, "Phacoemulsification and modern cataract surgery," *Surv Ophthalmol*, vol. 44, no. 2, pp. 123–147, 1999.

[75] D. E. Brooks, "Phacoemulsification cataract surgery in the horse," *Clinical Techniques in Equine Practice*, vol. 4, no. 1, pp. 11 – 20, 2005.

[76] R. S. Hoffman, I. H. Fine, M. Packer, and L. K. Brown, "Comparison of sonic and ultrasonic phacoemulsification using the Staar Sonic Wave system," *J Cataract Refract Surg*, vol. 28, pp. 1581–1584, Sep 2002.

[77] Y. K. Han and K. M. Miller, "Heat production: Longitudinal versus torsional phacoemulsification," *J Cataract Refract Surg*, vol. 35, pp. 1799–1805, Oct 2009.

[78] M. Topaz, M. Motiei, E. Assia, D. Meyerstein, N. Meyerstein, and A. Gedanken, "Acoustic cavitation in phacoemulsification: chemical effects, modes of action and cavitation index," *Ultrasound Med Biol*, vol. 28, pp. 775–784, Jun 2002.

[79] N. Suppipat, "Ultrasonics in periodontics," *J. Clin. Periodontol.*, vol. 1, no. 4, pp. 206–213, 1974.

[80] W. R. Laird and A. D. Walmsley, "Ultrasound in dentistry. Part 1–Biophysical interactions," *J Dent*, vol. 19, pp. 14–17, Feb 1991.

[81] A. D. Walmsley, W. R. Laird, and P. J. Lumley, "Ultrasound in dentistry. Part 2–Periodontology and endodontics," *J Dent*, vol. 20, pp. 11–17, Feb 1992.

[82] T. Arabaci, Y. iek, and C. F. anaki, "Sonic and ultrasonic scalers in periodontal treatment: a review," *Int J Dent Hyg*, vol. 5, pp. 2–12, Feb 2007.

[83] A. D. Walmsley, W. R. Laird, and A. R. Williams, "Displacement amplitude as a measure of the acoustic output of ultrasonic scalers," *Dent Mater*, vol. 2, pp. 97–100, Jun 1986.

[84] A. D. Walmsley, W. R. Laird, and A. R. Williams, "Dental plaque removal by cavitational activity during ultrasonic scaling," *J. Clin. Periodontol.*, vol. 15, pp. 539–543, Oct 1988.

[85] B. J. O'Daly, E. Morris, G. P. Gavin, J. M. O'Byrne, and G. B. McGuinness, "High-power low-frequency ultrasound: A review of tissue dissection and ablation in medicine and surgery," *Journal of Materials Processing Technology*, vol. 200, no. 1-3, pp. 38 – 58, 2008.

[86] J. F. Amaral, "The experimental development of an ultrasonically activated scalpel for laparoscopic use," *Surg Laparosc Endosc*, vol. 4, pp. 92–99, Apr 1994.

[87] L. A. Wetter, J. H. Payne, G. Kirshenbaum, E. F. Podoll, T. Bachinsky, and L. W. Way, "The ultrasonic dissector facilitates laparoscopic cholecystectomy," *Arch Surg*, vol. 127, pp. 1195–1198, Oct 1992.

[88] C. G. Huscher, M. M. Lirici, M. Di Paola, F. Crafa, C. Napolitano, A. Mereu, A. Recher, A. Corradi, and M. Amini, "Laparoscopic cholecystectomy by ultrasonic dissection without cystic duct and artery ligature," *Surg Endosc*, vol. 17, pp. 442–451, Mar 2003.

[89] T. Aoki and S. Kaseda, "Thoracoscopic resection of the lung with the ultrasonic scalpel," *Ann. Thorac. Surg.*, vol. 67, pp. 1181–1183, Apr 1999.

[90] C. Koch, T. Friedrich, F. Metternich, A. Tannapfel, H.-P. Reimann, and U. Eichfeld, "Temperature elevation in tissue during ultrasonic dissection," *Ultrasonics Symposium, 2002. Proceedings. 2002 IEEE*, vol. 2, pp. 1469–1472 vol.2, 2002.

[91] http://www.ethiconendosurgery.com/, "Accessed 11th september 2013."

[92] M. Robiony, F. Polini, C. F., and M. Vercellotti, T. Politi, "Piezoelectric bone cutting in multipiece maxillary osteotomies," *Journal of oral and maxillofacial surgery*, vol. 62, pp. 759–761, 2004.

[93] J.-L. Beziat, J.-C. Bera, B. Lavandier, and G. A., "Ultrasonic osteotomy as a new technique in craniomaxillofacial surgery," *International journal of oral and maxillofacial surgery*, vol. 36, pp. 493–500, 2007.

[94] http://www.mectron.com, "Accessed 11th september 2013."

[95] A. Gonzlez-Garca, M. Diniz-Freitas, M. Somoza-Martn, and A. Garca-Garca, "Ultrasonic osteotomy in oral surgery and implantology," *Oral Surgery, Oral Medicine, Oral Pathology, Oral Radiology, and Endodontology*, vol. 108, no. 3, pp. 360 – 367, 2009.

[96] T. Vercellotti, "Technological characteristics and clinical indications of piezoelectric bone surgery," *Minerva Stomatol*, vol. 53, pp. 207–214, May 2004.

[97] S. Pappalardo and R. Guarnieri, "Randomized clinical study comparing piezosurgery and conventional rotatory surgery in mandibular cyst enucleation," *J Craniomaxillofac Surg*, Aug 2013.

[98] D. J. Hoigne, S. Stubinger, O. Von Kaenel, S. Shamdasani, and P. Hasenboehler, "Piezoelectric osteotomy in hand surgery: first experiences with a new technique," *BMC Musculoskelet Disord*, vol. 7, p. 36, 2006.

[99] N. B. Smith, "Perspectives on transdermal ultrasound mediated drug delivery," *Int J Nanomedicine*, vol. 2, no. 4, pp. 585–594, 2007.

[100] E. Maione, K. K. Shung, R. J. Meyer, J. W. Hughes, R. E. Newnham, and N. B. Smith, "Transducer design for a portable ultrasound enhanced transdermal drug-delivery system," *IEEE Trans Ultrason Ferroelectr Freq Control*, vol. 49, pp. 1430–1436, Oct 2002.

[101] N. B. Smith, S. Lee, and K. K. Shung, "Ultrasound-mediated transdermal in vivo transport of insulin with low-profile cymbal arrays," *Ultrasound Med Biol*, vol. 29, pp. 1205–1210, Aug 2003.

[102] B. Snyder, S. Lee, N. Smith, and R. E. Newnham, "Ferroelectric transducer arrays for transdermal insulin delivery," *Journal of Materials Science*, vol. 41, pp. 221–216, 2006.

[103] E. J. Park, J. Werner, and N. B. Smith, "Ultrasound mediated transdermal insulin delivery in pigs using a lightweight transducer," *Pharm. Res.*, vol. 24, pp. 1396–1401, Jul 2007.

[104] S. Dostrovsky, "Early vibration theory: Physics and music in the seventeenth century," *Archive for History of Exact Sciences*, vol. 14, pp. 169–218, 1975.

[105] R. Lindsay, *Acoustics : historical and philosophical development.* Stroudsburg, Pa: Dowden, Hutchinson & Ross, 1973.

[106] R. Urick, *Principles of underwater sound.* Los Altos, CA: Peninsula Pub, 1983.

[107] K. Graff, "Ultrasonics: Historical aspects," in *Ultrasonics Symposium, 1977*, pp. 1–10, 1977.

[108] K. Graff, "Historical highlights in ultrasonics - 2," in *Frequency Control Symposium and Exposition, 2004. Proceedings of the 2004 IEEE International*, pp. 5–10, 2004.

[109] A. Manbachi and R. S. C. Cobbold, "Development and application of piezoelectric materials for ultrasound generation and detection," *Ultrasound*, vol. 19, no. 4, pp. 187–196, 2011.

[110] W. P. Mason, "Sonics and ultrasonics: Early history and applications," *Sonics and Ultrasonics, IEEE Transactions on*, vol. 23, no. 4, pp. 224–231, 1976.

[111] R. Wood and A. L. Loomis, "The physical and biological effects of high-frequency sound-waves of great intensity," *Philosophical Magazine Series 7*, vol. 4, no. 22, pp. 417–436, 1927.

[112] F. Williamson Jr, "Richard courant and the finite element method: A further look," *Historia Mathematica*, vol. 7, no. 4, pp. 369 – 378, 1980.

[113] M. J. Turner, "Stiffness and deflection analysis of complex structures," *Journal of the Aeronautical Sciences*, vol. 23, pp. 805–823, 1956.

[114] H. Allik and T. J. R. Hughes, "Finite element method for piezoelectric vibration," *International Journal for Numerical Methods in Engineering*, vol. 2, no. 2, pp. 151–157, 1970.

[115] J. F. Tressler, R. E. Newnham, and W. J. Hughes, "Capped ceramic underwater sound projector: The transducer," *The Journal of the Acoustical Society of America*, vol. 105, no. 2, pp. 591–600, 1999.

[116] M. Fyfe and M. Bullock, "Therapeutic ultrasound: some historical background and development in knowledge of its effect on healing," *The Australian Journal of Physiotherapy*, vol. 31, pp. 220–224, 1985.

[117] W. J. Fry, "Intense ultrasound in investigations of the central nervous system," *Adv Biol Med Phys*, vol. 6, pp. 281–348, 1958.

[118] W. J. Fry and F. J. Fry, "Fundamental neurological research and human neurosurgery using intense ultrasound," *IRE Trans Med Electron*, vol. ME-7, pp. 166–181, Jul 1960.

[119] P. N. T. Wells, "The medical applications of ultrasonics," *Reports on Progress in Physics*, vol. 33, no. 1, p. 45, 1970.

[120] M. Catuna, "Sonic energy: A possible dental application," *Annals of dentistry*, vol. 12, pp. 100–101, 1953.

[121] T. Thoe, D. Aspinwall, and M. Wise, "Review on ultrasonic machining," *International Journal of Machine Tools and Manufacture*, vol. 38, no. 4, pp. 239 – 255, 1998.

[122] L. Balamuth and A. Kuris, "Ultrasonic cutting tool," July 4 1961. US Patent 2,990,616.

[123] L. Balamuth and A. Kuris, "Ultrasonically vibrated cutting knives," Apr. 23 1963. US Patent 3,086,288.

[124] H. H. Postle, "Ultrasonic cavity preparation," *The Journal of Prosthetic Dentistry*, vol. 8, pp. 153–160, 1958.

[125] D. Zinner, "Recent ultrasonic dental studies, including periodontia, without the use of an abrasive," *Journal of Dental Research*, vol. 34, pp. 748–749, 1955.

[126] W. Johnson and J. Wilson, "The application of the ultrasonic dental unit to scaling ?procedures," *Journal of Periodontology*, vol. 28, pp. 264–271, 1957.

[127] A. D. Walmsley, W. R. Laird, and P. J. Lumley, "Ultrasound in dentistry. Part 2– Periodontology and endodontics," *J Dent*, vol. 20, pp. 11–17, Feb 1992.

[128] N. Suppipat, "Ultrasonics in periodontics," *Journal of Clinical Periodontology*, vol. 1, no. 4, pp. 206–213, 1974.

[129] M. J. Richman, "The use of ultrasonics in root canal therapy and root resection," *Journal of Dental Medicine*, vol. 12, pp. 12–18, 1957.

[130] H. Martin, "Ultrasonic disinfection of the root canal," *Oral Surgery, Oral Medicine, Oral Pathology*, vol. 42, no. 1, pp. 92 – 99, 1976.

[131] J. E. Horton, T. M. T. Jr., and L. D. Wood, "The healing of surgical defects in alveolar bone produced with ultrasonic instrumentation, chisel, and rotary bur," *Oral Surgery, Oral Medicine, Oral Pathology*, vol. 39, no. 4, pp. 536 – 546, 1975.

[132] J. E. Horton, T. M. Tarpley Jr., and J. R. Jacoway, "Clinical applications of ultrasonic instrumentation in the surgical removal of bone," *Oral Surgery, Oral Medicine, Oral Pathology*, vol. 51, pp. 236–242, 1981.

[133] P. Leclercq, C. Zenati, S. Amr, and D. M. Dohan, "Ultrasonic bone cut part 1: State-of-the-art technologies and common applications," *J. Oral Maxillofac. Surg.*, vol. 66, pp. 177–182, Jan 2008.

[134] M. Labanca, F. Azzola, R. Vinci, and L. F. Rodella, "Piezoelectric surgery: twenty years of use," *Br J Oral Maxillofac Surg*, vol. 46, pp. 265–269, Jun 2008.

[135] S. Schaeren, C. Jaquiery, M. Heberer, M. Tolnay, T. Vercellotti, and I. Martin, "Assessment of nerve damage using a novel ultrasonic device for bone cutting," *J. Oral Maxillofac. Surg.*, vol. 66, pp. 593–596, Mar 2008.

[136] R. J. Meyer Jr, A. Dogan, C. Yoon, S. Pilgrim, and R. Newnham, "Displacement amplification of electroactive materials using the cymbal flextensional transducer," *Sensors and Actuators A: Physical*, vol. 87, no. 3, pp. 157 – 162, 2001.

[137] A. Dogan, E. Uzgur, D. C. Markley, R. J. M. Jr., A. C. Hladky-Hennion, and R. E. Newnham, "Materials for high performance cymbal transducers," *Journal of Electroceramics*, vol. 13, pp. 403–407, 2004.

[138] K. Lam, X. Wang, and H. Chan, "Lead-free piezoceramic cymbal actuator," *Sensors and Actuators A: Physical*, vol. 125, no. 2, pp. 393 – 397, 2006.

[139] J. Tressler, W. Cao, K. Uchino, and R. E. Newnham, "Finite element analysis of the cymbal-type flextensional transducer," *Ultrasonics, Ferroelectrics and Frequency Control, IEEE Transactions on*, vol. 45, no. 5, pp. 1363–1369, 1998.

[140] J. Zhang, A. C. Hladky-Hennion, W. J. Hughes, and R. E. Newnham, "A miniature class V flextensional cymbal transducer with directional beam patterns: the double-driver," *Ultrasonics*, vol. 39, pp. 91–95, Mar 2001.

[141] J. Tressler, A. Dogan, J. Fernandez, J. Fielding, J.T., K. Uchino, and R. Newnham, "Capped ceramic hydrophones," in *Ultrasonics Symposium, 1995. Proceedings., 1995 IEEE*, vol. 2, pp. 897–900 vol.2, Nov 1995.

[142] R. E. Newnham, A. Dogan, D. C. Markley, J. F. Tressler, J. Zhang, E. Uzgur, J. Meyer, R. J., A. C. Hladky-Hennion, and W. J. Hughes, "Size effects in capped ceramic underwater sound projectors," in *OCEANS '02 MTS/IEEE*, vol. 4, pp. 2315–2321 vol.4, Oct 2002.

[143] R. J. Meyer Jr, W. J. Hughes, T. C. Montgomery, D. C. Markley, and R. E. Newnham, "Design of and fabrication improvements to the cymbal transducer aided by finite element analysis," *Journal of Electroceramics*, vol. 4, pp. 2315–2321, 2002.

[144] P. Ochoa, J. Pons, M. Villegas, and J. Fernandez, "Advantages and limitations of cymbals for sensor and actuator applications," *Sensors and Actuators A: Physical*, vol. 132, no. 1, pp. 63 – 69, 2006.

[145] P. Ochoa, J. Pons, M. Villegas, and J. Fernandez, "Effect of bonding layer on the electromechanical response of the cymbal metal-ceramic piezocomposite," *Journal of the European Ceramic Society*, vol. 27, no. 2-3, pp. 1143 – 1149, 2007.

[146] D. a. R. Markley, S.E.Danley, R.J.Meyer, W.J.Hughes, A.Dogan, J. E.Uzgur, and A.C.Hladky, "Size and material effects on cymbal transducers for underwater applications : hydrophones and projectors," *2003 US Navy Workshop on Acoustic Transduction Materials and Devices*, 2003.

[147] I. Hibbitt, Karlesson & Sorensen, *ABAQUS User's Manual Version 6.10*. SIMULIA.

[148] G. Nader, E. Silva, and J. Adamowski, "Effective damping value of piezoelectric transducer determined by experimental techniques and numerical analysis," in *ABCM symposium series in mechatronics*, vol. 1, pp. 271–279, 2004.

[149] P. Ochoa, M. Villegas, and J. F. Fernandez, "Resonant frequency response of cymbal transducer," *Ferroelectrics*, vol. 273, no. 1, pp. 321–326, 2002.

[150] C.-L. Sun, S. Guo, W. Li, Z. Xing, G. Liu, and X.-Z. Zhao, "Displacement amplification and resonance characteristics of the cymbal transducers," *Sensors and Actuators A: Physical*, vol. 121, no. 1, pp. 213 – 220, 2005.

[151] D. J. Ewins, *Modal testing : theory, practice, and application.* Baldock, Hertfordshire, England Philadelphia, PA: Research Studies Press, 2000.

[152] A. Mathieson, *Nonlinear Characterisation of Power Ultrasonic Devices Used in Bone Surgery.* PhD thesis, University of Glasgow, UK, 2012.

[153] Data Physics Corporation, *Signal Calc. 240V 4.2.207 Users manual*, 2007.

[154] J. Tressler and R. E. Newnham, "Doubly resonant cymbal-type transducers," *Ultrasonics, Ferroelectrics and Frequency Control, IEEE Transactions on*, vol. 44, pp. 1175–1177, Sept 1997.

[155] J. Zhang, W. Hughes, A. C. Hladky-Hennion, and R. Newnham, "Concave cymbal transducers," in *Applications of Ferroelectrics, 1998. ISAF 98. Proceedings of the Eleventh IEEE International Symposium on*, pp. 255–258, 1998.

[156] P. Ochoa, M. Villegas, J. Pons, P. Leidinger, and J. F. Fernandez, "Tunability of cymbals as piezocomposite transducers," *Journal of Electroceramics*, vol. 14, no. 3, pp. 221–229, 2005.

[157] Y. Ke, T. Guo, and J. Li, "A new-style, slotted-cymbal transducer with large displacement and high energy transmission," *Ultrasonics, Ferroelectrics and Frequency Control, IEEE Transactions on*, vol. 51, pp. 1171–1177, Sept 2004.

[158] J. Yuan, X. Shan, T. Xie, and W. Chen, "Modeling and improvement of a cymbal transducer in energy harvesting," *Journal of Intelligent Material Systems and Structures*, vol. 21, no. 8, pp. 765–771, 2010.

[159] J. Ueda, T. Secord, and H. Asada, "Large effective-strain piezoelectric actuators using nested cellular architecture with exponential strain amplification mechanisms," *Mechatronics, IEEE/ASME Transactions on*, vol. 15, pp. 770–782, Oct 2010.

[160] S. Lin, "An improved cymbal transducer with combined piezoelectric ceramic ring and metal ring," *Sensors and Actuators A: Physical*, vol. 163, no. 1, pp. 266 – 276, 2010.